DYNAMICS OF QUASI 2D CO-ROTATING VORTEX MERGER

By

AKSHAY G. KHANDEKAR

Bachelor of Science in Mechanical Engineering

Oklahoma State University

Stillwater, OK

2011

Submitted to the Faculty of the
Graduate College of the
Oklahoma State University
in partial fulfillment of
the requirements for
the Degree of
MASTER OF SCIENCE
May, 2014

DYNAMICS OF QUASI 2D AND 3D CO-ROTATING

VORTEX MERGER

Thesis Approved:

Dr. Jamey Jacob

Thesis Adviser

Dr. Arvind Santhanakrishnan

Dr. Brian Elbing

Name: AKSHAY GIRISH KHANDEKAR

Date of Degree: MAY, 2014

Title of Study: DYNAMICS OF QUASI 2D AND 3D CO-ROTATING MERGER

Major Field: Mechanical & Aerospace Engineering

ABSTRACT: Merger of vortices is examined experimentally to explore the merger characteristics under different conditions. It is known that like-signed vortices rotate around a common center of circulation and merger between the vortices may occur under certain conditions. This merger is dependent on the strength of the individual vortex circulation, distance of separation between the centers of the two vortices, Re_{Γ}, and vorticity distribution. The quasi-2D experiments conducted in a vortex generator tank uses high aspect ratio rotating paddles. The vortex merger tank generates slender co-rotating vortices and are examined using PIV (Particle Image Velocimetry). Experimental data is examined and merger relations are derived. Merger characteristics are compared at centerline, 25% span and 5% span from the tank wall for different circulation strengths. Symmetric and asymmetric mergers are studied and it is found that in both cases, the vortex pair rotates around an axis perpendicular to the plane of the vortex pair. Symmetric merger is seen to occur at the center between the two vortices whereas in asymmetric merger the stronger vortex breaks the weaker vortex filaments and continues to follow its path. Wall effects seem to have an effect of vortex braiding and vortex stretching. Closer to the wall, the merger time increases while the merged vortex dissipates faster than at the centerline. Dimensionless relationships are also examined.

TABLE OF CONTENTS

Chapter Page

LIST OF TABLES

Table Page

LIST OF FIGURES

CHAPTER I

INTRODUCTION

1.1 Motivation:

Lift generating systems create vorticity and circulation in the fluid that the object is flying in. Aircraft create circulation in the wake in the form of a vortex sheet that remains even after the aircraft has passed away. The rotation of the vortex behind the aircraft is usually along the streamline axis. It is observed that co-rotating vortices merge whereas counter-rotating vortices push each other and travel along the streamline. The wake vortex behind an aircraft can be complex and evolves in space as it is advected downstream as viewed by the wing or in time as viewed by a stationary observer (Figure 1). The strength of the circulation of the vortex is dependent on the Reynolds number of the flow, hence large aircraft generate high circulation that persists for longer duration and dissipates at a much lower rate. These vortices create a potential threat for vehicles that encounter them, and hence two aircraft have to keep a mandated distance while flying. This in return has an effect on take-off and landing, thus impacts air traffic scheduling.

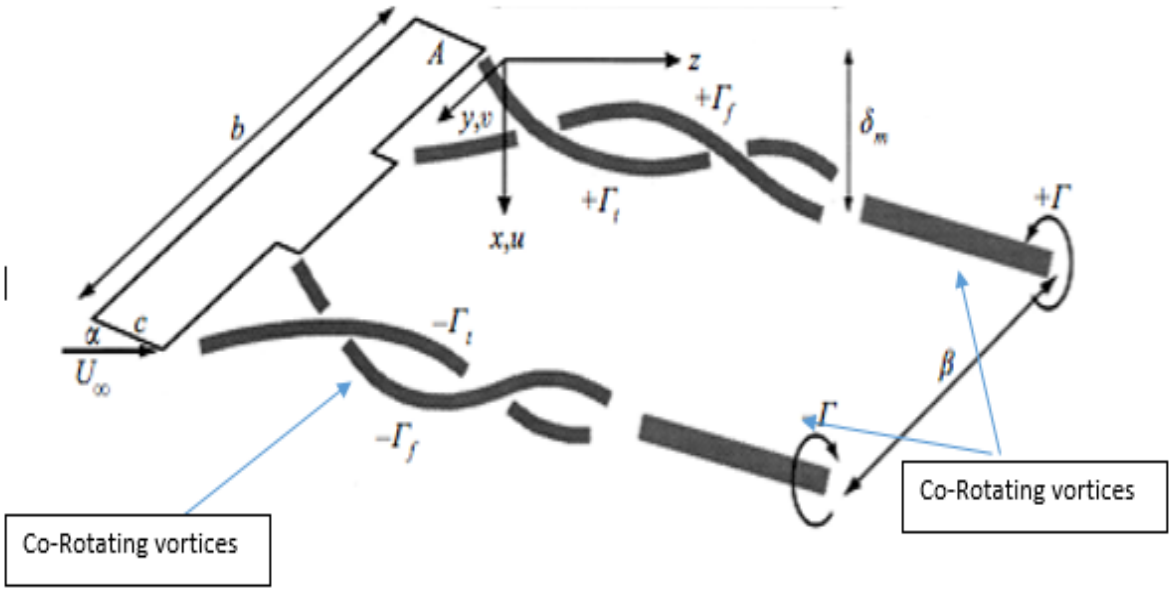

Figure 1 Schematic of co and counter rotating vortices in a wake.

Vortices are formed because of circulation created by an object when it travels in the fluid. The rotation of these vortices can be clockwise or counter clockwise. When such vortices come in the vicinity of each other they behave in a certain way. Co-rotating vortex pairs may merge when near each other to form one large vortex and then dissipate eventually. The merger depends on the strength of the individual vortex pair. The equation for the total circulation (Γ) is given by:

$$\Gamma = \oint_C V * dl = \oint_S \omega * dA$$

where V is the fluid velocity and dl is the differential length of the closed curve element C. Circulation can also be written in terms of vorticity ω and the area dA of the closed surface S. Vorticity can be defined as rotational motion of a fluid in a given local area and can be mathematically written as the curl of velocity field.

$$\vec{\omega} = \nabla \times \vec{v}$$

A co-rotating vortex pair rotates around a common center of vorticity along the axis that joins the center of the two vortices. If they have the same strength, they merge near the center of that axis. It is seen that for an aircraft each wing produces multiple co-rotating vortices due to the flap and wing tip and they eventually merge to form one big vortex, as shown in Figure 2. Thus, each wing produces a vortex and the wake sees a counter rotating vortex pair.

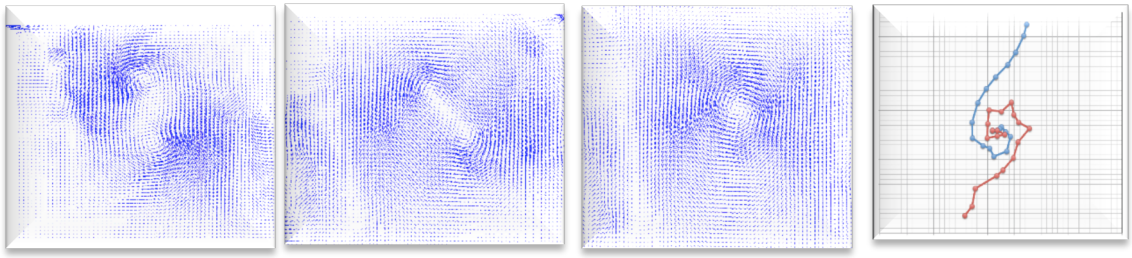

Figure 2 Vortex merger and path using PIV data.

1.2 Goals and Objectives:

The goal of this thesis is to study the merger of a co-rotating vortex pair in 2D state using a vortex tank and in 3D state by collecting data in the wake of two wings. The pair considered for this project is going to be symmetric, i.e. both the vortices have the same amount of circulation Γ, but also consider asymmetric merger where Γ would be different for each vortex.

A vortex tank is to be used with long filaments which rotate creating circulation and a co-rotating vortex pair. Particle Image Velocimetry (PIV) method is used to examine the vortex pair and data collection. Merger behavior is studied based on strength and separation distance between the vortex pair.

1.2.1 Objectives:

1. Develop a Labview program to run stepper motors to drive the filaments in the vortex tank and have independent drive system to each stepper motor.
2. Develop Labview program to run stepper motors to control the traverse system for in the wind tunnel scanning section for future efforts.
3. Calibrate the 7-hole probe and use Labview to collect data using a DSA 3217 pressure scanner.
4. Use MatLab code for processing the data collected from the PIV experiments and from the 7-hole probe.

The experiments consist of rotating the long filaments in the vortex tank at different speeds. That would generate a vortex pair of different strengths and the merger can be studied. Also effects of spacing can be examined by changing the distance between the two filaments. A time relation based on circulation strength is to be determined to study the dynamics of the merger. A relation between number of rotations for the merger and strength of circulation is to be determined. In the 3D experiments, the merger is experimented using different angle or attacks of the wings and separation distance between them. Symmetric vortices are created as the flow velocity is constant. Time relation and spacing effects are studied based on the circulation of each vortex.

CHAPTER II

PREVIOUS WORK

Lift is the most important force that drives any vehicle to fly in the air. As circulation in the wake of that vehicle is a result of lift, since the early stages of aerodynamics circulation has always been an important part of study. Vortices are a result of this circulation and thus understanding the dynamics of vortices got attention. It is known that co-rotating or similar rotating vortices merge along the axis perpendicular to the plane in which the two vortices are observed. While a counter-rotating vortex pair is observed to follow the line of symmetry between the pair.

Wings help generate lift for an airplane and each wing produces a large number of co-rotating vortices which merge to form one big vortex at the tip and the two wings form a vortex sheet in the wake of counter rotating vortices. As shown in Figure 1, we can see how vortex pairs merge and we end up with a counter rotating pair in the wake, which advects until it dissipates. This vortex system in the wake caused by the circulation is a

main concern for aircraft separation distance between two aircraft. The main aim is to accurately understand and make a prediction on the wake vortex system over its life span and the trajectory of it so as to minimize the effect of turbulence caused by it on the succeeding aircraft.

A lot of study has been done in the past about the mechanics behind a vortex merger. Interaction of two co-rotating trailing vortices is studied by C. Cerrettelli and C.H.K. Williamson from the Cornell University. They worked on measuring the structure of the asymmetric vorticity field that causes the vortex pair to be pushed towards each other and eventually merge. They discovered that the co-rotating vortex pair evolves through four distinct phases. The first stage is a diffusive growth, which could be viscous or turbulent. The second stage corresponds to where the vortices move towards each other and the process is almost independent of viscosity. Later the vortices start to diminish by a symmetrization process which is the third stage and in the last or fourth stage is where the vortex core grows by diffusion. Thus, the physical mechanism of a vortex merger is divided in four different stages.

Cerritelli and Williamson used a computer-controlled XY towing tank driven by a continuous cable and pulley system that is powered by a DC servomotor. The driving system gives a range of Reynolds number ranging from 400 to 5700. Digital particle image velocimetry (DPIV) method was used to take quantitative measurements. Figure 3 shows the schematic of the setup that they used for their experiments.

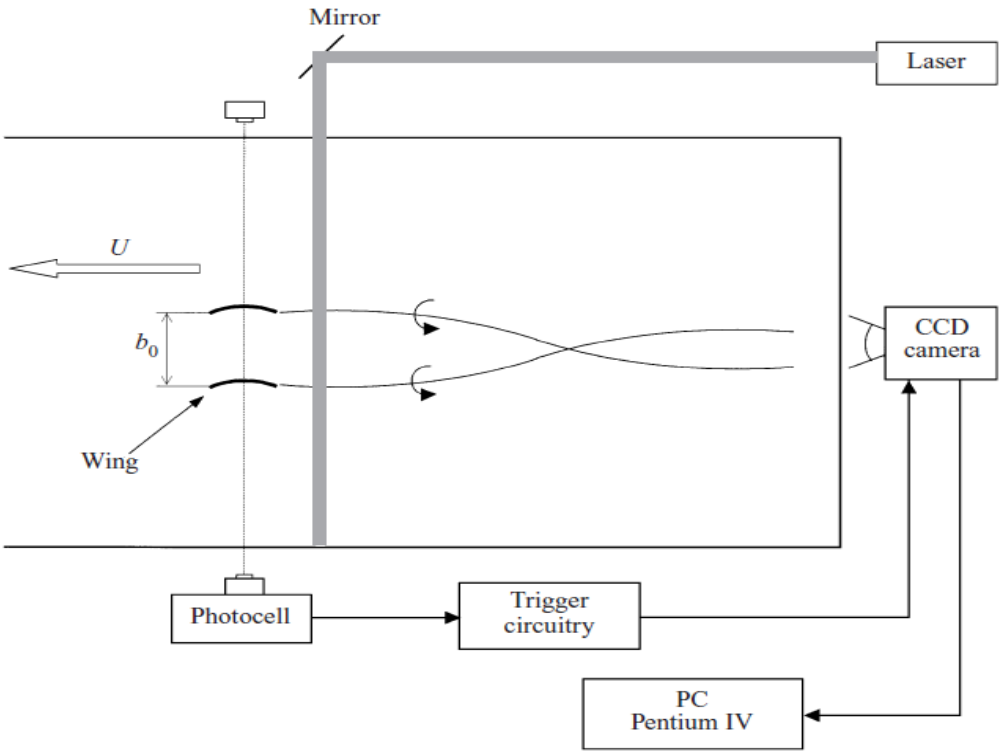

Figure 3 Cerretelli and Williamson setup.

The group performed a number of experiments with varying Reynolds number, i.e. making it laminar and turbulent flows. The convective period for all the stages to get over is given by the following equation for laminar and turbulent case where b_0 is the initial vortex spacing while Γ_o is the strength of the vortices.

For Laminar case: $t_c = 8.1 \frac{b_o^2}{\Gamma_o}$

For Turbulent case: $t_c = 16.1 \frac{b_o^2}{\Gamma_o}$

The number of turns that the vortex pair undergoes before merging with each other is determined by the total merger time t_m and the period T.

The number of turns (N) is given by: $N \sim \frac{t_m}{T}$

A general representation of the vortex merger can be shown in the Figure 4 below. The (a) and (b) images are of the vortex pair in the diffusive stage while images (c) and (d) are in the convective merging stage. Image (a) is at t=2.1sec, (b) at 13.3sec, (c) at 19.6 sec and (d) at 30.8 sec. and vorticity is counterclockwise.

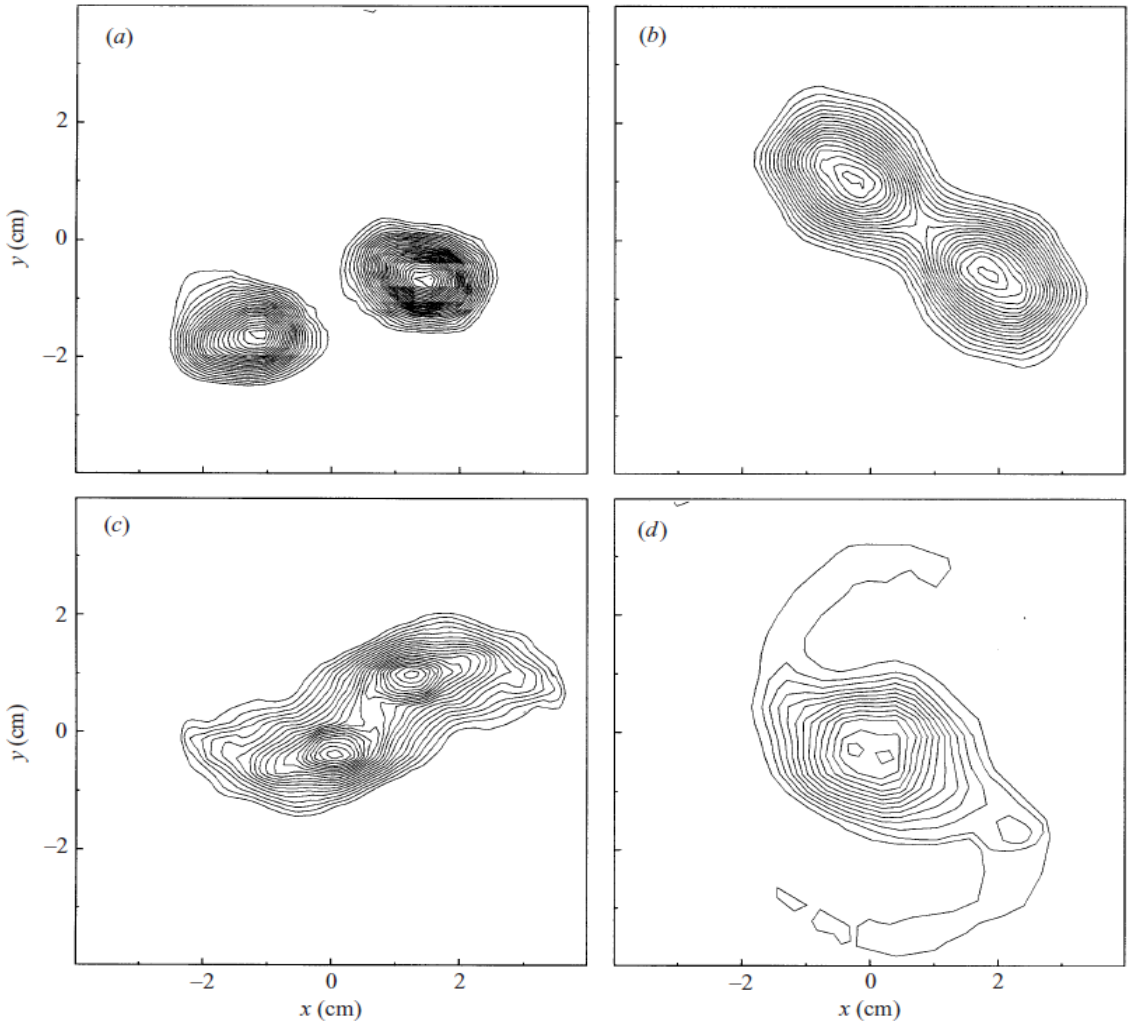

Figure 4 Vorticity fields during merger of 2 co-rotating vortices.

Xinyu Lu and J.D. Jacob also observed effects of initial spacing on co-rotating vortex formation and merger. Experiments were performed in the wind tunnel to understand and study the formation, evolution, interaction and merger of trailing vortices formed by a pair of NACA 0012 wings. A 7-hole probe is being used to get an average velocity profile in 3-D of the vortex wake. It was observed that it took at least one orbit period for the merger to finish.

The experiment was set up utilized the split wing combination since vortices are generated relatively free of external effects and can be easily implemented in the wind tunnel. The tunnel used was a low turbulence open loop tunnel. The NACA 0012 wings were half span of 13" and 13.5" and had chord length of 6". The 7-hole probe used was of outer diameter of 2mm. the pressure scanner used was a DAS08 scanner with a sampling frequency of 200 Hz. Data was collected at several distances in the wake of the two wings. The x/c distance was 0.21, 2.94, 8.04, 9.62, 11.62, and 16.50 downstream of the trailing edge. For each distance a coarse mesh was run to find the vortices and then a fine mesh was run to get detailed velocity profile with higher resolution. Six wing configurations were ran as shown in the following table

Case	Wing configuration	AOA	Half span length
1	Single NACA 0012	3	13.5
2	Double NACA 0012	3,0	13.5
3	Double NACA 0012	+3,-3	13.5
4	Single NACA 0012	5	13.0
5	Double NACA 0012	+5,-5	13.5
6	Double NACA 0012	+3,-3	13.5

Table 1. Wing configuration for Xinyu Lu and J. D. Jacob experiment

In case 1, a single vortex was studied and in case 2 the existence of an extra wing in the vortex formation was studied. In case 3, the $\pm 3^0$ orientation was used to generate vortices of same strength of circulation. The schematic of the experimental set up is as shown below:

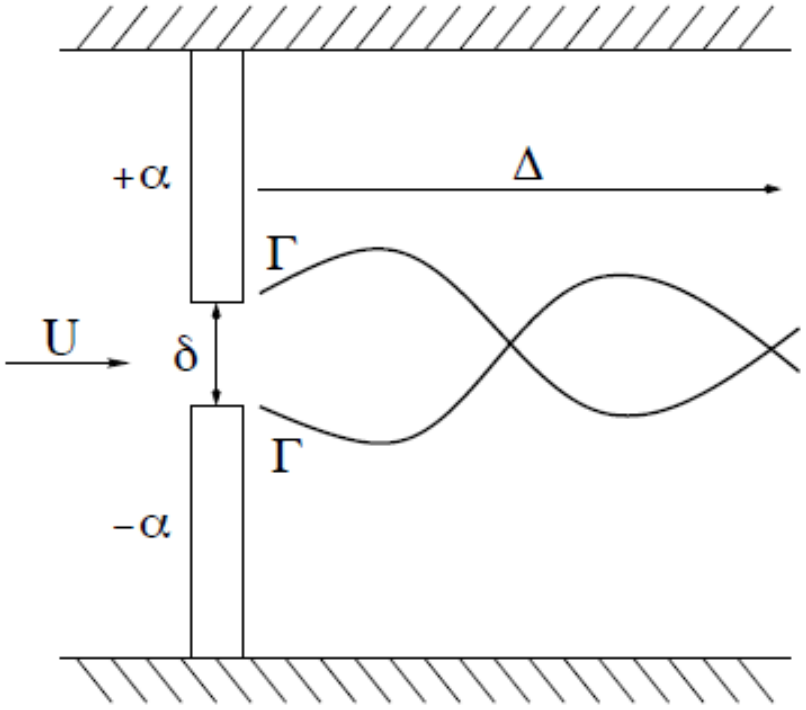

Wing semi-spans are placed at opposite attack angles α to generate co-rotating trailing vortices. These are expected to merge at some downstream distance Δ_m.

Figure 5 Schematic of Xinyu and Jacob experiment setup.

They observed that merger time t_m was about the same as one orbital period τ and the merger distance can be estimated using the following equation from Li, Chen et al and Devenport et al:

$$\Delta m = U_\infty * \tau = U_\infty * \frac{4\pi^2 l^2}{\Gamma}$$

The theoretical and experimental data was compared. For case 4, for a total circulation of 0.62 m^2/s and separation of 2.6" the separation ratio was 0.43 and predicted distance was Δ_m/c of 45. And from the experimental results it's found that the one period orbital motion would happen at distance of 44. Similarly for case 5, the predicted distance was 9.0 while the experimental result was found to be 7.8. For case 6, the distance predicted theoretically was x/c as 14 while experimentally was observed as 9.62. It was observed that when initial spacing ratio decreases the prediction is not as accurate as when the ratio is higher. This could be an effect off line vortices assumption in theoretical analysis and can be said that it's not valid over smaller spacing. Thus it can be said that smaller initial spacing between the vortex pair the merger happens closer in the downstream from the trailing edge.

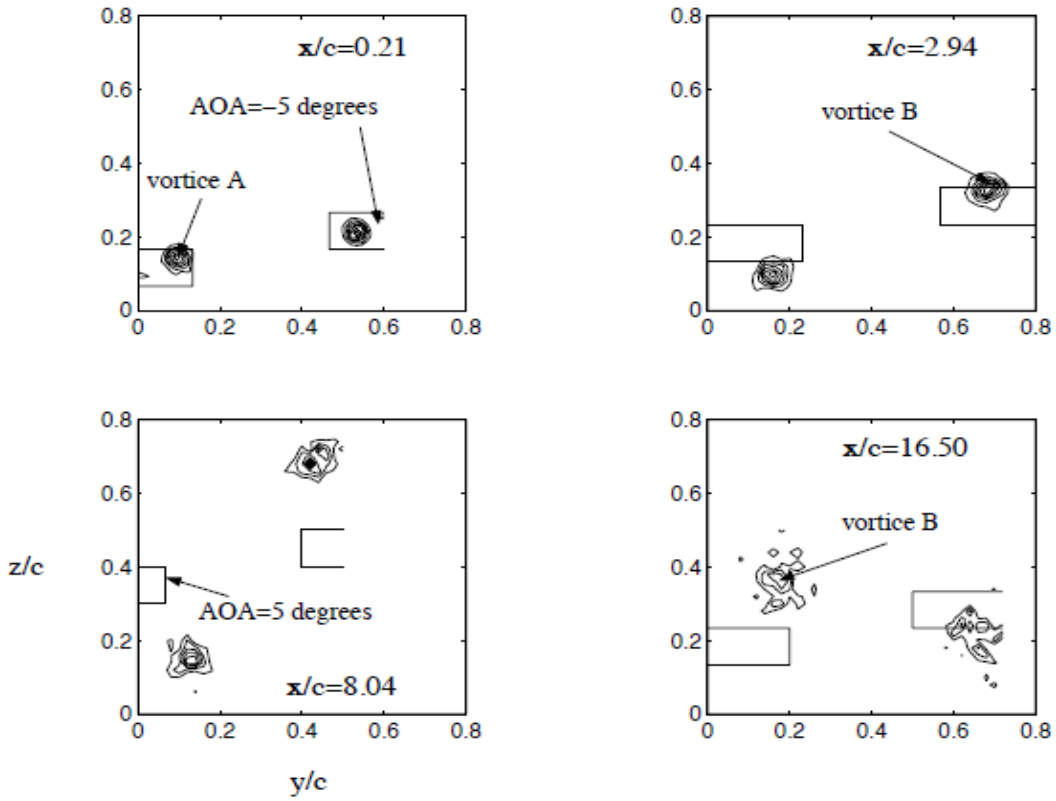

Figure 6: Xinlyu and Jacob Experiment result for case 6.

Chen, Jacob and Savas studied the dynamics of co-rotating vortex pairs in the wakes of flapped airfoils in the University of California at Berkley. The behavior of a pair of co-rotating vortex pair was studied in water towing tank. Reynolds numbers from a range of $1x10^4$ to $6.4x10^4$ were varied for the experiments. PIV method was used to collect data quantitatively. The goal of their project was to understand the dynamics of a co-rotating pair by treating it as a 2-D system which should not merge unless the vortex cores are sufficiently large. The towing tank used for the experiments were 70m long and 2.4m across and a depth of 1.7m. The speed U_∞ is varied from 10 to 160 cm/s. The following Figure 7 shows the experimental setup of the experiment.

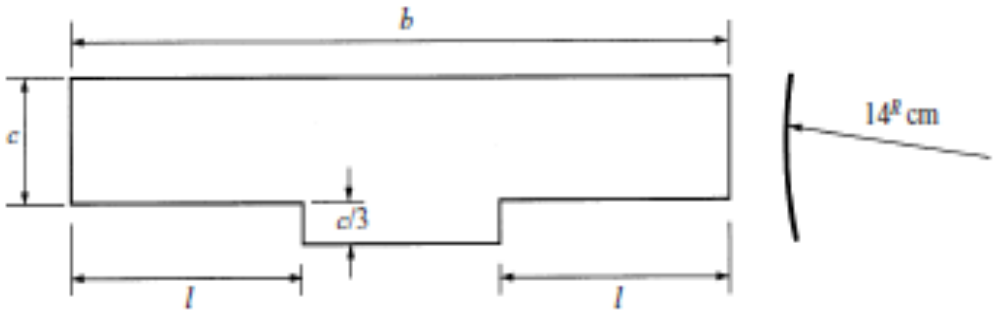

FIGURE 2. Wing geometry showing plan view, circular profile, and dimension definitions.

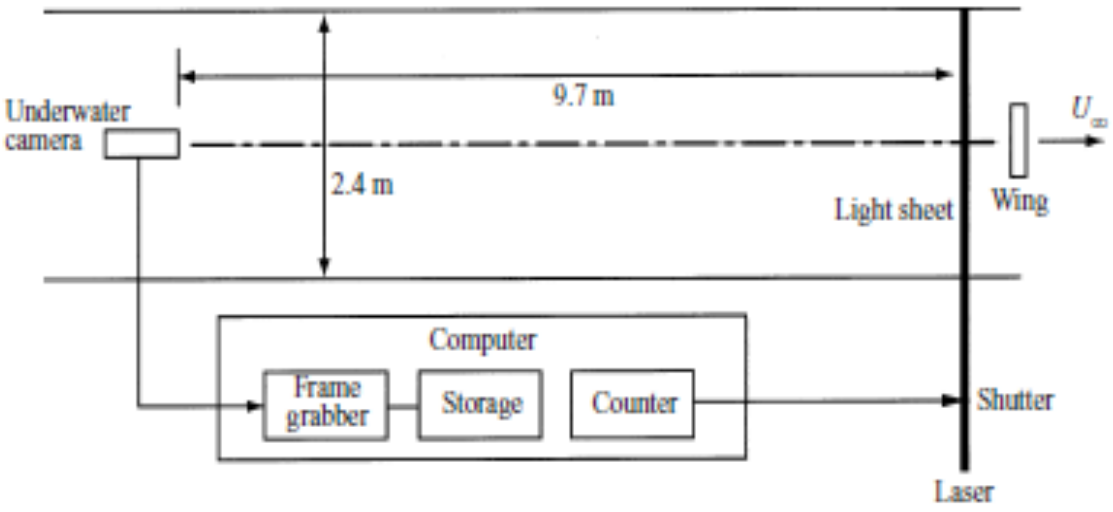

Figure 7 Experimental setup used by Chen, Jacob and Savas.

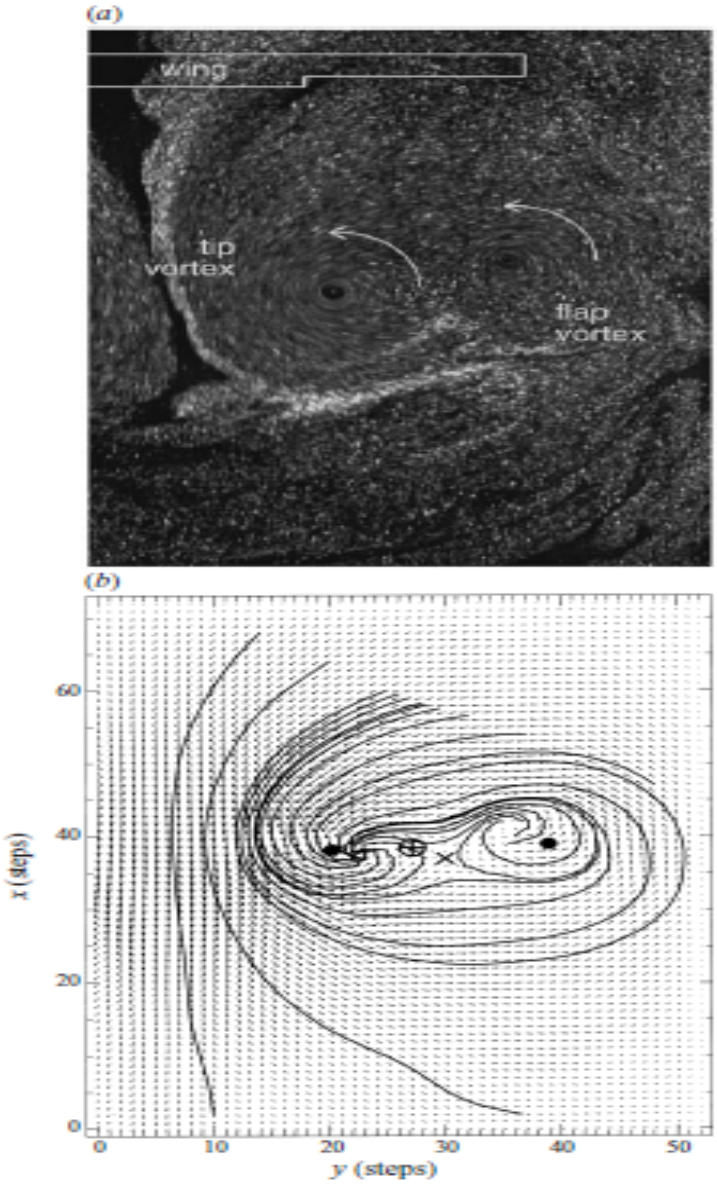

Figure 8 The PIV image and the processed data using image pair.

The above images are from the quantitative analysis using the PIV method. Image (a) is an actual image from the camera while image (b) is processed velocity vector plot of image (a). Vortex formed by tip and flap of the wing are clearly seen. It was found that the total circulation was addition of the tip and the flap. $\Gamma_{total} = \Gamma_{tip} + \Gamma_{flap.}$ A pair of co-

rotating vortex merges in approximately 0.8 orbit times. The time scale is dependent on Re_Γ or strength ratio of flap to tip circulations. The orbit time determines scale of events that result in the merger of the pair. Usually the merger distance is a lot more than the usual span of a wing. Experimental data suggests that the process of merger is 3-D and inviscid. Vortices are either wrapped around each other to merge or shrink and spread over large regions around the dominant filament. The first indication of the merger is dissolving of filaments of the vortices. The process depends directly on the strength of individual vortex. When one vortex is weaker the filament dissolution starts quicker weakening the vortex and merges with the dominating vortex.

The main interest of this project is to see the effects of initial spacing on the vortex merger and understanding the dynamics behind the process of merger. Symmetric or equal strength merger is studied along with the effects of asymmetric merger is also studied. Number of rotations are calculated and vortex paths are also tracked. Vortex merger is studied on a 2D and a 3D phase. Comparisons and relations are driven on experiments conducted in a vortex generator water tank using PIV and in wind tunnel in the wake of NACA 0015 wings pair placed at opposite angle of attacks.

CHAPTER III

METHODOLOGY

3.1 Overview

The purpose of this experiment is to study the dynamics of a co-rotating vortex pair. Two sets of experimental setup was used for 2D merger study and 3D merger studies. The former was performed in a water tank which has two long filaments that could rotate and generate circulation and data was collected using PIV method, while the later was performed in a wind tunnel using NACA 0015 wings and a 7-hole probe to collect data.

The filaments are connected to a stepper motor respectively and hence an individual control on the speed of rotation for each filament was achieved. The strength of the circulation is directly dependent on the rotational speed of the filament. Experiments are conducted at different speed variations and separation distance between the two vortex centers and the data collected is analyzed to find relations of circulation of a vortex to the time of merger, dynamics of merger geometry and number of rotations for merger. For a

3D case, NACA 0015 wings are placed at opposite angle of attacks and separated by a distance and data is collected at different velocities which is directly proportional to the strength of the individual tip vortex. The wings are mounted on portable polycarbonate plates which can be moved inside the tunnel thus helping collect data at different distances in the wake of the wings. The traverse system attached to the tunnel using stepper motors guide the 7-hole probe to scan a section behind the wings. Collaborating data at different distances behind the wings can help us predict how the merger behind an aircraft based on Reynolds number of the flow and strength of circulation of a vortex pair. The schematic of the two experiments is shown in the Figures 23 and 28 below.

3.2 Stepper motor control

Stepper motors play a very vital role in these experiments. They are the driving blocks for the filaments in the vortex tank to generate vortices and to run the traverse system to guide the 7-hole probe for scanning the section in the wake. Stepper motors can be controlled using stepper motor drivers that are available in the market. For independent access to both stepper motor and having a reliable and cost effective system, an Arduino Uno board was used as a micro controller which would then command to the stepper motor driver. The driver receives commands from the micro controller which in return turns the stepper motor accordingly. Labview is used as a base software for the entire stepper motor control. Figure 9 shows how the control is actually set up.

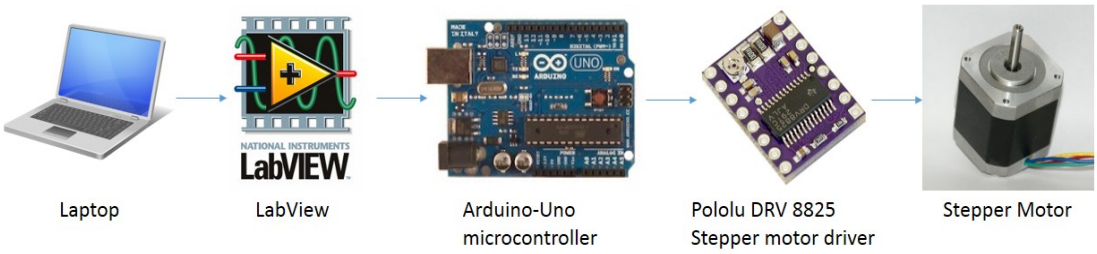

Figure 9 Stepper motor control schematic.

3.2.1 Arduino board

Arduino UNO is a microcontroller that is based on Atmega 328. The microcontroller has 14 Digital I/O pins out of which 6 pins provide a PWN output. 2 of those pins are of importance to drive the stepper motor. The specifications of the Arduino Uno are as follows:

Microcontroller	ATmega328
Operating Voltage	5V
Input Voltage (recommended)	7-12V
Input Voltage (limits)	6-20V
Digital I/O Pins	14 (of which 6 provide PWM output)
Analog Input Pins	6
DC Current per I/O Pin	40 mA

DC Current for 3.3V Pin	50 mA
Flash Memory	32 KB (ATmega328) of which 0.5 KB used by bootloader
SRAM	2 KB (ATmega328)
EEPROM	1 KB (ATmega328)
Clock Speed	16 MHz

Table 2. Arduino Uno spec sheet.

Two PWN outputs are required to control one stepper motor. Thus one Arduino microcontroller is enough to run the filaments in the vortex tank and the traverse system. The two PWM outputs control the Step and Direction for the stepper motors. We initially have to upload the stepper motor program that is provided by Arduino using the Arduino sketch compiler. The sketch is shown in Figure 11. After uploading the sketch the Arduino is ready to go for being used to drive stepper motors. Later it is important for the Arduino to be able to receive commands using LabView as that is going to be the base software of the entire project. There is an Arduino Library available for LabView which has to be downloaded and installed, which helps to program the Arduino so as to run stepper motors. Figure 10, shows how Arduino is initialized in the Labview. We select the VISA resource (COM port), Baud rate (115200), Type of Arduino board (Arduino UNO), bytes of data to be sent (15), connection type (USB) and create a block for error which can be passed on to debug the code in case of errors. Using the Arduino close block in Labview we disconnect the Arduino serial after the experiment is done. The Step

PWM output is used to govern the number of steps that the stepper motor is to spin while the Direction PWN output governs if the steps taken are to be in clockwise or counter clockwise direction.

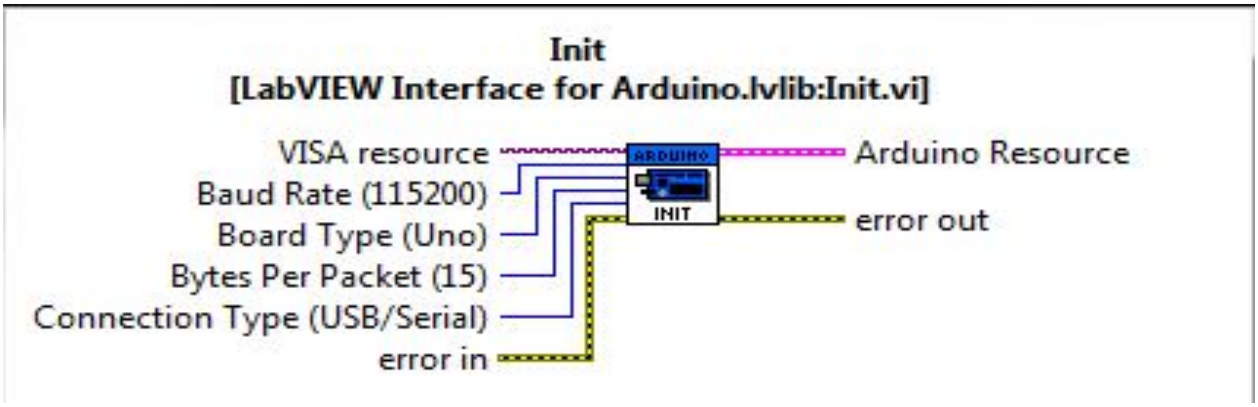

Figure 10 Arduino initialization block for Labview.

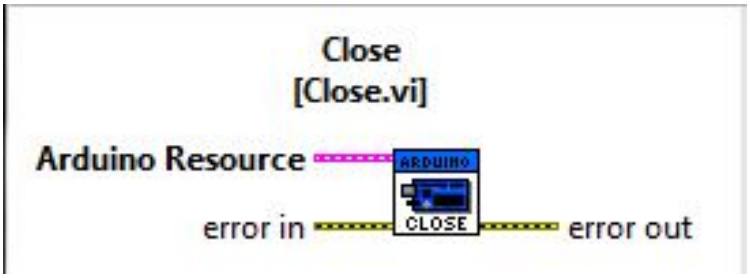

Figure 11 Arduino close block for Labview.

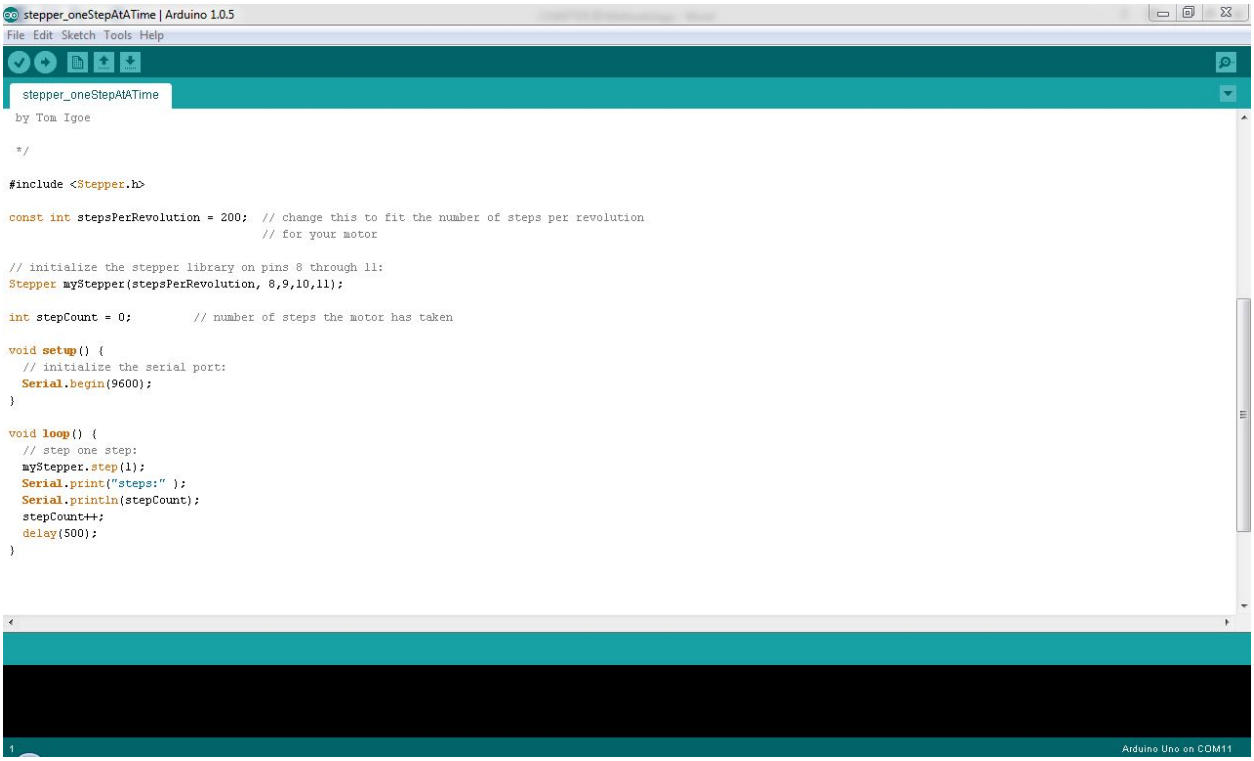

Figure 12 Arduino stepper motor sketch.

3.2.2 Stepper Drivers Pololu

Stepper driver is a motion control module which can be connected in a circuit to drive stepper motors and commanded by a microcontroller using digital input. The stepper driver used in this project is the Pololu DRV8825 stepper motor driver with high current functionality. The DRV8825 can be used to drive bipolar stepper motors by connecting the A+ A- B+ B- leads to the output of the driver. Two sets of voltage inputs are required, a 5V input is used for the control logic of the driver. This input helps to power the functioning of the driver. Another voltage input is required depending on the stepper

motor specification and that input voltage is used to power the motor. A current of 2.2A can be drawn per phase via the stepper driver, which shows that a high torque bipolar motor can be easily driven using the DRV8825. The driver is to be soldered with header pins and can be easily used on a breadboard. The specifications and schematic of the circuit for the DRV8825 are shown below, along with the actual circuit built in the interest of this project.

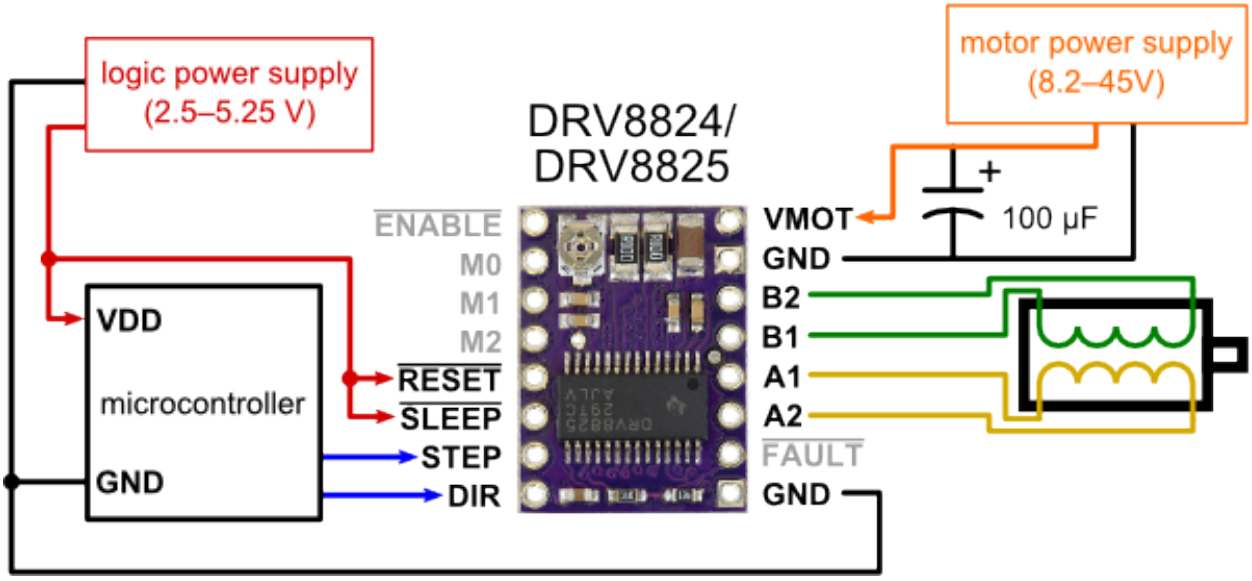

Figure 13 Circuit schematic for DRV8825.

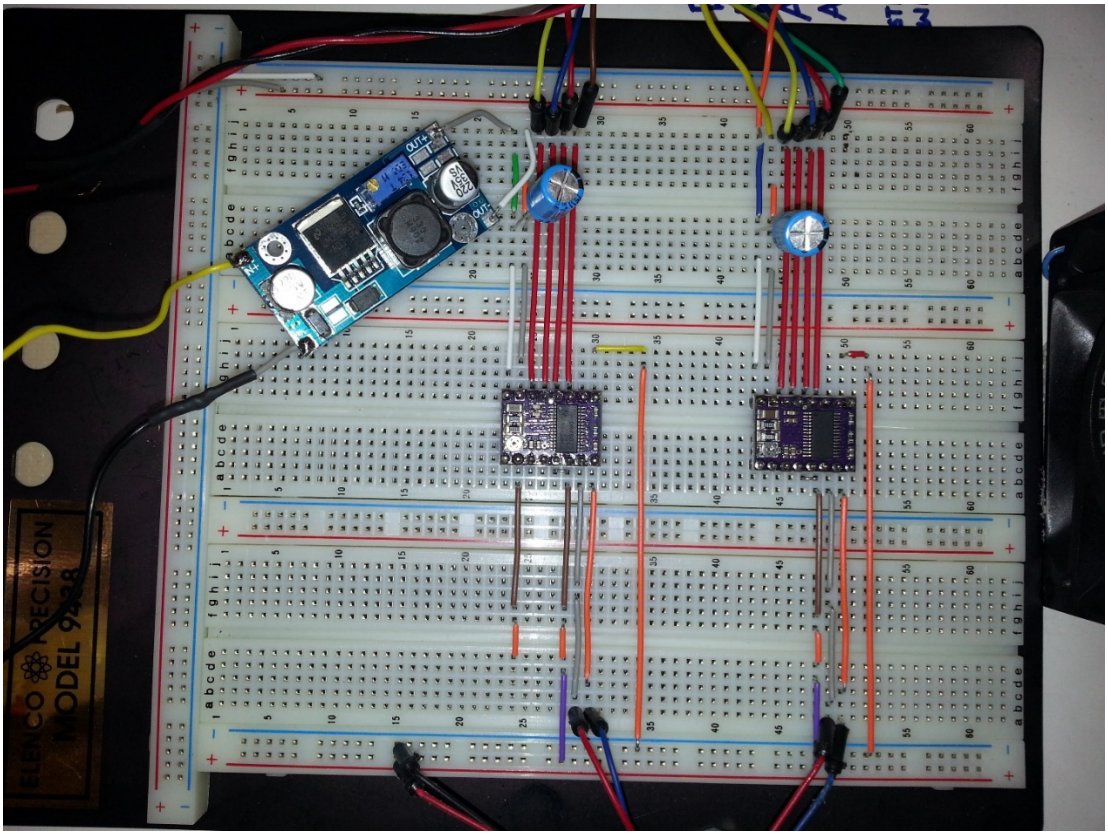

Figure 14 Circuit built for controlling stepper motors.

Dimensions

Size:	0.6″ × 0.8″
Weight:	1.6 g[1]

General specifications

Minimum operating voltage:	8.2 V
Maximum operating voltage:	45 V
Continuous current per phase:	1.5 A[2]
Maximum current per phase:	2.2 A[3]
Minimum logic voltage:	2.5 V[4]
Maximum logic voltage:	5.25 V[4]
Microstep resolutions:	full, 1/2, 1/4, 1/8, 1/16, and 1/32
Reverse voltage protection?:	N

Figure 15 DRV8825 specification data sheet.

3.2.3 Stepper Motors For Vortex tank and Traverse

Stepper motors are brushless DC motors which have the capability to convert one full rotation in equal number of steps. The position of the motor can be controlled to hold at a specific step without any feedback sensor as long as the initial zero position of the motor is set for a desired application. There are two types of stepper motors, unipolar and bipolar. For this project we use bipolar motors for both the vortex tank experiments and the wind tunnel experiments. The reason behind using the bipolar stepper motor is that the DRV8825 stepper driver is compatible with only bipolar motors and bipolar motors have high torque productivity as compared to unipolar motors. Hence bipolar motors were the best fit for the project. The most important specifications on selection the stepper motors was the torque output, the current required per phase as the DRV8825 could provide with a maximum of 2.2Amps per phase and the leads of the stepper motor. The leads of a stepper motor are the wires that drive the stepper motor. The DRV8825 driver has position to connect 4 lead wires namely A+ A- B+ B- that would drive the steps and direction of the respective stepper motor.

The stepper motor selected for the vortex tank experiment was a NEMA 23 stepper motor. The voltage required per phase was 6.5V while current was 1.3A which was as per the stepper driver. Step angle was 1.8 degrees and is a 2 phase Bi-Polar 5 lead stepper motor. It was manufactured by Shinano Kenshi and was purchased from www.steppermotordepot.com

Figure 16 NEMA 23 vortex tank stepper motor.

The stepper motor selected for the vortex tank experiment was a NEMA 23 stepper motor. The voltage required per phase was 5.7V while current was 2.3A which was as per the stepper driver. Step angle was 1.8 degrees and is a 4 phase Bi-Polar 6 lead stepper motor. It had a capacity of 16 kg.cm holding torque which was enough to drive the traverse system. It was purchased from www.steppermotordepot.com

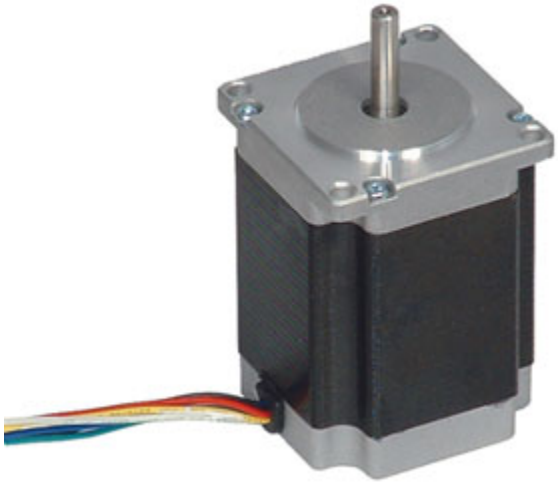

Figure 17 NEMA 23 traverse system stepper motor.

3.3 Setups

3.3.1 Vortex tank

The vortex tank is as the name suggests is a polycarbonate tank of dimensions 4ft x 1ft x 1ft i.e. it holds about 30 gallons of water as shown in Figure 18. This tank has side plates of 1ft x 1ft which can be removed as per the requirement and different sides can be bolted into. Each pair of side plates have two holes aligned along the diagonal of the square separated by a specific distance. These holes hold the long filaments. The filaments are made out of polycarbonate that are bolted into steel rods that pass through the side plate holes. One end of the steel rods are connected to a shaft that is coupled with the shaft of the stepper motor. The stepper motors then move the filaments as per the requirement of the experiment.

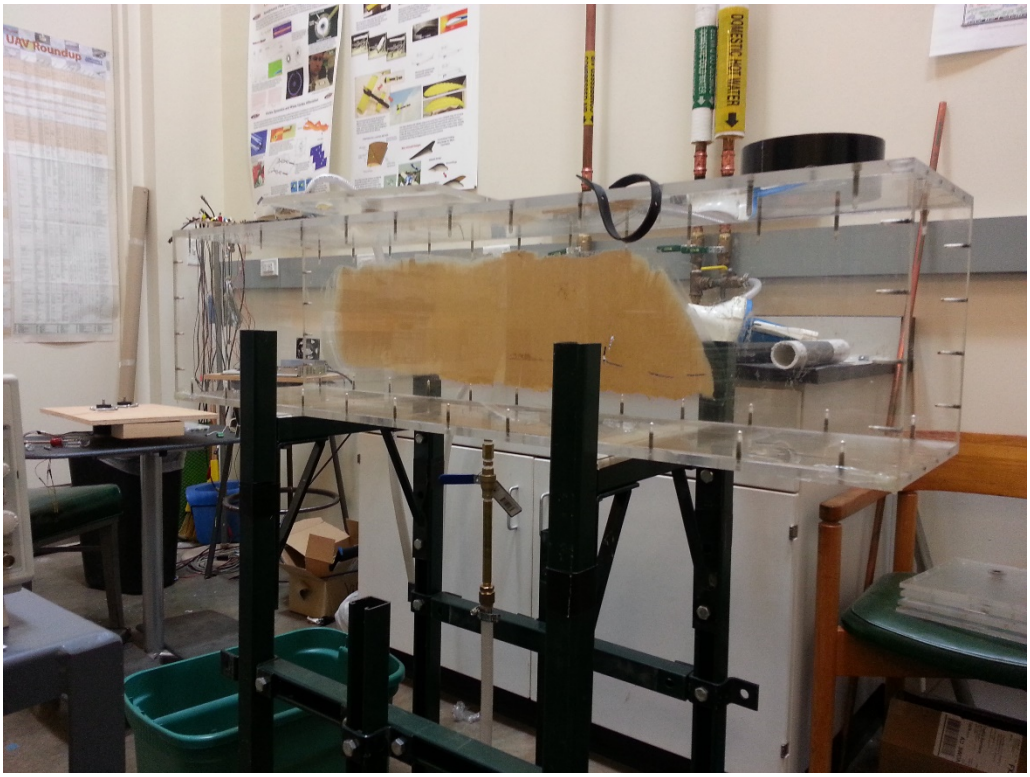

Figure 18 Vortex tank of dimensions 4ft x 1ft x 1ft.

The above picture shows the vortex tank that is supported and leveled on strut rod table. The pictures below are of the side plates with separated holes for filaments, the filaments that generate vortices, shaft coupling that attaches filaments to the stepper motors and stepper motor mount. The data is collected using Particle Image Velocimetry which is described more in section 3.3 of the Thesis report.

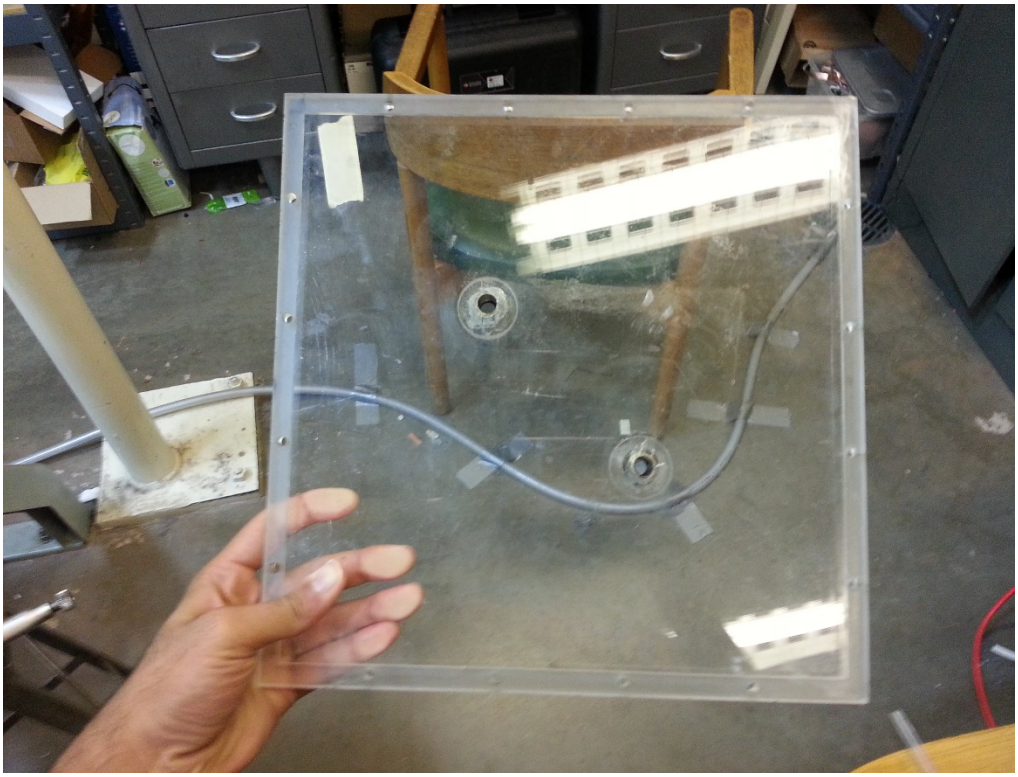

Figure 19 Side plates for the vortex tank.

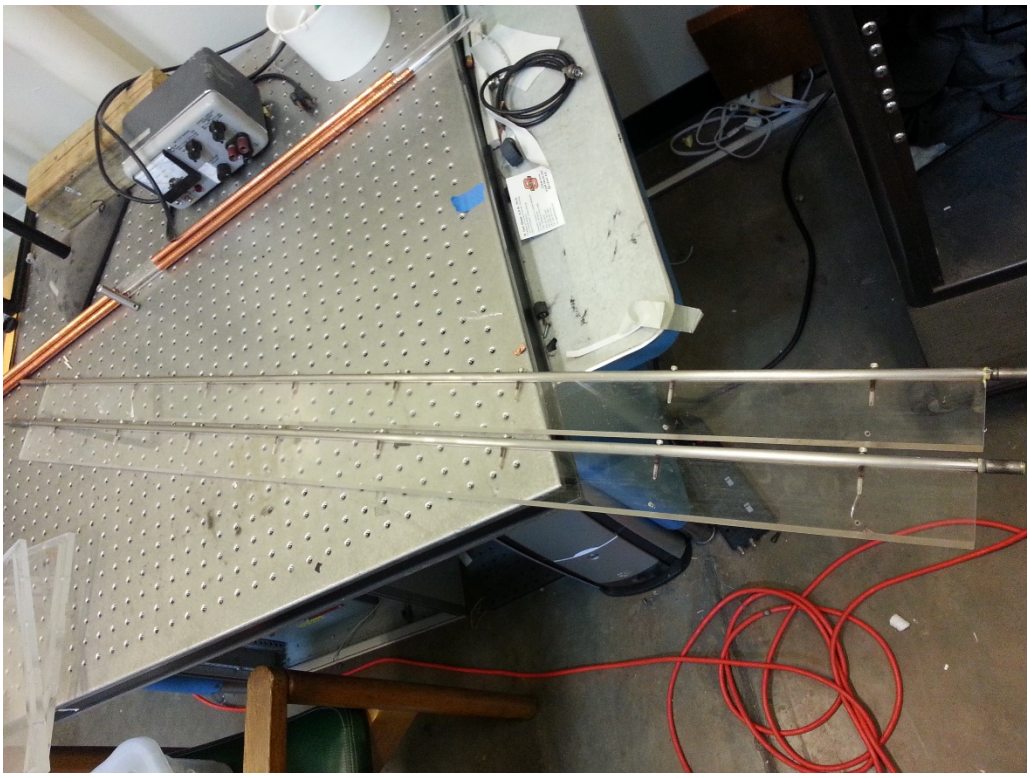

Figure 20 Filament paddles for the vortex tank.

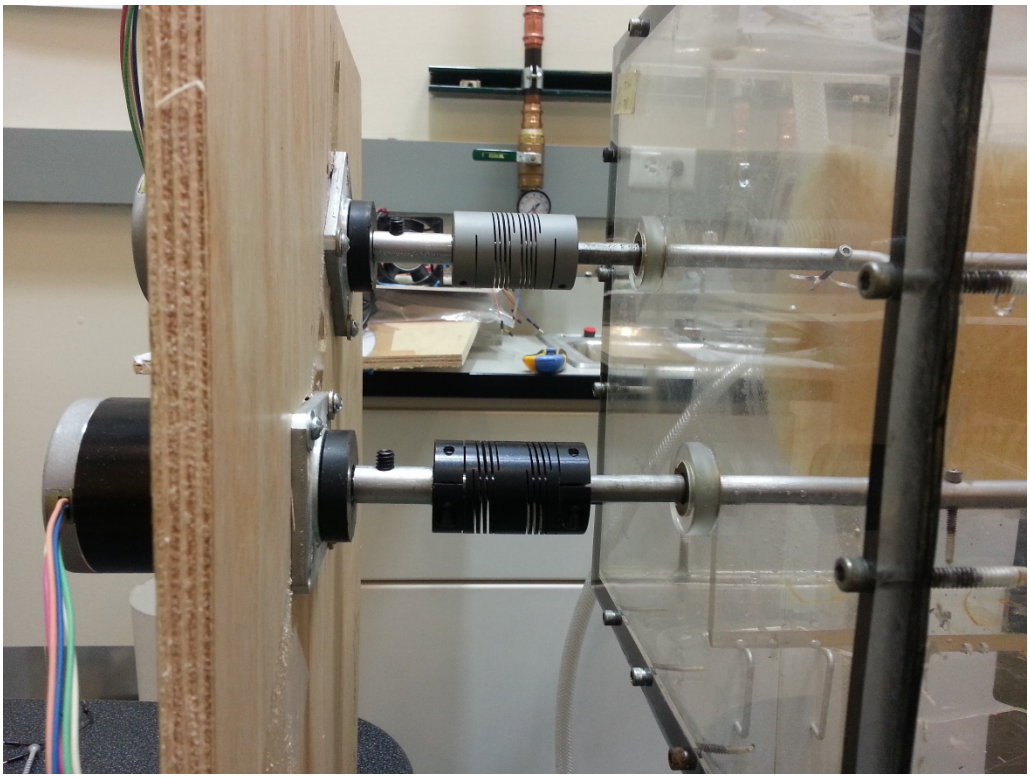

Figure 21 Motor to filament coupling.

Figure 22 Stepper motor mount for vortex tank.

3.3.2 Traverse system

The traverse system is a mechanical device that is controlled by stepper motors so as to move the 7-hole pitot probe from starting point to the designated end point. The system comprises of 2 stepper motors connected to threaded rods. A flange nut is positioned on the threaded rods which moves the probe holder in the X and Y directions. The stepper motors can be controlled individually and the probe is guided in a specific path so as to collect data. Figure 23 shows the schematic of the traverse path.

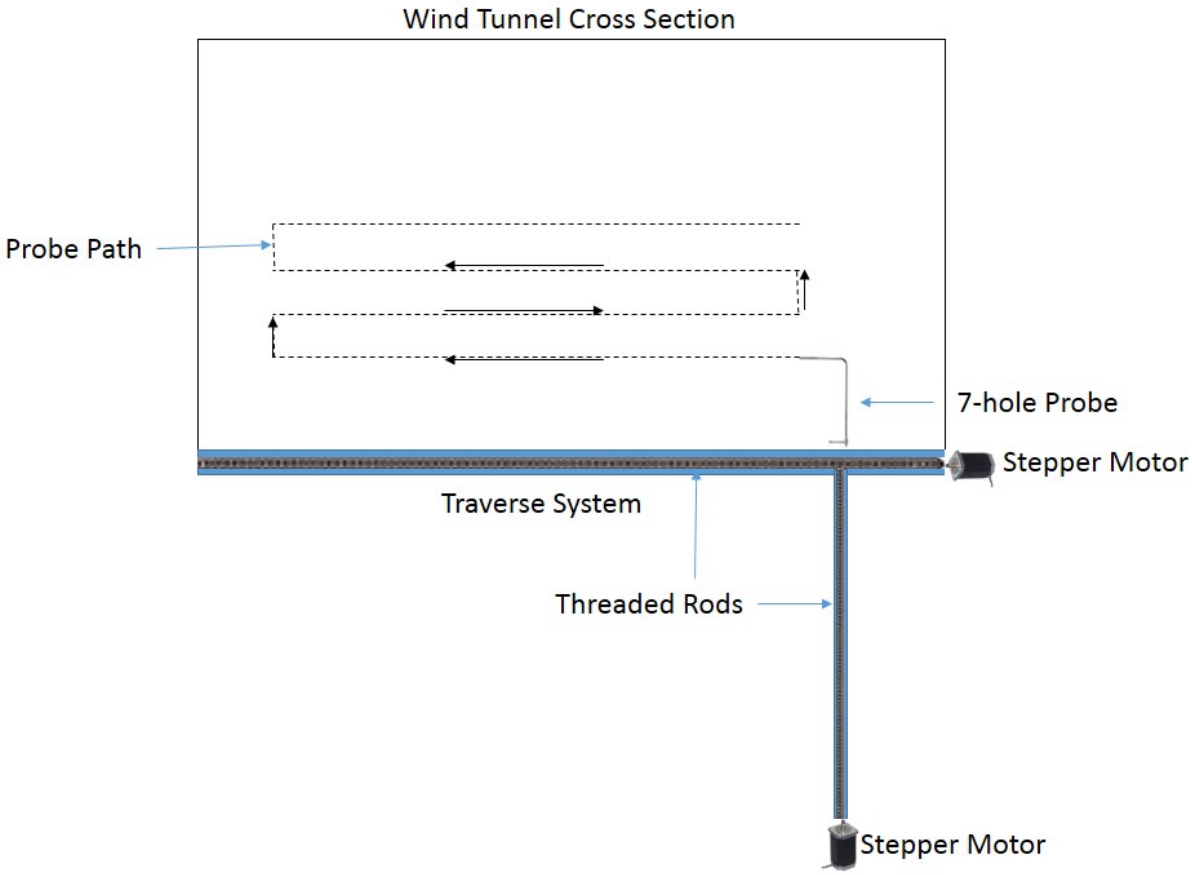

Figure 23 Schematic of traverse guided path.

As shown in Figure 23 the X stepper motor is the horizontally placed while the Y stepper motor is vertically placed. Control of the motors is discussed more in Section 3.4.2. The probe in the schematic is out of the page and it follows the dotted line path as shown. The arrows indicate the direction of the movement of the probe. Stepper motors are controlled in a way that they take a pause at designated intervals on the path so as to collect data. The data is collected using DSA Scanivalve for which a Labview interface is developed. Data collection and analysis is discussed further in section 3.4. Figure 24 shows the actual traverse system that replicates the schematic diagram which is attached under the

floor of the wind tunnel. The stepper motors are connected to the DRV 8825 drivers and the system is also connected to a few rods that help in stability of the probe holder so that it does not swing along the axis.

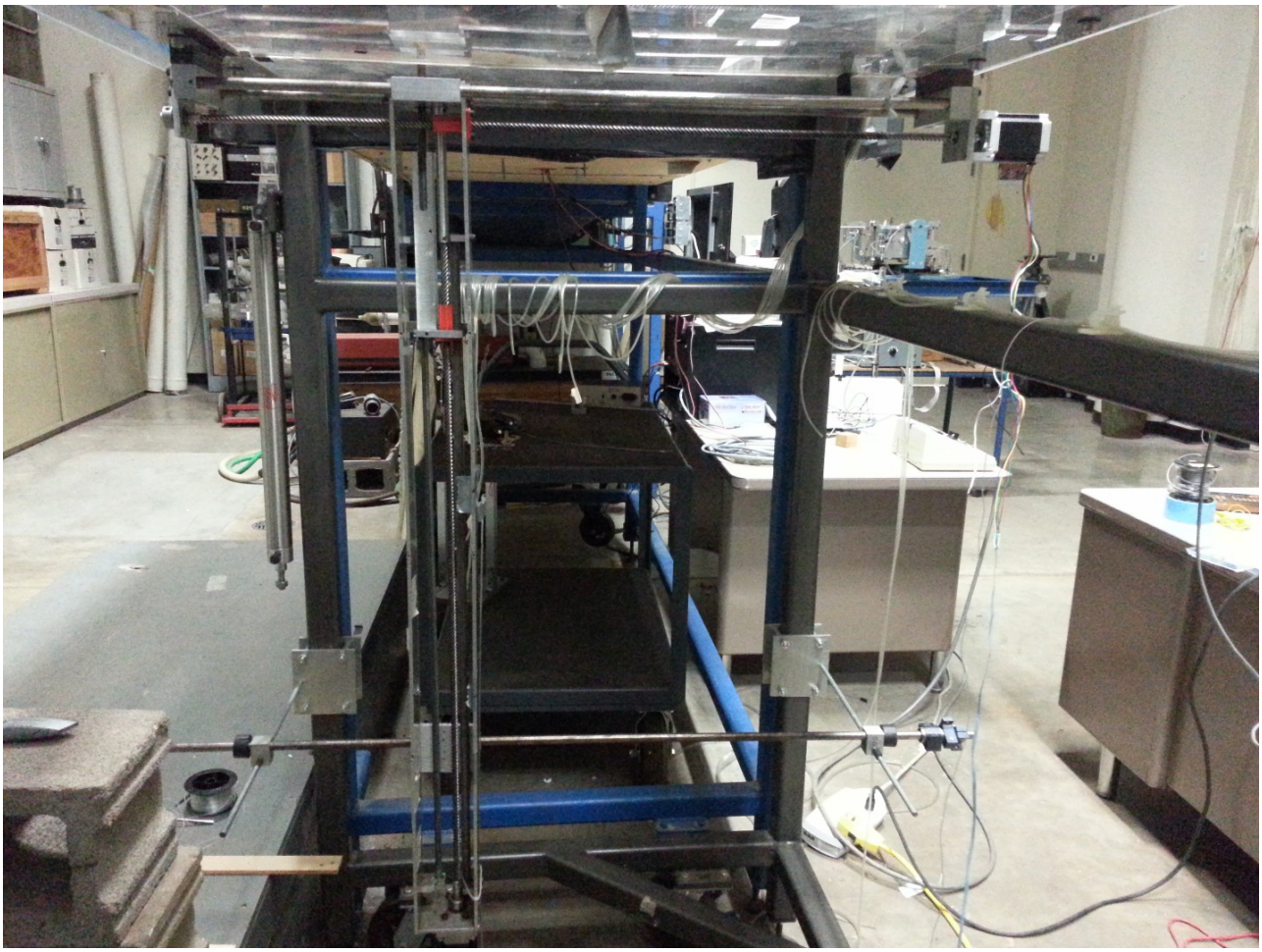

Figure 24 Traverse system.

3.4 Vortex generator tank data collection

The vortex tank is first set up by using side plates of desired separation distance and installed with the long filaments fit into it. The next step is to attach the motor couplings

and connect the motors to motor mounts. Once everything is set the stepper motor leads are connected according to A+ A- B+ B- to the DRV8825 control driver. The stepper motor control is used as discussed in section 3.2.2. The tank is then filled with water and seeded with particles that help to track the motion of the vortices. The method is discussed under Particle Image Velocimetry. The Lasers are focused at the center of the tank perpendicular to the length. The camera is focused at the laser sheet. The laptop used controls the camera using the MotionPro software which triggers the Laser pair. A time delay is to be set between the first and the second laser so as to capture pair of images that can be correlated while processing. The laser and camera are hence synchronized and is discussed in section 3.3.3. The following Figure 25 show the stepper motor control, the main ground control and the lasers used for collecting data.

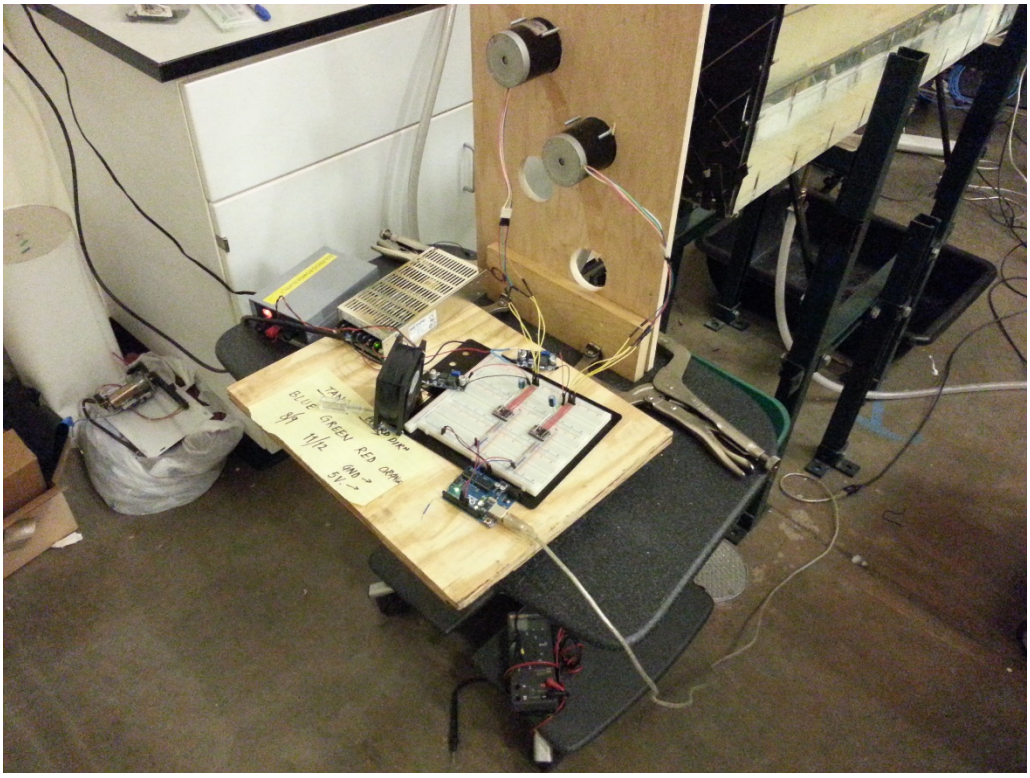

Figure 25 Stepper motor controller.

Figure 26 Ground Control for Experiments

As shown in the above Figure 26, the computer communicates with the IDT camera and activates the process of data collection. The camera communicates to the lasers through a timing box. The timing box is triggered once the camera is ready to start taking pictures. The camera is set to take pictures at the rate of 30 Hz using Motion Pro software. Each laser is triggered by the timing box at a delay time of 0.003 seconds. The exposure time of the camera is set so as to match the time delay at which lasers are triggered. Thus a pair of image is taken each time the two lasers are triggered. The camera is placed perpendicular to the laser sheet, i.e. the camera is focused through the side plates.

Figure 27 Laser setup for PIV.

The lasers are leveled at the same height as that of the tank so as to get a good sheet of laser focused onto it. The laser has 3 lenses in front of it to convert the beam into a nice sheet. There is a convex lens followed by a concave lens and a cylindrical lens. Each lens is adjusted in a way to get a vertical sheet of laser. The following Figure 28 shows the schematic of the entire setup.

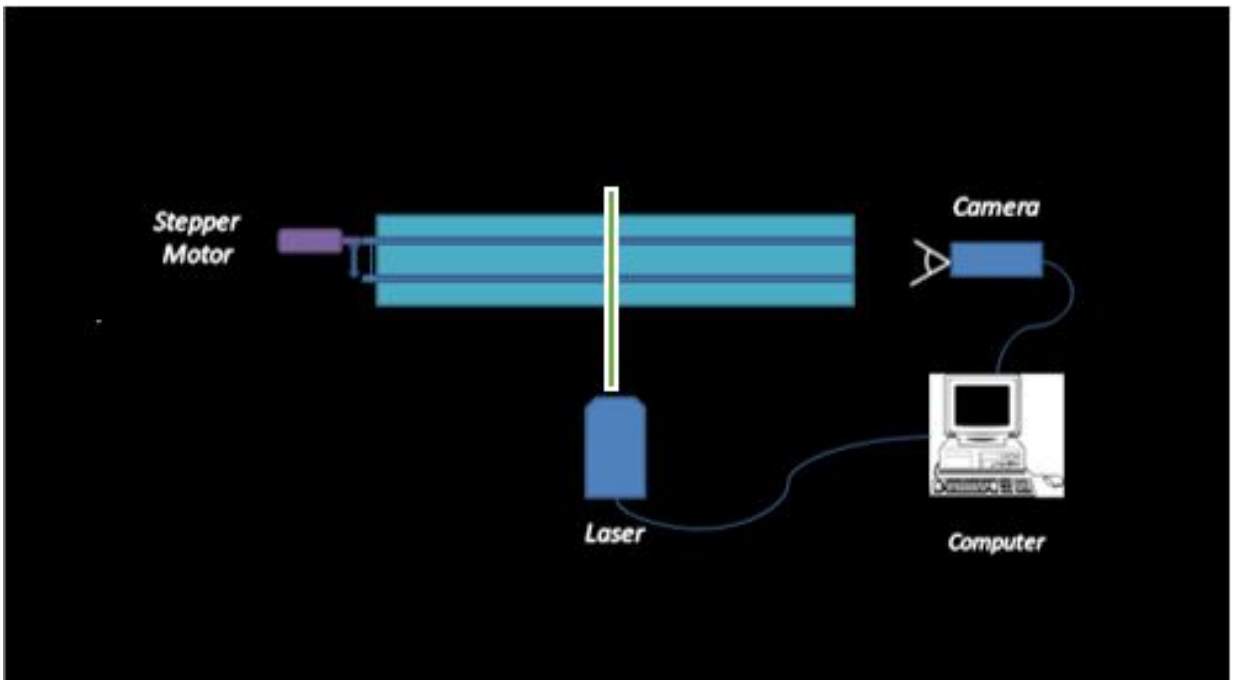

Figure 28 Vortex tank schematic.

3.4.1 Particle Image Velocimetry

PIV or particle image velocimetry is an optical method of flow visualization technique that has been used in this project for experiments with the vortex tank. The method is used to obtain instantaneous velocity measurements thus helping us with understanding circulation of the fluid caused by the motion of the filaments. The fluid is difficult to track hence to track the fluid motion the fluid is seeded with a tracer particle of 40μm size. The tracer particles are really small sized and hence are assumed to follow flow dynamics and have no weight effects of their own. The fluid is illuminated with the laser sheet so that the particles in the fluid are visible. The IDT camera is capable of taking pictures in pairs at the rate of 30Hz and takes images in pairs. The two images are correlated from the two time exposures. The spatial displacement that statistically

produces the maximum cross-correlation approximates the average displacement of the particles in the interrogated cell. The analyzed data can be used to plot velocity vectors and hence determine the motion of particles. An example of two images and its correlated plot is shown below.

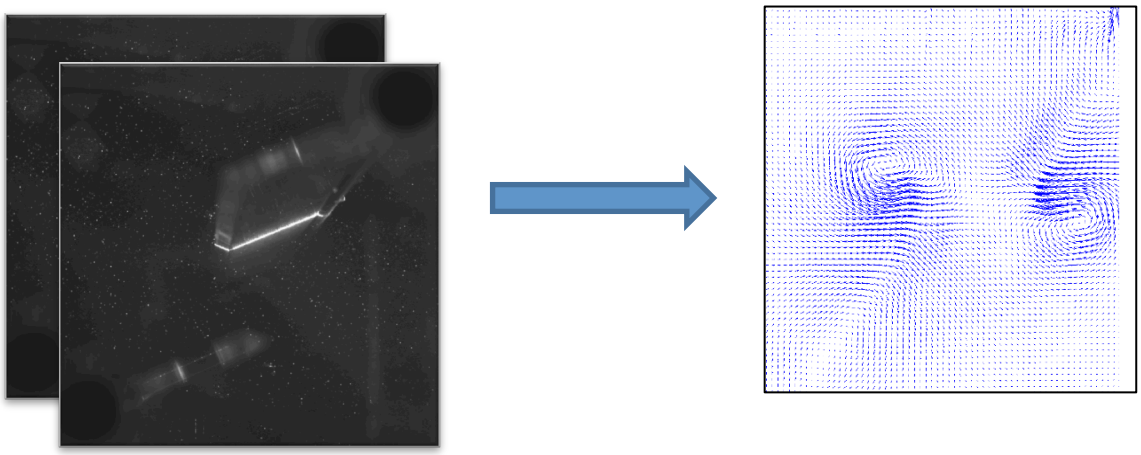

Figure 29 PIV images and processed data from 2 correlated images using MatLab.

3.4.2 Labview control for Vortex Tank

Labview is the main software for controls in this experiment. The stepper motors are commanded using this software to perform actions as required. At a step angle of 1.8 degrees it takes 50 steps to complete 1/4th of a revolution and 200 steps to complete a full revolution. As the stepper motor has enough torque to drive the filaments, we do get the same amount of revolutions with the filaments in place. The Labview code is shown below, the front panel of the Labview VI and also the block diagram.

The Front panel is where the control inputs are given for the filaments to perform. The number of steps is kept as constant as 50 steps while speeds are varied. 3 different speeds

are experimented i.e. 20, 30 and 40 steps per second which gives 6, 9 and 12 revolutions per min. Labview can be used to monitor the movement of stepper motors and help set the initial position of the filaments. The movement of the pedals or filaments is explained in the Figure 30 below.

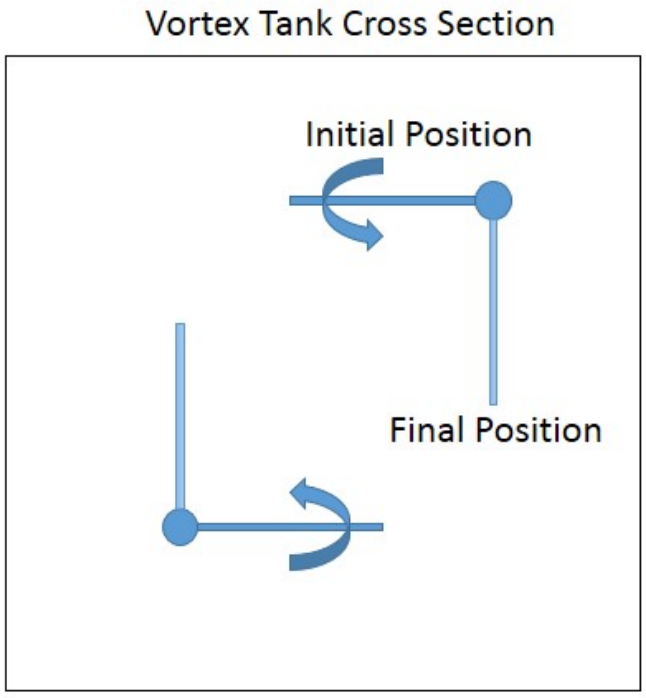

Figure 30 Cross-section and filament movement.

So the filaments can be controlled individually using the Labview front panel as shown below. The number of steps dictates the total movement and the speed decides on the time taken for filament to reach final position and the strength of the circulation. Hence symmetric vortices are produced when the speed is set equal on both the motors and asymmetric vortices are produced with different speed for the two motors.

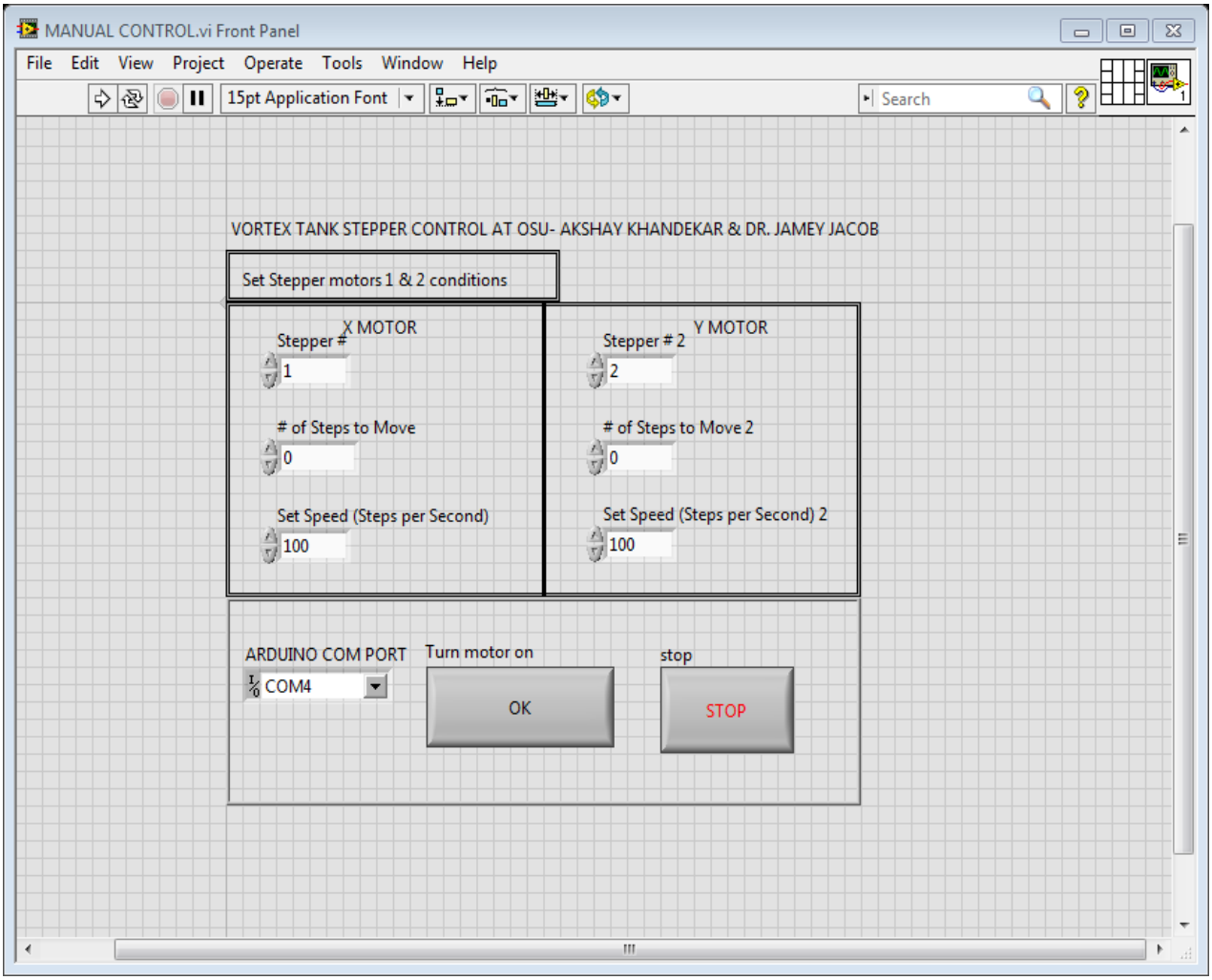

Figure 31 Front panel for the LabView vortex tank.

The Arduino com port is where you select the com port where the Arduino UNO board is connected. It has been observed that to stop the program it needs to be stopped using the VI stop button, in case the main Labview stop is used, the entire connection is lost and the Arduino and Labview needs to be restarted again and rebooted. The program behind the front panel runs inside of the block diagram which is shown in Figure 32.

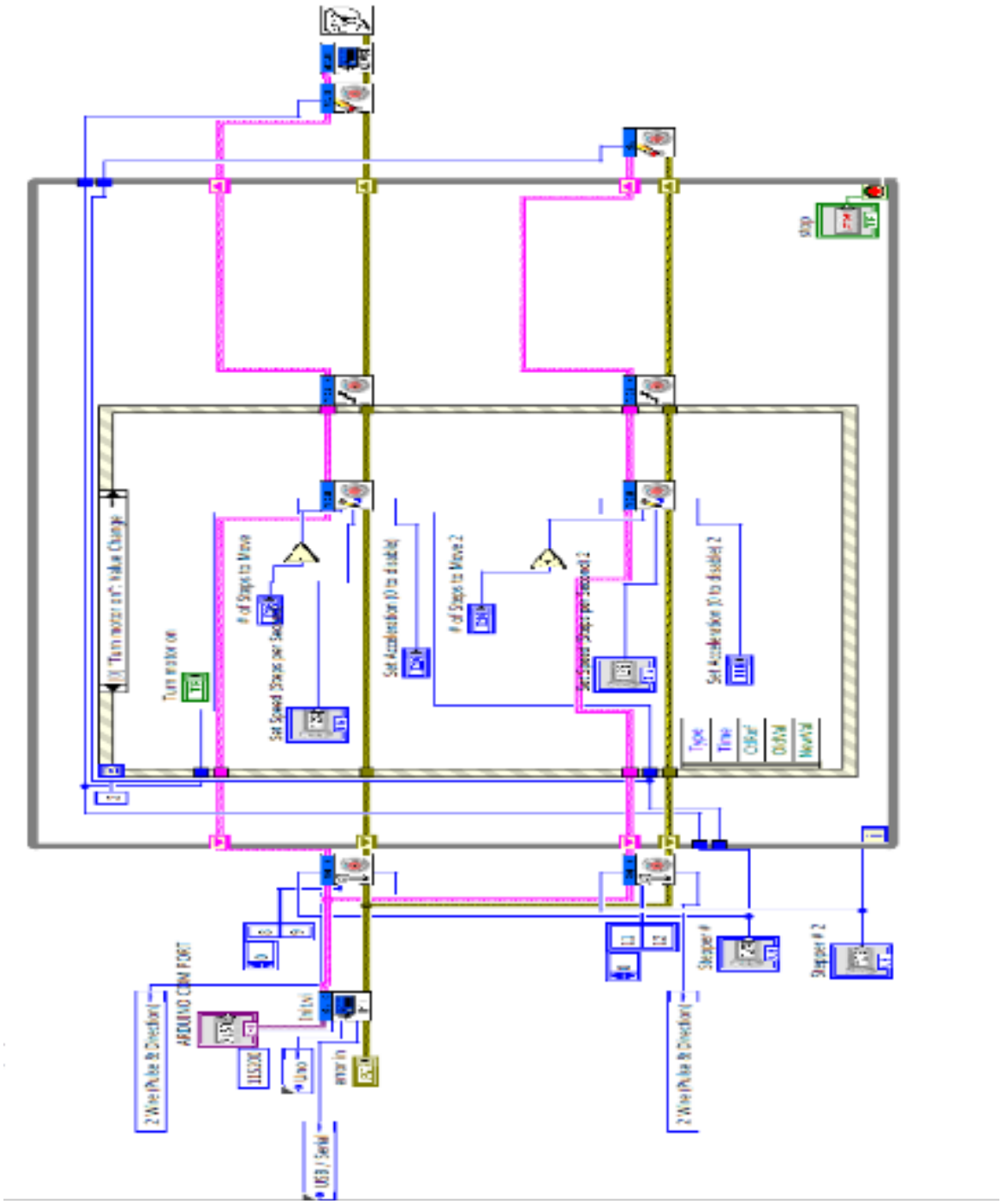

Figure 32 Block Diagram of Vortex tank Labview code

3.4.3 Laser and Camera synchronization

The laser and camera are the most important part of data acquisition in the PIV method. The laser provides a source of strong light sheet creating a 2D plane like a cross section and the camera takes the pictures, which when compared in pairs can be analyzed for movement of the fluid or the seeder particles. The laser used in this case is a Class IV Nd-YAg laser system. The max frequency of the laser is 15 Hz. Hence 2 lasers are used which are shot at a delay time which can be controlled by a timing box. Figure 27 shows the setup of the lasers in front of the camera. The camera used is X-Pro motion and has a minimum speed of 30 Hz to take pictures. The lasers have an individual speed of 15 Hz each and hence they are to be set at a delay time such that the lasers are shot when the picture is to be taken. The exposure time of the camera is set to be exactly like that of the delay time. The camera triggers the first laser via the timing box and then the timing box triggers the second laser at the given delay time. An oscilloscope can be used to check the signal of the camera, Laser1 and Laser2 so as to synchronize them accordingly. The signal coming from the camera is a square wave with a width of 30 Hz. The aperture of the camera opens at the side of the square wave and an image is taken that time. The signal of the lasers is to be synchronized with the sides of the square wave within the distance when the aperture is open. Thus Laser1 and Laser2 and connected to Channel 1 and Channel 2 respectively and the camera is connected to channel 3. The distance between the channel signals is measured and the delay time is calculated. The exposure time on the camera is then set equal to the delay time set. Figure 33 shows the signals on the oscilloscope that were to be synchronized.

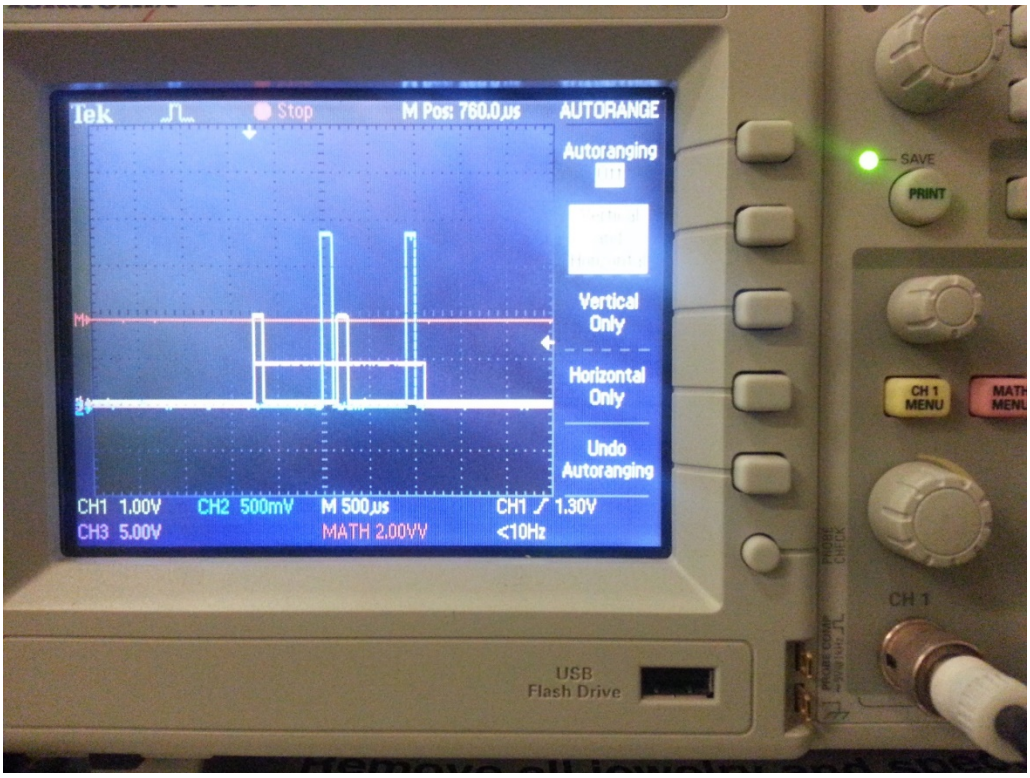

Figure 33 Laser and camera synchronization using oscilloscope.

Hence the pink square wave is that of the laser whereas the yellow and blue are those of the laser 1 and 2 respectively. The delay time is synchronized in a way that the laser 1 shoots at the start and laser 2 at the end. A delay time of 0.003 sec was used on the timing box and the exposure time was set as 0.002889 sec on the exposure of the camera.

3.4.4 Data Analysis

The data collected from the motion pro camera is saved on the hard disk of the computer as .tif files. These files are then exported to DPIV software where they are processed. DPIV is a digital particle image velocimetry software, which takes in two images and performs image processing so as to correlate them and track movement of particles. Number of iterations can be set as correlation parameters. Increasing the number of iterations gives better results thus increasing the resolution of the processed image. The output is the magnitude and direction of particle stored as vectors. These vectors are exported to a folder as batch files or data files or csv (comma separated values) files. The Figure 34 below shows how DPIV software correlates images to show vectors.

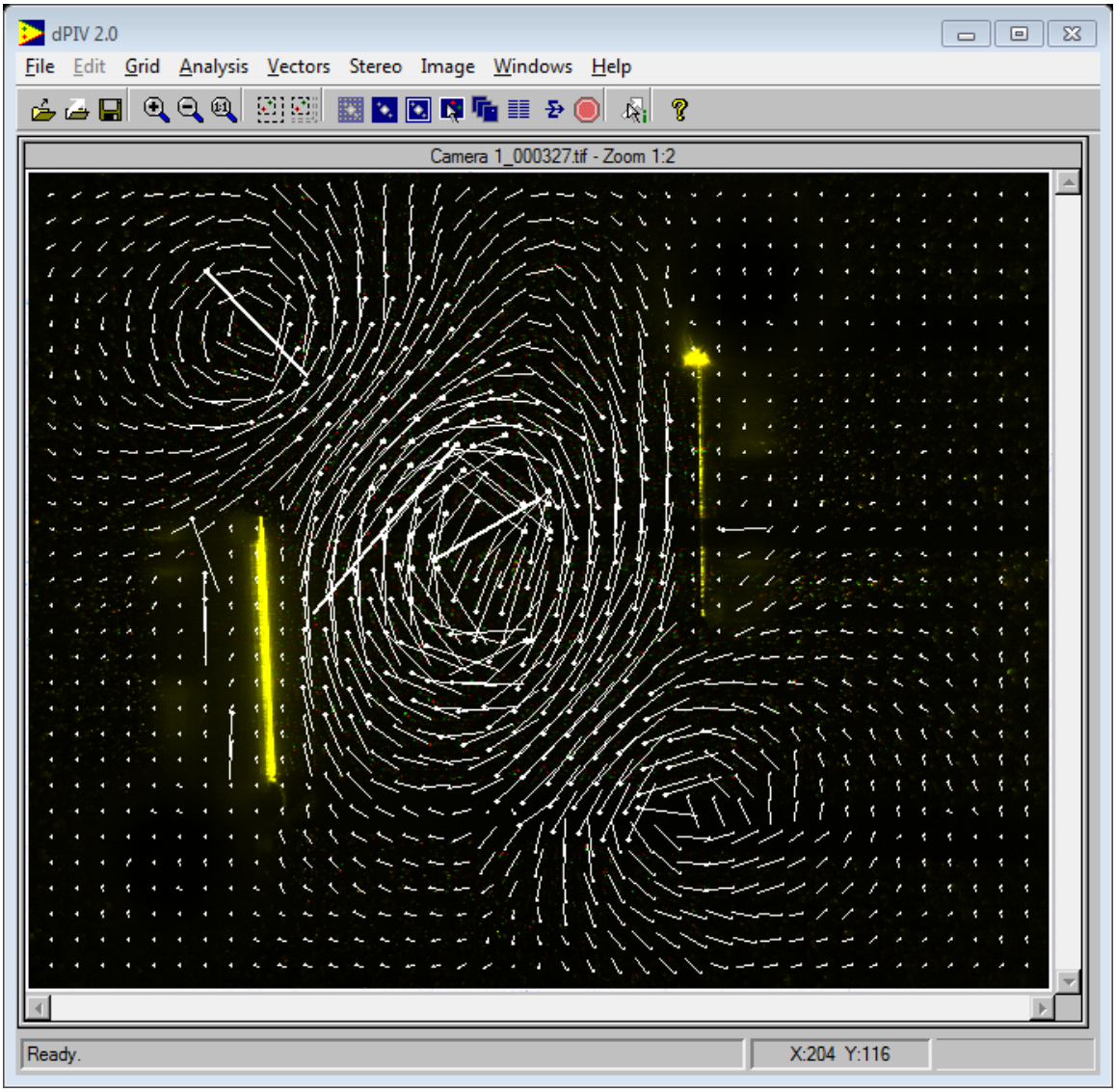

Figure 34 DPIV image correlations and vector plot

These data files can be imported to MatLab and processed to give vector plots and vorticity plots. The MatLab code used for processing of the data is provided in the Appendix. Vortices are tracked using the tracking method of MatLab to determine the paths of the vortex centers and hence number of orbits can be calculated. The vortex centers after being tracked can be used to plot their path along the centerline of the line

joining the centers of the pair when it was first generated. After vorticity is being calculated, we can find the total strength of the circulation using vorticity given by the following equation.

$$\Gamma = \oint_S \omega * dA = \int V * dl$$

Energy of the circulation needs to be conserved and hence it has been observed the the strengths of the merged vortex is approximately equal to the sum of the co-rotating vortex pair.

$$\Gamma_{total} = \Gamma_1 + \Gamma_2$$

The Reynolds number of the circulation caused by each filament can be calculated by

$$Re_\Gamma = \frac{\Gamma}{\vartheta}$$

Where ϑ the kinematic viscosity of water, as water is the working fluid and is 0.01cm/s^2.

All the data been collected is in terms of pixels that the camera has recorded. The camera captured images of size 1280 x 1024 pixels. Thus there is a need to scale it down in terms of actual lengths in order to analyze the data. First we need to calculate the scale for which the number of pixels are counter for an actual length in real setup. Hence scale can be given by:

$$scale = \frac{pixels\ between\ two\ points\ in\ an\ image}{actual\ distance\ between\ those\ two\ points}$$

Hence using this scale we can scale down the positions x and y and velocities u and v. This helps us to get positions and locations in terms of cm. We know that after the 2nd

iteration on the DPIV software it gives out 39 vectors in x direction and 31 vectors in y direction. These number of vectors can be specified as nxc and nyc. For calculating vorticity using velocity, we need to know the actual distance between the two vectors which can be calculated by:

$$dx = \frac{nxc}{scale * nx}$$

Scaling is very important for calculation of vorticity and eventually circulation as an integral of vorticity over a selected area. Without scaling all numbers exported from DPIV data files are in units of pixels which have no real time value in real world applications.

3.5 Wind tunnel data collection

The wind tunnel experiments are conducted as for the 3D aspect of the vortex merger in this project. A pair of NACA 0012 wings are used at opposite angle of attack (AoA) and separated by a distance are placed in the wind tunnel. A schematic of the entire experiment setup is as follows:

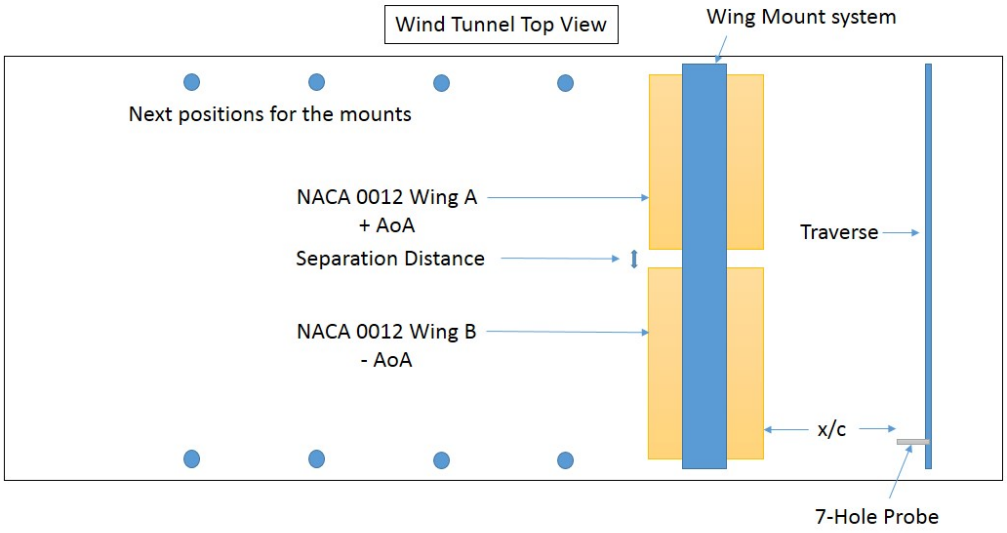

Figure 35 Wind Tunnel experiment setup schematic

The above Figure 35 is the top view section of the wind tunnel setup. The data is collected by the probe in the wake of the wings. The 7-hole probe moves along the traverse line in the X-direction and out of the page in the Y-direction and is guided by the traverse as discussed in the section 3.2.2 For taking data behind in the wake either the wings needed to move ahead upstream of the probe needed to be moved away. As the traverse system was fixed at one point on the wind tunnel, there would have been a need to use a really long rod as a probe holder. Having something really long in a flow would have caused a lot of bending and vibrations while moving in X and Y directions. That would have in turn ruined a lot of data as pressure would have changed. Hence it was decided on moving the wings upstream of the probe. For that a small setup was made in order to hold the wings inside of the tunnel without making changes on the tunnel wall. The following Figure 36 shows the plates.

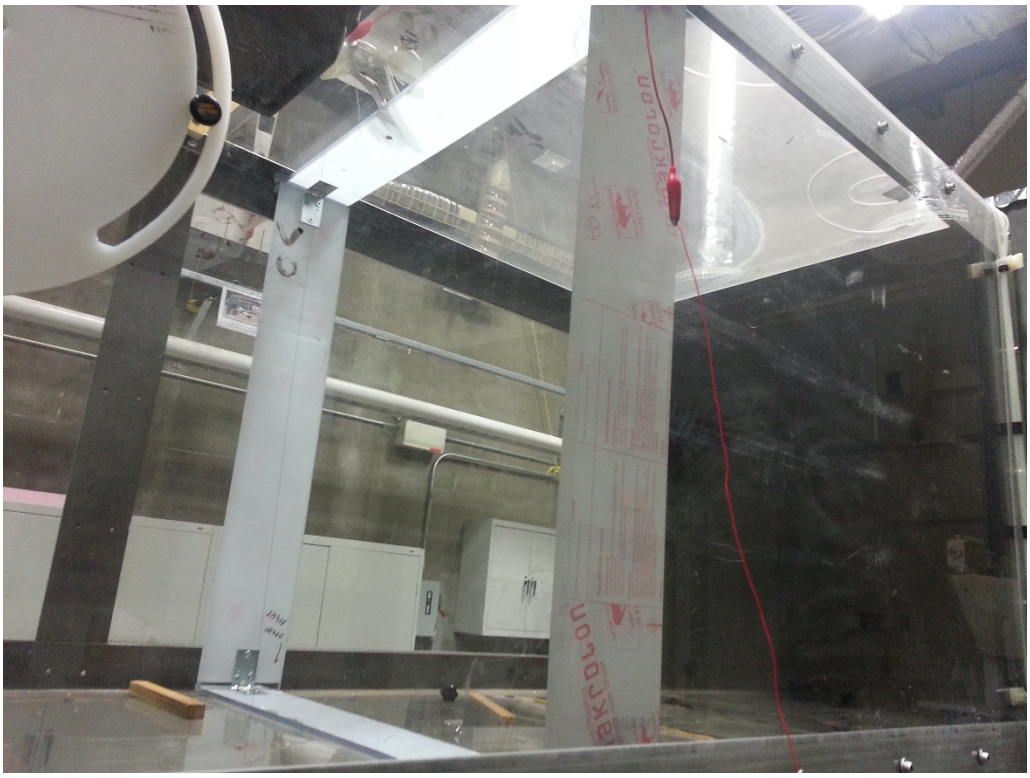

Figure 36 Portable wing mounts for wind tunnel

The portable wing plates help us move the wings upstream so that data can be collected at different x/c (distance/chord) length behind the wings. The bottom plate is bolted on the floor of the wind tunnel at locations which ate 8 inches apart. The chord of the wings is also 8 inch which helps us to get a consistent multiple of the x/c ratio. The side plates are connected to the top and bottom plates using L-brackets and ¼" countersunk bolts. The top plate is pressure fit to the ceiling of the wind tunnel, which makes the entire structure very rigid and eliminates vibrations and bending of the plates. The side plates were cut at angles of 45 degrees on the leading edge and two cuts were made on the trailing edge. The Figure 37 shows the top view section of the places and the wings were placed in

between the two plates. These cuts helped to reduce the effects of boundary layer formed because of the plates on the wing. Having an angled cut on the leading edge would help in having the flow divert towards the wall instead of having it flow inward on the wings. Reducing the boundary effects helps in getting good results as compared to having the boundary effects.

Figure 37 Top view of plates to reduce boundary layer effects on wings

3.5.1 DSA Scanivalve

The 7-hole probe is connected to a pressure scanned or transducer to collect the pressure. The DSA 3217 is a Scanivalve product that is a pressure transducer which is calibrated and reads pressure in user defined units. The units used in the project is psi. The DSA 3200 series of pressure transducer is a multi-point electronic pressure scanner with 16 ports to measure pressure and temperature data. It has pressure sensors with pneumatic calibration valves, RAM, 16 bit A/D converter and a microprocessor all fit in one compact unit. The DSA3217 can be communicated with either RS232 terminal or has an

easier way using the Ethernet cable. The microprocessor compensates for pressure changes and also helps in unit conversion as and when needed. The unit has an accuracy of ±0.5% and a tremendous sampling rate of 500Hz per channel. The range of the sensors are 10 inch H2O which is 0.336psi and is sufficient for the experimental data collection for the scope of this project.

Figure 38 DSA 3217

The DSA 3217 can be communicated using the Ethernet and a software that comes from Scanivalve company called Scantel, but having to manually use Scantel to collect data while running the probe on the traverse would not have worked out properly. Hence there

was a need to create a Labview VI for the Scanivalve which could be integrated with the Labview module of the traverse system. As Ethernet port was a possible way of communication the DSA3217 was established on the Labview as a VISA source. A new connection was made using the MAX i.e. measurement and automation explorer. The IP address can be set up of the DSA3217 and a sub VI was created. The pressure scanner needs to be established a connection with the computer using HyperTerminal. It helps create a secured TCP/IP connection with the device by selecting the host IP address and device IP address. The front panel of the Scanivalve VI is shown in Figure 39, where the inputs are Average samples to be collected and averaged, period for the sampling rate and gives an output of 16 pressure points as an array.

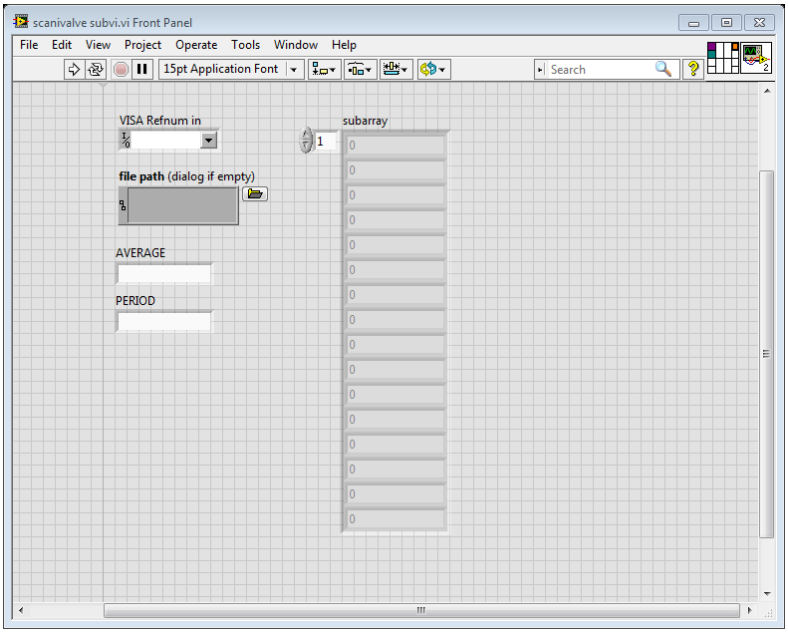

Figure 39 Scanivalve VI

The program that goes behind this is shown in the block diagram below.

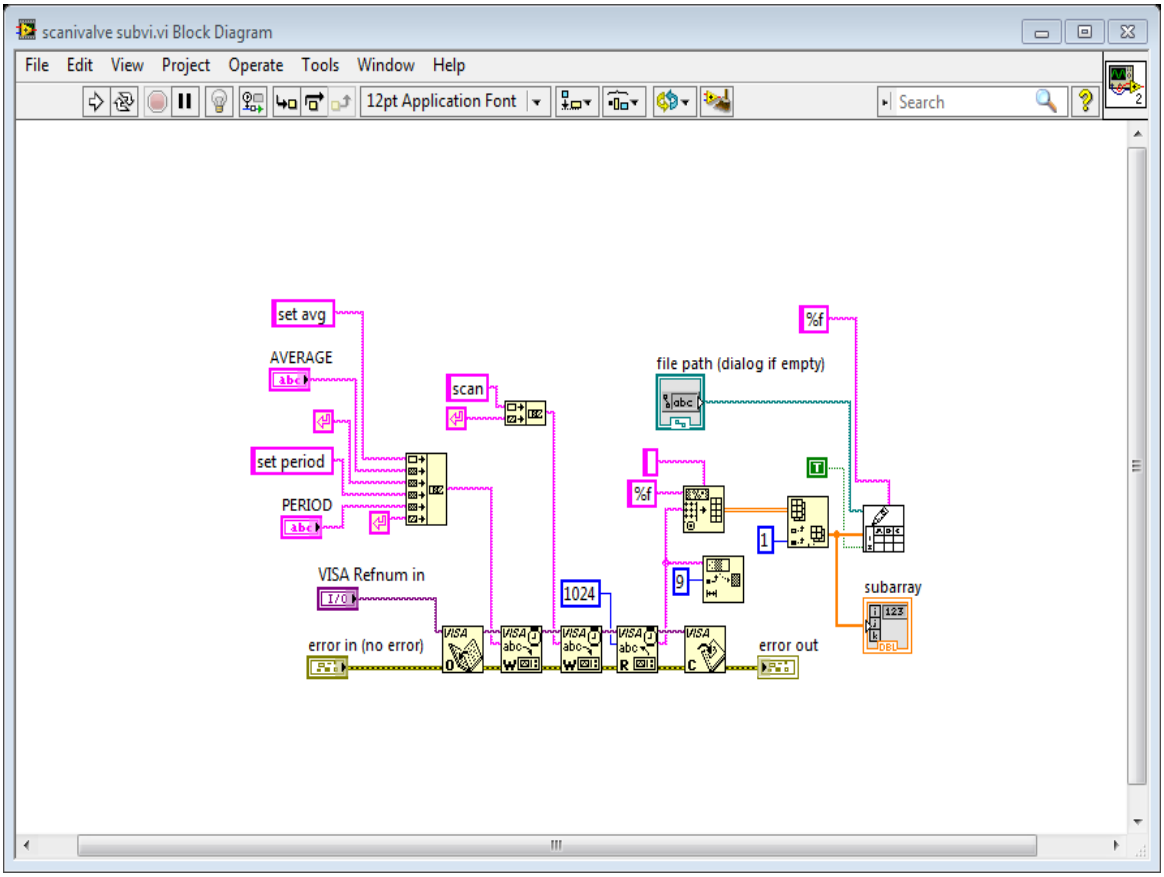

Figure 40 Scanivalve VI block diagram

Selecting different values for the average and period helps set used defined sampling rate. Having a high average number reduces the sampling rate but gives precise values of pressure. For this project the traverse stops the 7-hole probe at intervals where the probe is to collect just one pressure value. Hence for increasing the accuracy of the data, the

average used is around 100 while only one data point is collected at that interval. This data is then undergone through the processing and results are analyzed.

3.5.2 Labview control for Traverse

Labview was the driving software for running the traverse and collecting data for the 7-hole probe. Section 3.2.2 explains more about the working of the traverse. The Labview front panel for the traverse is as below.

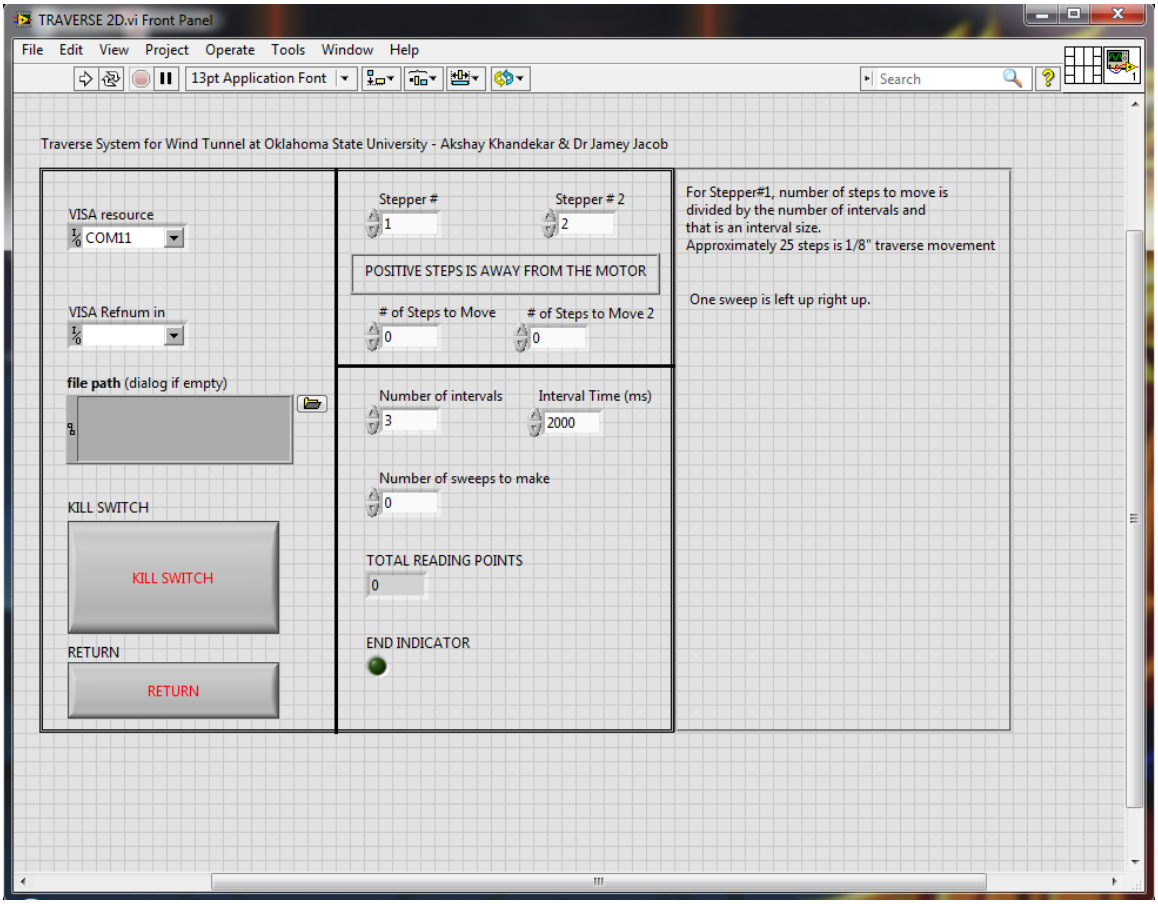

Figure 41 Front panel for traverse VI

The block diagram is shown in the Figure 42 below.

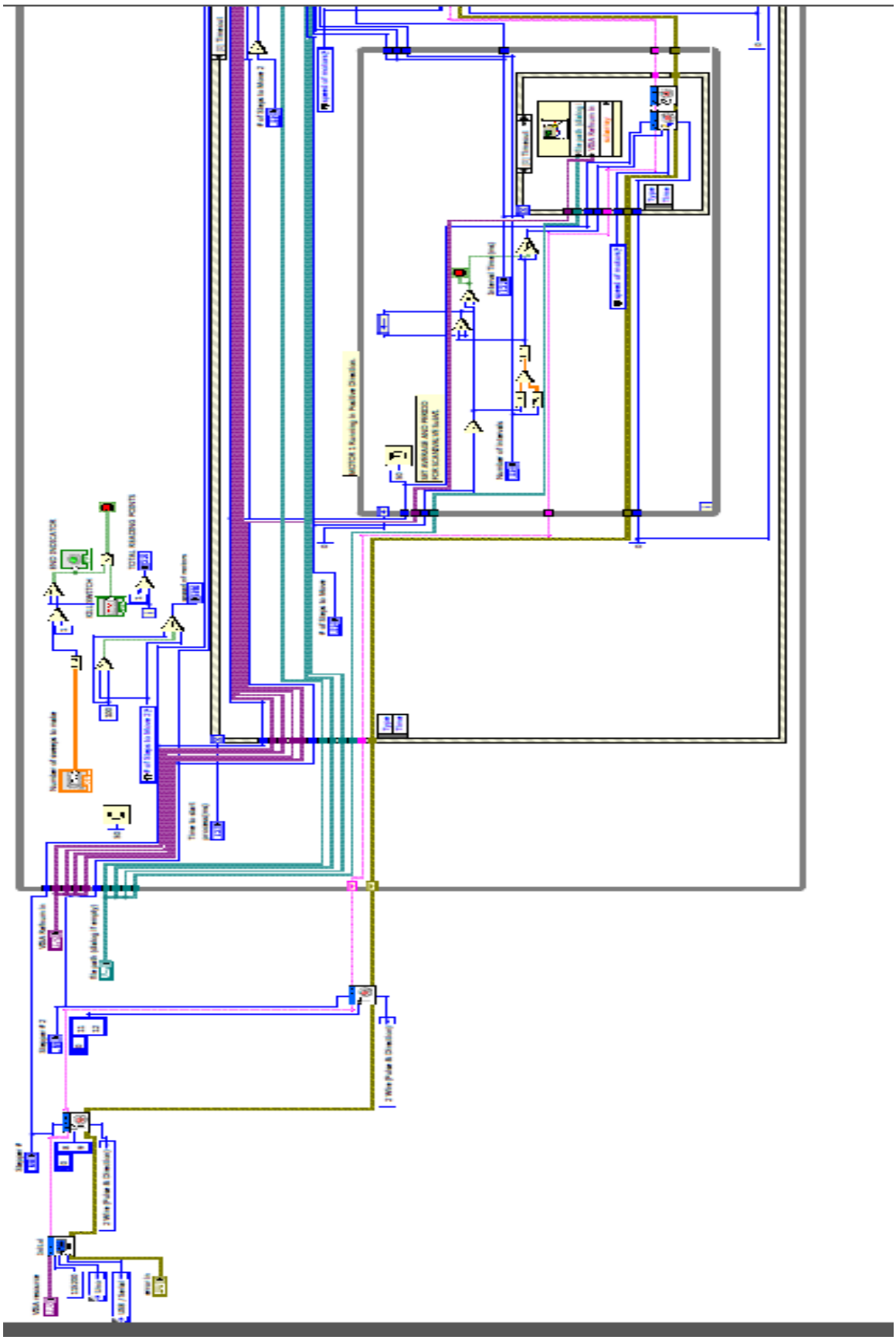

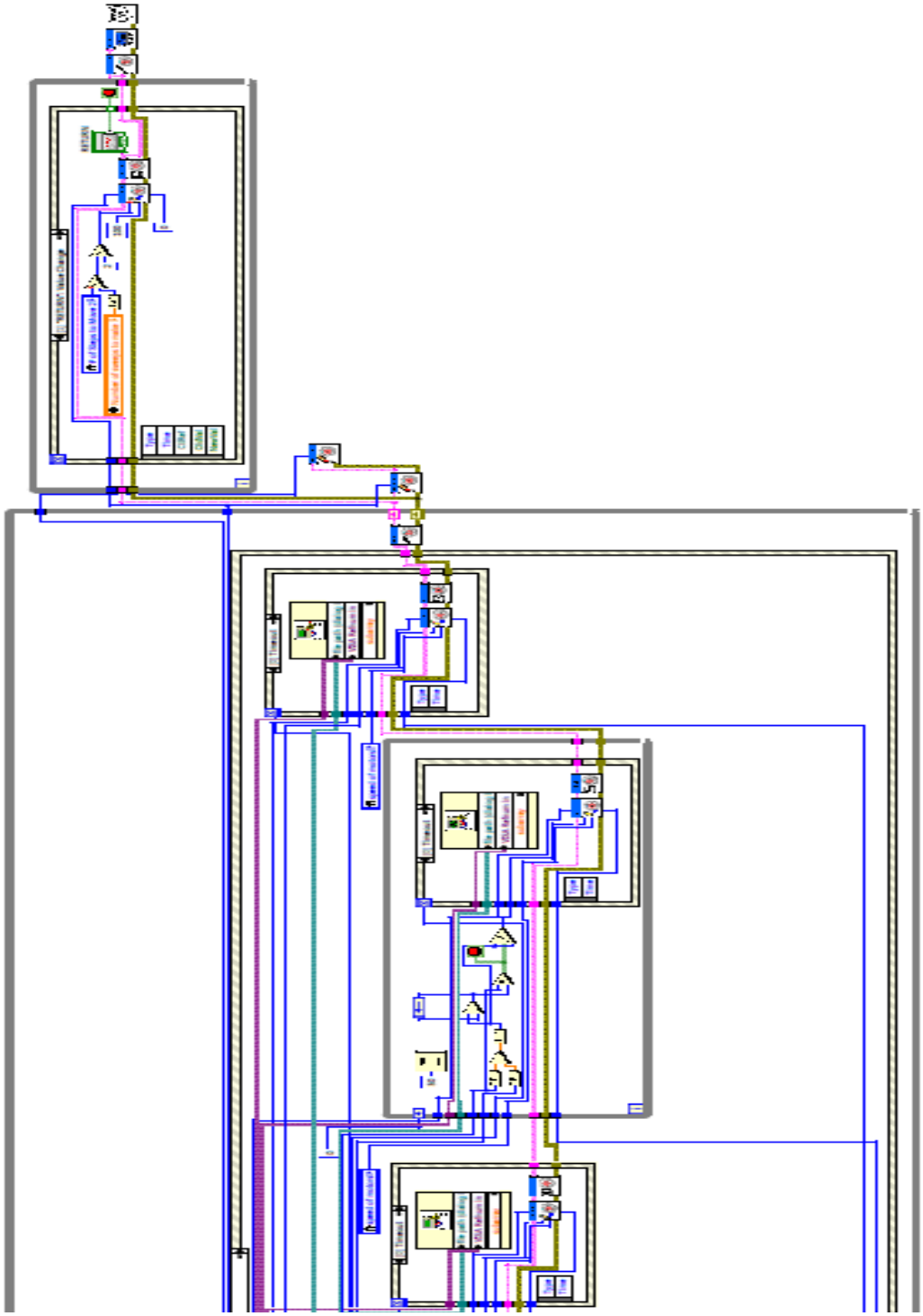

Figure 42 Block Diagram for Traverse system

The Labview front panel is where the COM port for the Arduino is selected. For both the motors the number of steps are selected. For motor 1 or the X direction motor, the number of steps is divided by number of intervals or data points to be collected gives the distances between two data points. This distance between two intervals on the X-axis is selected as the distance on the Y-axis so as to keep uniformity between the data collected and help the gird of data collection to be consistent. Movement of the probe is explained in section 3.2.2. At each interval point the Scanivalve is run to collect pressure values using the 7-hole probe. Once the number of sweeps to cover is completed, the return button helps the traverse go back to the initial position where it started from. In case of emergency when the traverse has vibrational problems or is moving in an undesired direction a kill switch has been initialized. Once the kill switch is pressed the entire Labview program quits and the traverse stops instantaneously. Thus data is collected accordingly and processed using MatLab.

CHAPTER IV

RESULTS

4.1 Velocity and Vorticity Plots

The dynamics of vortex merger are studied for co-rotating symmetric and asymmetric vortices generated in a vortex tank. Different cases are studied primarily based on initial spacing between the filaments generating the co-rotating vortex pair. The distance was set to be 0.75" and 1". Strength of a vortex i.e. circulation (Γ) is directly proportional on the rotational speed of the filament. Three speeds are considered in this project, 6rpm, 9rpm and 12rpm. Therefore we get 6 cases to study for each initial spacing and a total of 12 data cases. This data is then secondarily based on the location of the laser sheet, to study the wall effects of the tank on the vortex formation and merger. Hence the laser sheet is focused in the center of the tank i.e. half distance, one quarter close to a wall i.e. $1/4^{th}$ distance and very close to the wall i.e. approximately at the wall. Thus we have a total of 36 data cases to study and observe the vortex merger.

After processing of data from MatLab, the velocity plots can be obtained as follows:

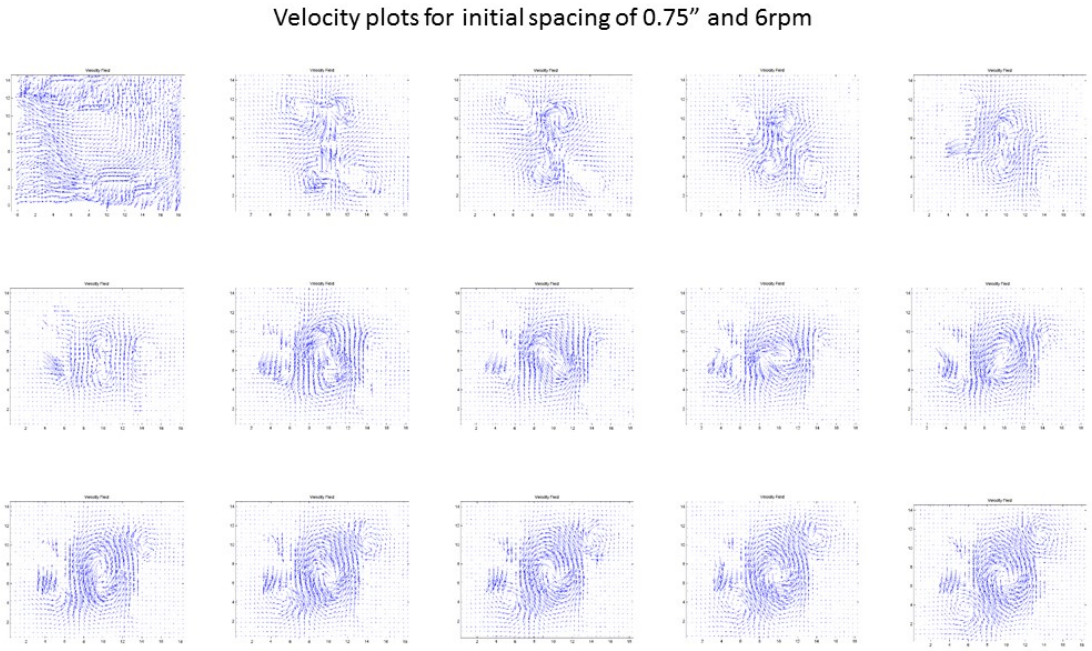

Figure 43 Velocity Plots for 0.75" spacing and 6rpm symmetric vortex pair

The above plots are images processed from the batch files imported from the DPIV data. Images are captured at a sampling rate of 30 Hz and each pair of images are processed together for correlation. Therefore after plotting the velocities we have data at the rate of 15Hz. above images are at a time interval of 1/2 second each. As you can see the circulation is counterclockwise for the co-rotating pair. Hence the pair revolves around the axis perpendicular to the plane of the vortex and in clockwise action.

Vorticity can be calculated at a specific location based of u and v velocities at the adjacent locations. Thus after an iterative process of the vectors used for velocity plots, a contour plot of the vorticity can be shows as below.

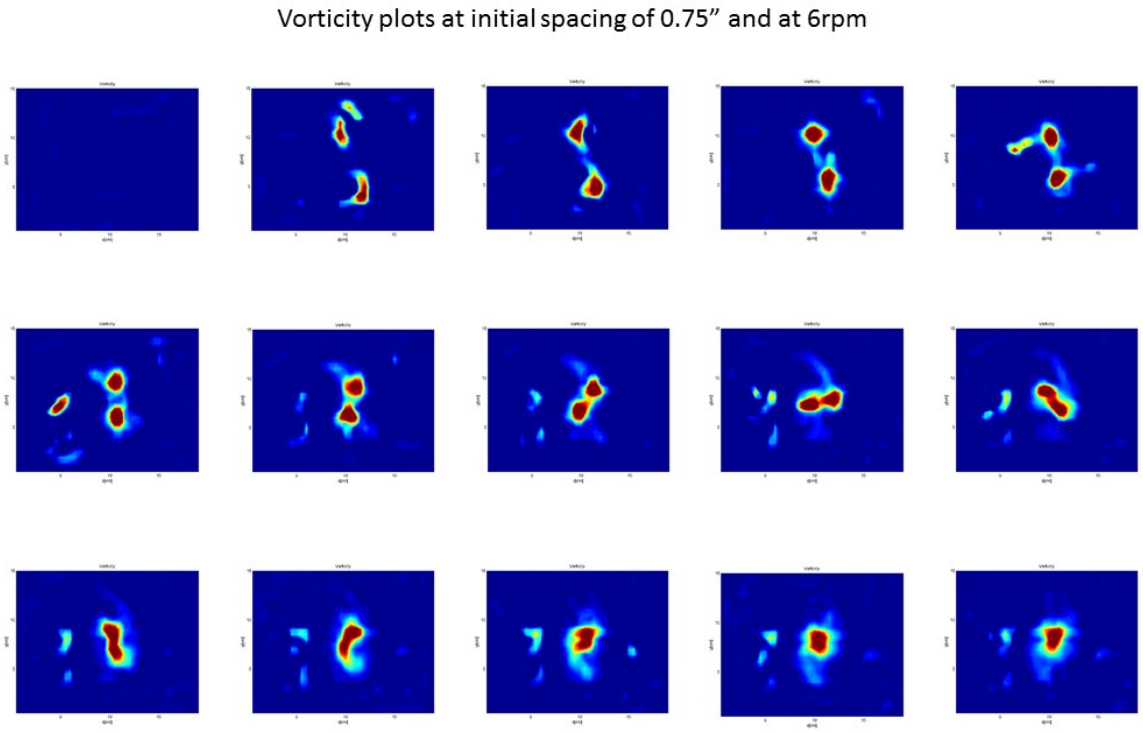

Figure 44 Vorticity plots for 0.75” spacing at 6rpm symmetric vortex pair

4.2 Circulation via Velocity and Vorticity

Circulation is calculated from velocity and vorticity at a specific location by selecting a point on the vorticity plot. Using equation for calculation circulation (Γ) from the adjacent velocity and vorticity values a box of desired area is drawn. Points are selected

for each image and the calculated circulation is then plotted with time. The Figure 45 below shows how a box is selected for calculating circulation at a chosen point.

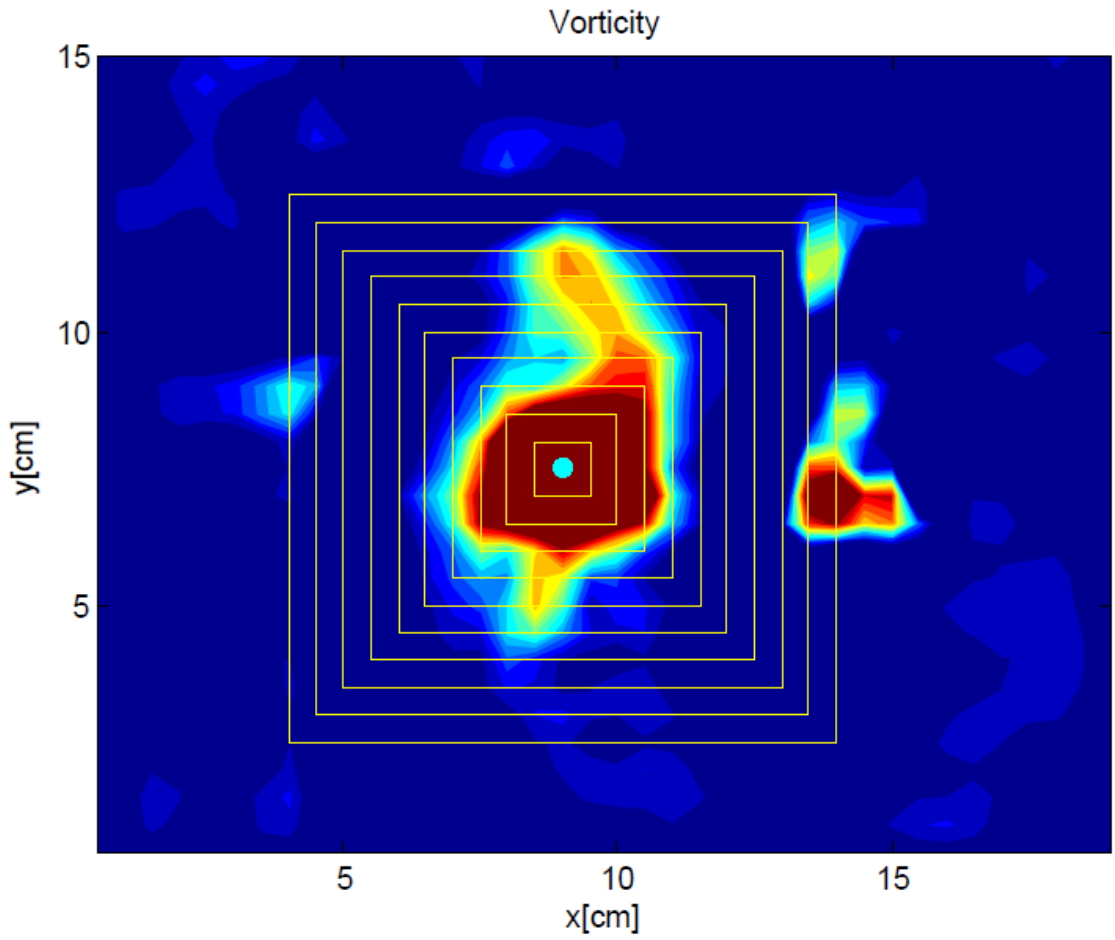

Figure 45 Circulation at a selected location

Selection of such individual points for each image is time consuming and also an inefficient method. Such manual point selections can miss out the important location where the circulation at that time frame could be maximum. Hence the need of scanning

of the image to calculate for maximum circulation was a must and was obtained. The following Figure 46 shows the auto selection of maximum circulation.

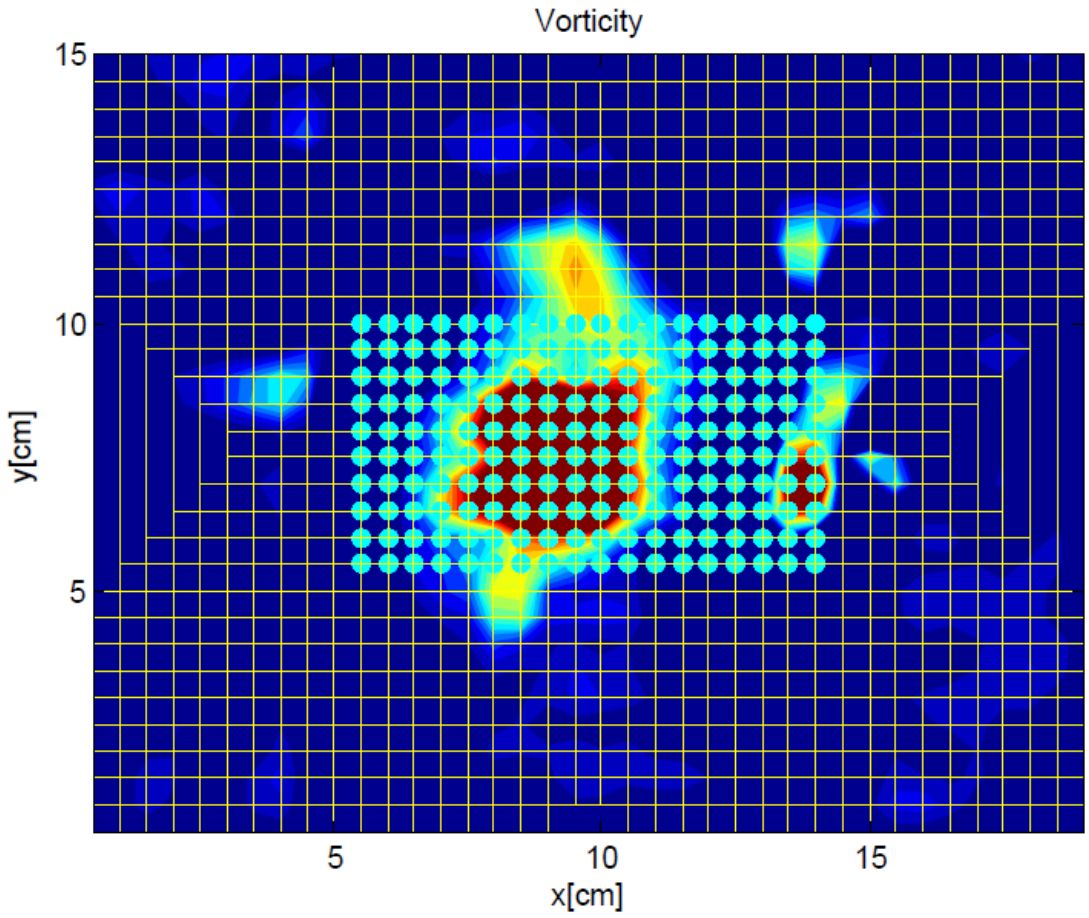

Figure 46 Maximum circulation scan from vorticity

The multiple dots are the points where circulation was calculated and the maximum circulation value was saved. As vorticity is derived from velocity, as a result the circulation from vorticity is under predicted as compared to the one from velocity. Hence

for further study and comparisons circulation from vorticity is used in all cases. The Figure 47 below shows the comparison of circulation calculated from vorticity in red and from velocity in blue. Maximum circulation from the point scan was selected and plotted for each image, hence we get circulation over a period of time for which the data was collected.

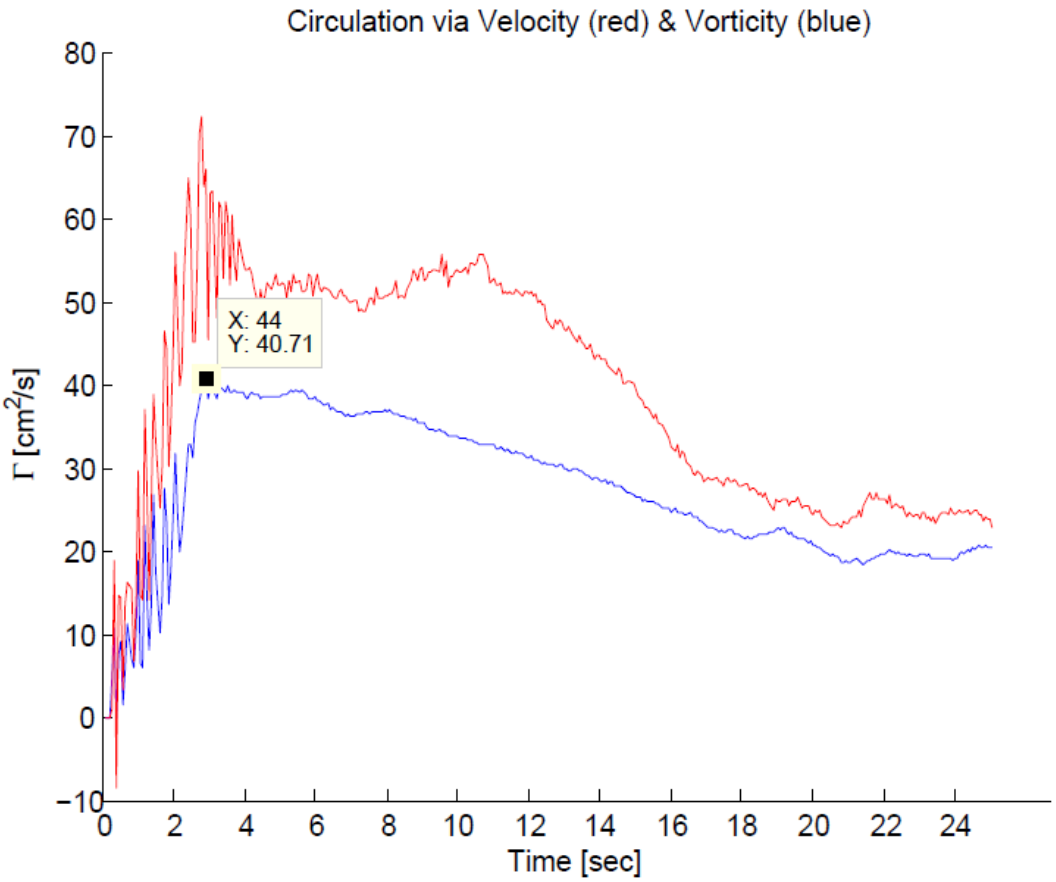

Figure 47 Circulation from velocity and vorticity for 0.75" separation at centerline

Circulation from vorticity is calculated and recorded for each of the case. The different cases vary from initial spacing between the vortex pair and different speed of the pedals to generate the vortices and the location of the vortex pair in the vortex generator tank.

That gives a total of 36 case studies. Circulation is plotted against time for separation distance of 0.75" and at centerline. Different pedal speeds give symmetric and asymmetric vortices, which are plotted against time and compared.

The images are processed using DPIV software where a pair of image is considered to know the movement of the particles. The processed image has a grid of velocity vectors that are stored as a data batch file. For better resolution of data, we can increase the number of vectors. A normal 2 iterative process gives a vector grid of 39x31 for an image of 1280x1024 pixels. Increasing the resolution of processing we can get 79x63 vector grid on an image of 1280x1024 pixels. That's doubling the resolution which improves the data trend. But the time consumed for 2 iterations i.e. the lower resolution in this case is 6 hours per case study, whereas for higher resolution of 3 iterations it takes around 10 hours per case study. As the maximum value of each run is to be considered, a comparison between lower and higher resolution is done in order to see if the maximum value is different.

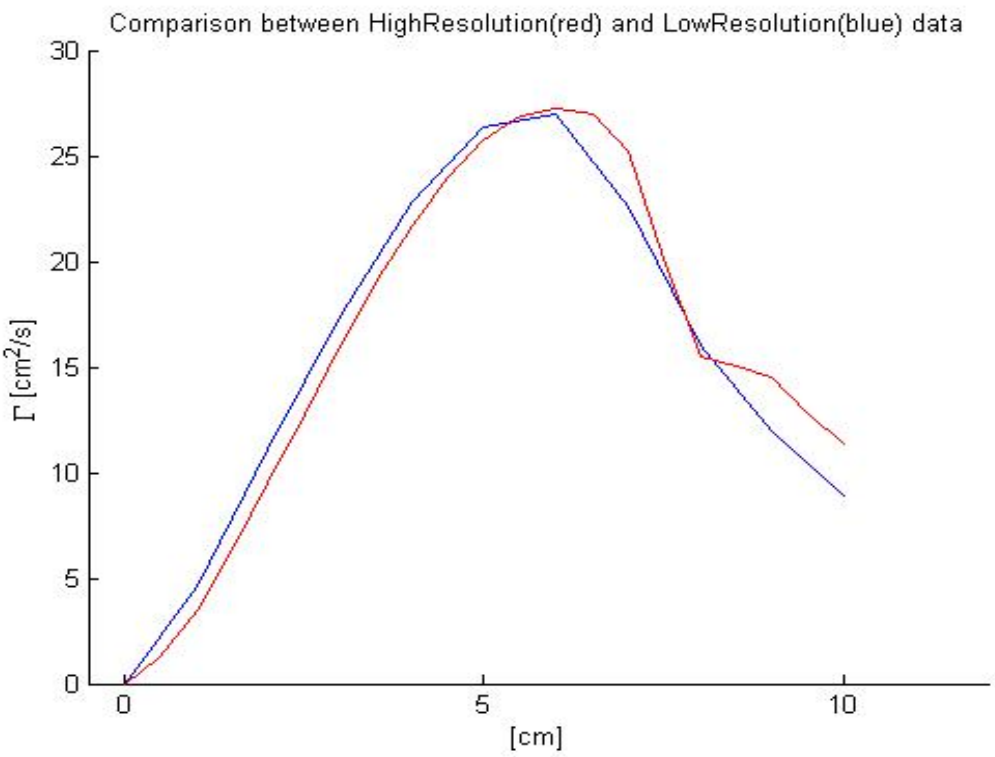

Figure 48 Comparison of high and low resolution circulation calculation

In the Figure 48 above, we observe that increasing the resolution does give better and smooth curve, but as only the maximum value is to be considered they both show the same max value. Hence, an increment in resolution is not necessary and we can avoid the penalty on time. The comparison gives a good check that both low and high resolution follow a similar trend.

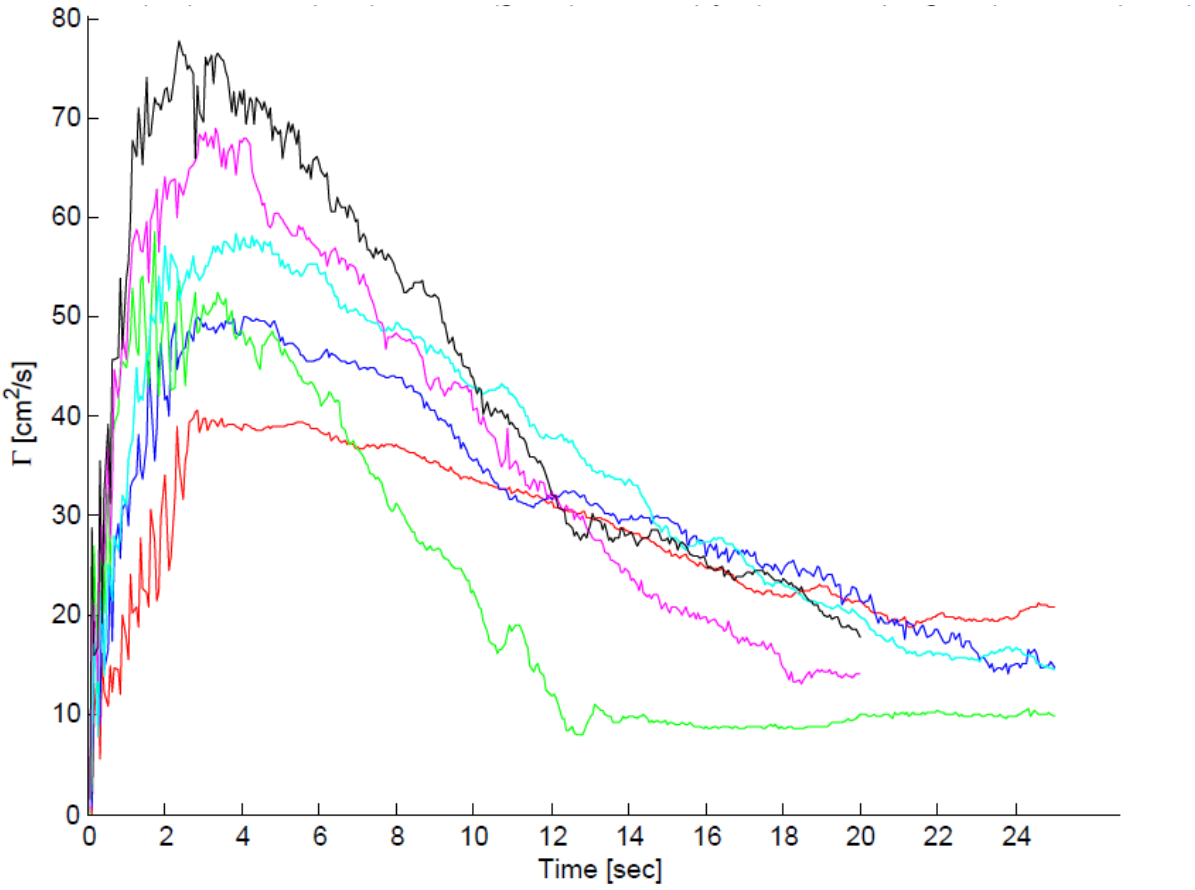

Figure 49 Circulation vs time for 0.75" separation at centerline

The above Figure 49 shows circulation (Γ) against time. Different pedal speeds create vortices of different strengths. In the above Figure 49, we have 6 different cases with varying pedal speeds. Test001 (red) is with both pedals at 6rpm, Test002 (blue) is with pedal 1 at 6rpm and pedal 2 at 9rpm, Test003 (green) is with pedal 1 at 6rpm and pedal 2 at 12rpm, Test004 (cyan) is with pedal 1 at 9rpm and pedal 2 at 9rpm, Test005 (magenta) is with pedal 1 at 9rpm and pedal 2 at 12 rpm and Test006 (black) with pedal 1 at 12rpm and pedal 2 at 12rpm. As strength of circulation increases with higher pedal speed, we observe that total circulation (Γ) also increases from Test001 to Test006. Test001, 004 and 006 are symmetric vortex pair merger while 002, 003 and 005 are asymmetric vortex

pair merger. Similar plots for separation distance of 0.75" and 1" and position of centerline, 25% span and 5% span are provided in the Appendix under Additional Plots. They all show similar trend from Test001 to Test006.

4.3 Non Dimensional Analysis

Comparing absolute values of strength of circulation (Γ) against time for different cases would not give a good enough way to measure the actual changes. Hence circulation and time both need to be non-dimensionalized. We first start with non-dimensionalizing the circulation. It can be given as follows:

$$\emptyset_1 = \frac{\Gamma}{\omega c^2} = \frac{\left[\frac{cm^2}{s}\right]}{\left[\frac{rad}{s}\right][cm^2]} = dimensionless\ quantity$$

The figure (50) below is for 0.75" separation distance and at centerline.

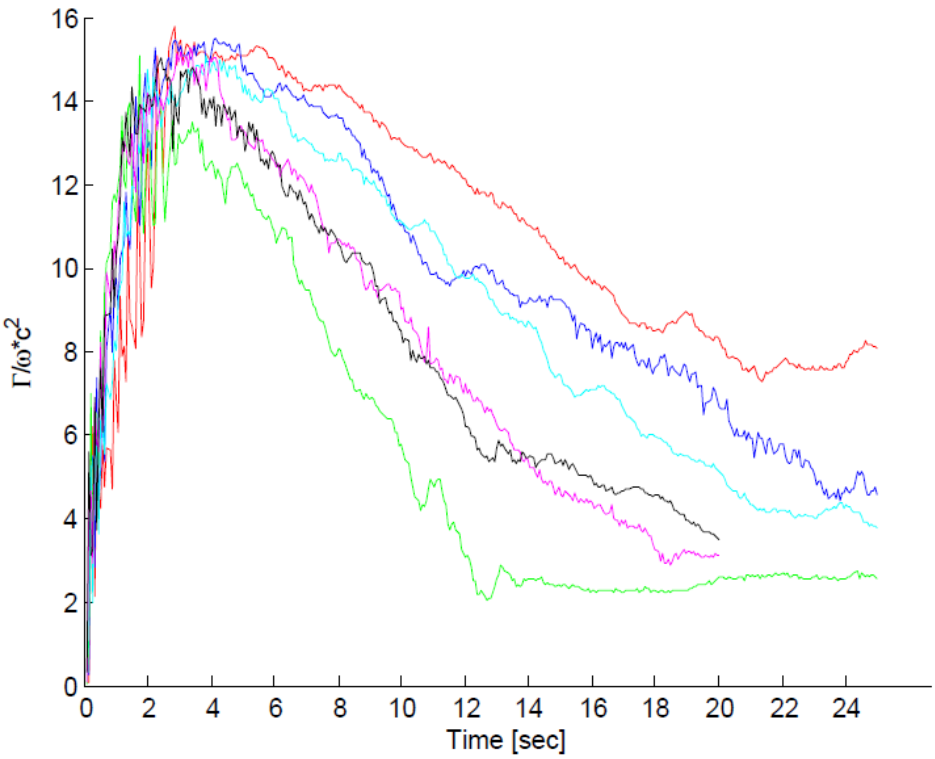

Figure 50 Non dimensional circulation vs time for 0.75" separation at centerline

As we non-dimensionalize the circulation, we observe that the plots get more comparable and follow a likewise trend than just plotting circulation against time. The maximum for each case for the non-dimensional values seem to be similar. For more comparisons the plots for other cases are provided in the Appendices. We can further non-dimensionalize time. We first non-dimensionalize time using the rotational speed of each pedal and plot the non-dimensional circulation with non-dimensional time.

$$\emptyset_2 = t\omega = [s]\left[\frac{1}{s}\right] = dimensionless\ quantity$$

The Figure 51 below is for 0.75” separation distance and at centerline.

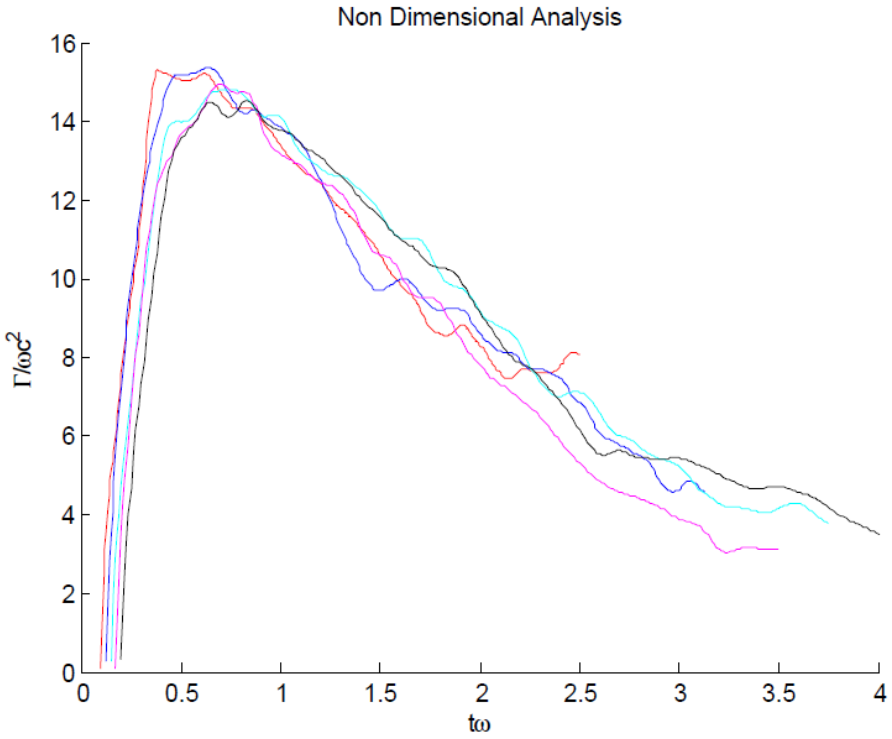

Figure 51 Non Dimensional Analysis for 0.75" separation at centerline

The plots seem to follow a similar trend, hence an average of all the values is taken. The yellow scatter plot in the Figure 52 below is an average for a specific separation distance at a specific position in the tank with varying pedal speeds.

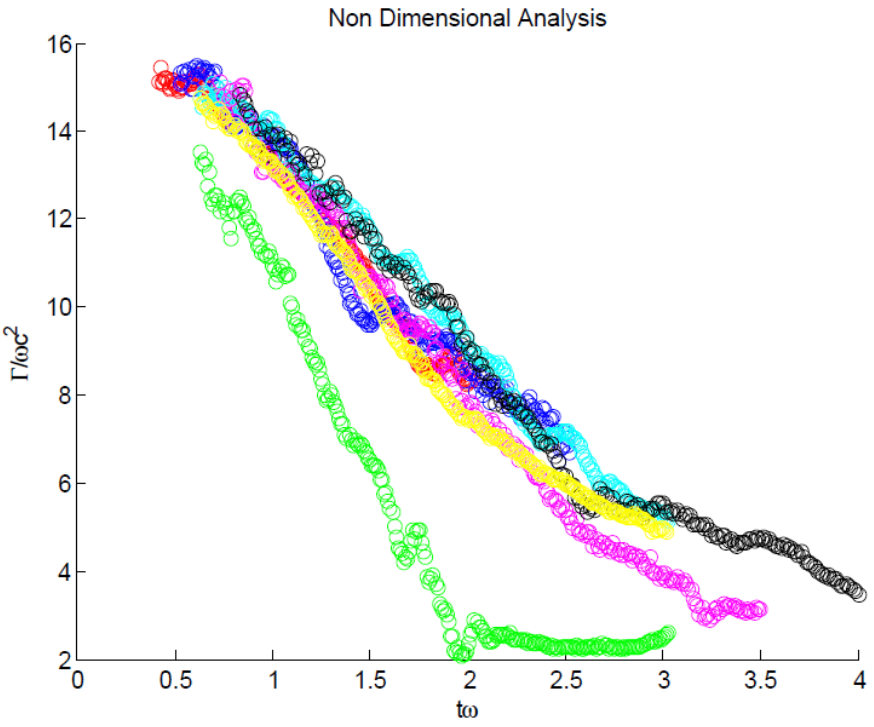

Figure 52 Non Dimensional Analysis for 0.75" separation at centerline scatter plot

Non-dimensional plots for rest of the cases are shown in the appendices. We can then take average for each condition and reducing the 36 cases down to 6 cases. Average of 6 data cases for varying speeds is taken and plotted in the Figure 53 below. Figure 54 shows non-dimensional circulation vs non dimensional time for 0.75” and 1” separation distance at centerline, 25% span and 5% span. The red plot is for 0.75” at centerline, blue for 0.75” at 25% span, green for 0.75” at 5% span, yellow for 1” at centerline, cyan for 1” at 25% span and magenta for 1” at 5% span. The green data for close to the wall for 0.75” separation does not seem to follow the same data trend, is because of physical disturbances while collecting the data. The leakage in the vortex generator tank and

settling of particles at the bottom of the tank are guessed to have brought such different trend of the data.

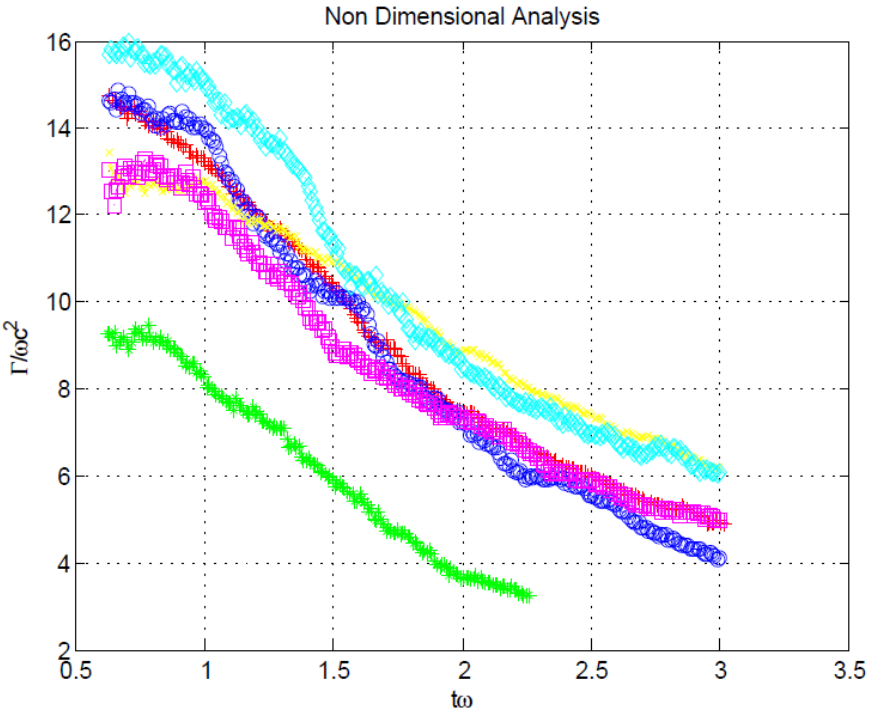

Figure 53 Non dimensional analysis for 0.75" and 1" separation scatter plot

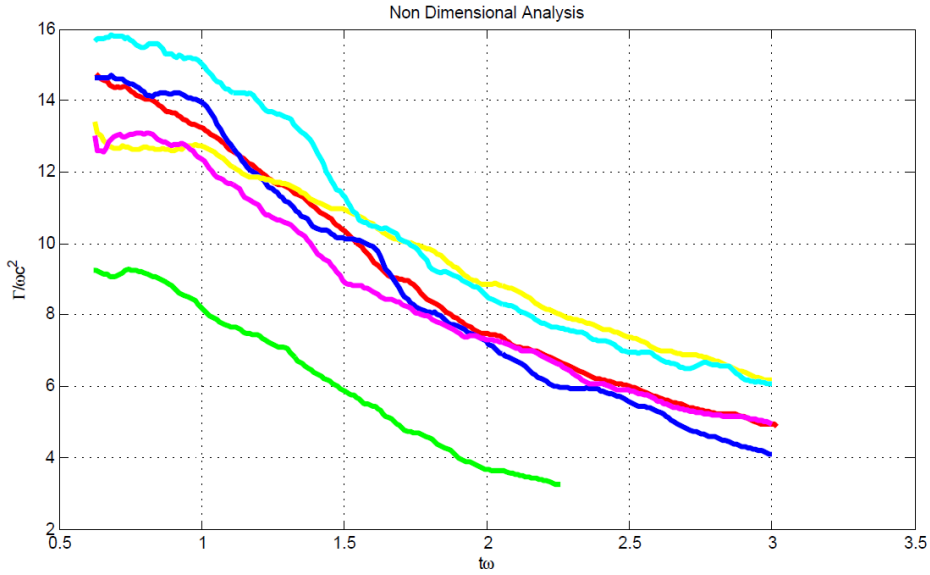

Figure 54 Non dimensional analysis for 0.75" and 1" separation smooth plot

Time is non-dimensionalized based on the properties of the vortex pair as follows:

$$\emptyset_3 = \frac{t\Gamma}{c^2} = \frac{[s]\left[\frac{cm^2}{s}\right]}{[cm^2]} = dimensionless\ quantity$$

The Figure 55 below is for 0.75" separation distance at the centerline.

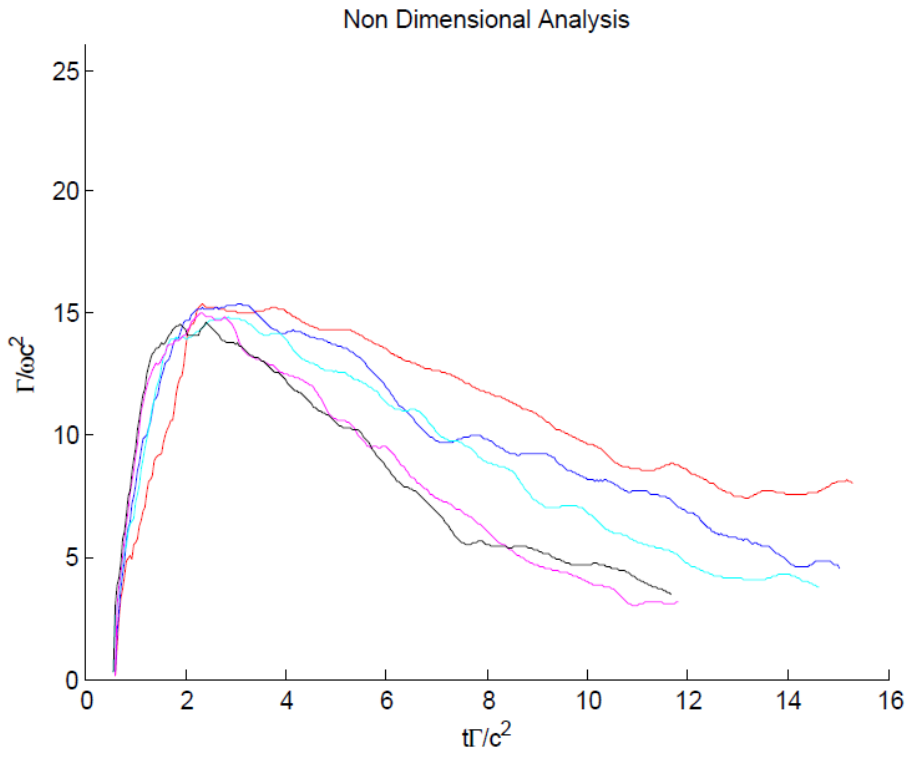

Figure 55 Non Dimensional Analysis for 0.75" separation at centerline

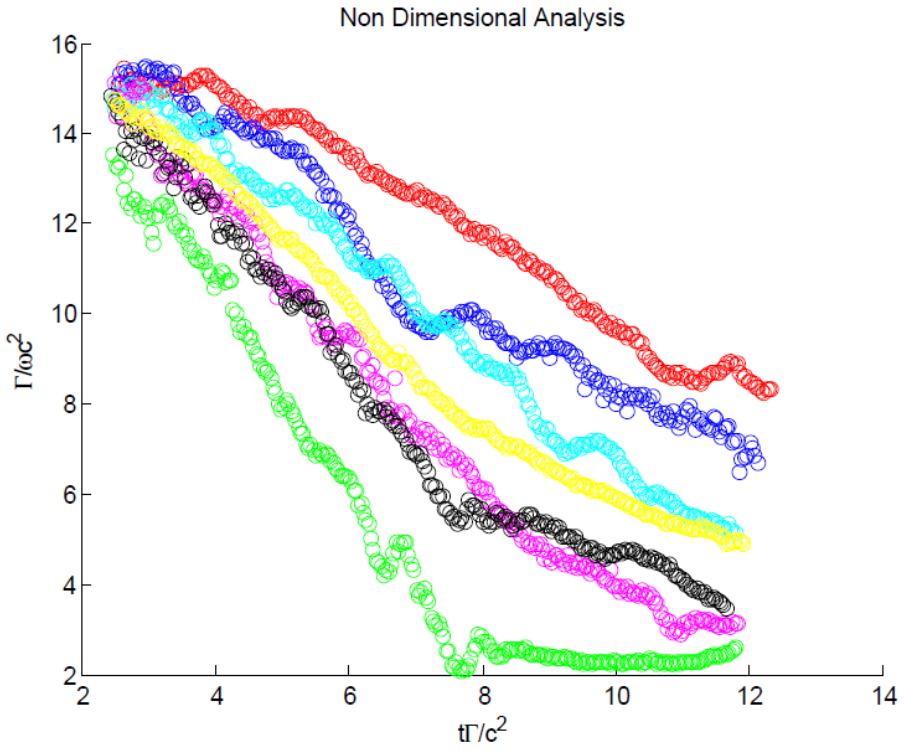

Figure 56 Non dimensional analysis for 0.75" separation scatter plot

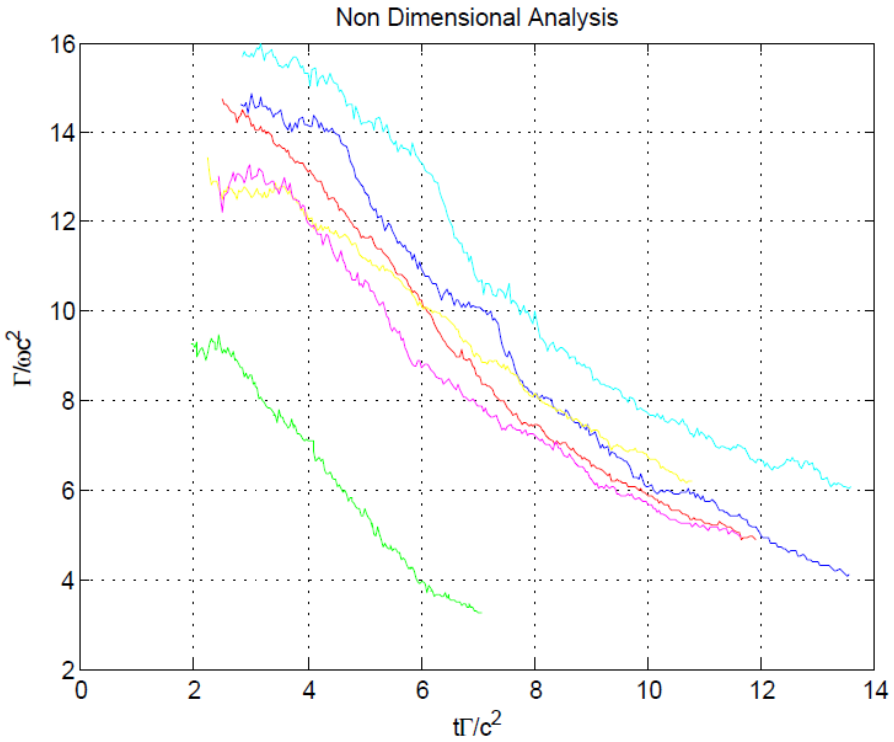

Figure 57 Non Dimensional Analysis for 0.75" and 1" separation

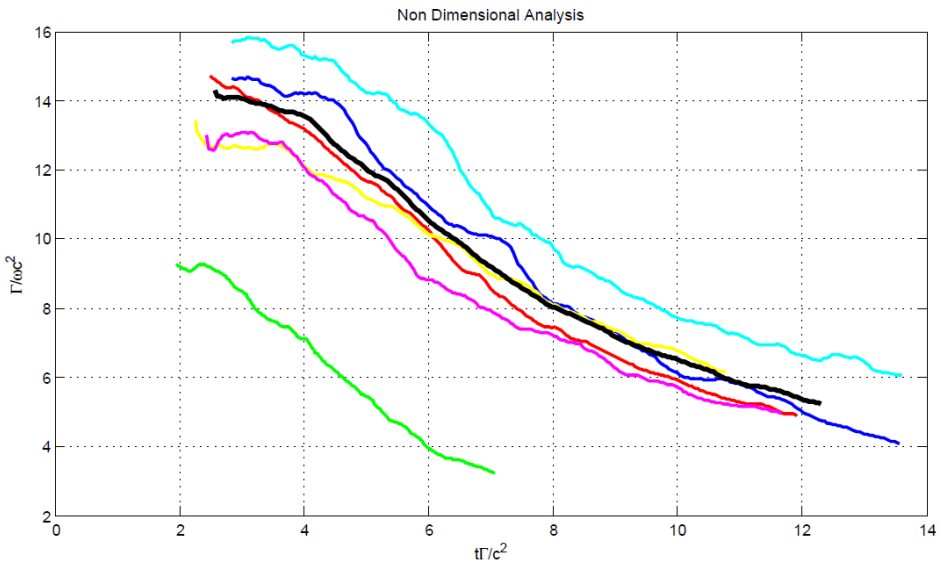

Figure 58 Non Dimensional Analysis for 0.75" and 1" separation smooth plot

4.4 3D Contour Plot Volume Visualization

Vorticity plots can be collaborated and merged as a 3d volume visualization against time to observe the merger process. Below are the 3d visual plots for symmetric and asymmetric vortex merger.

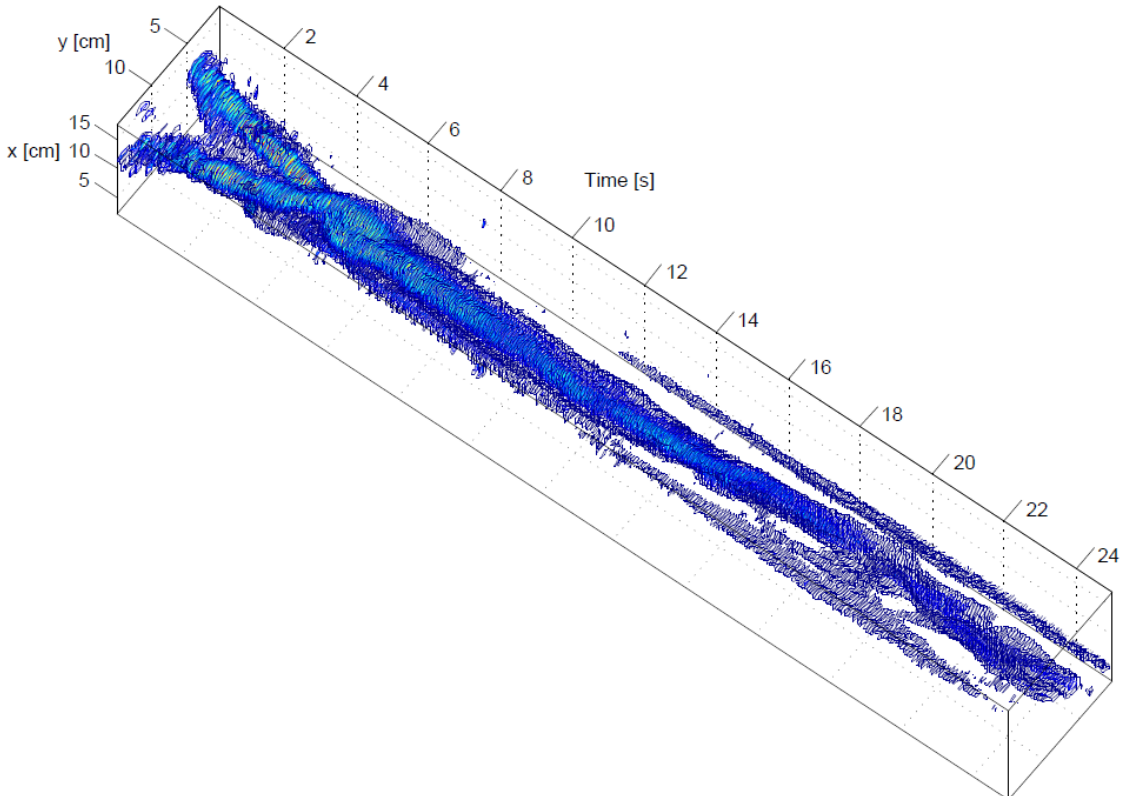

Figure 59 3D contour vorticity plot vs time for 0.75" separation at centerline symmetric merger

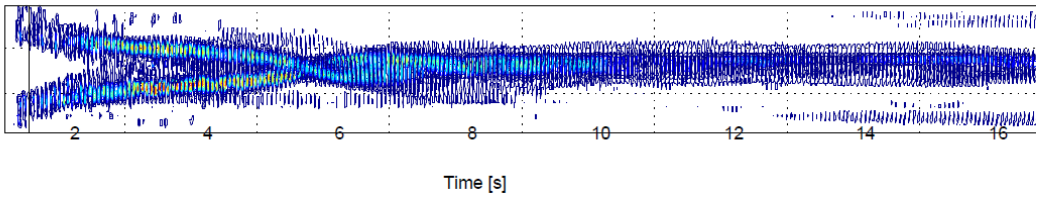

Figure 60 3D contour vorticity plot vs time for 0.75" separation at centerline side view symmetric merger

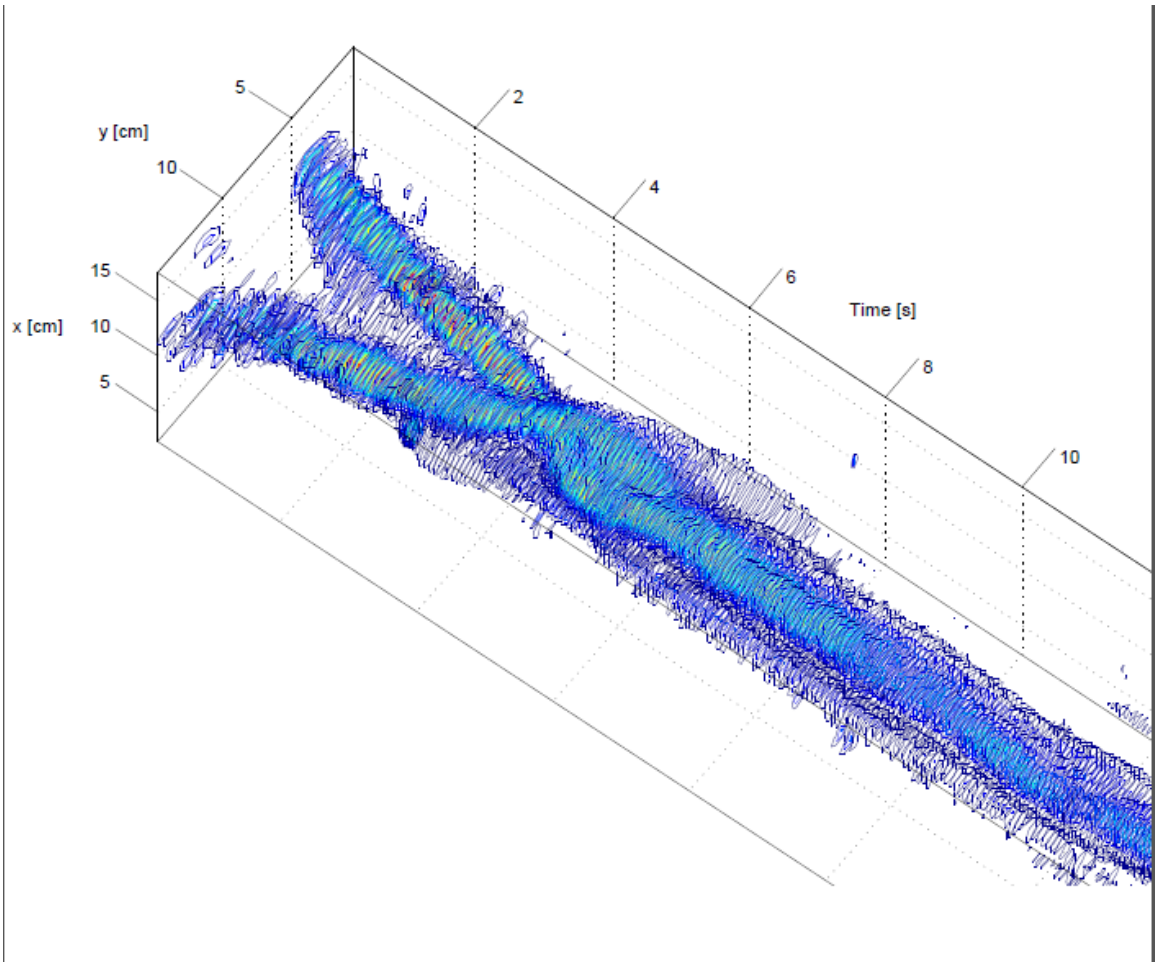

Figure 61 3D contour vorticity plot zoom in for 0.75" separation at centerline symmetric merger

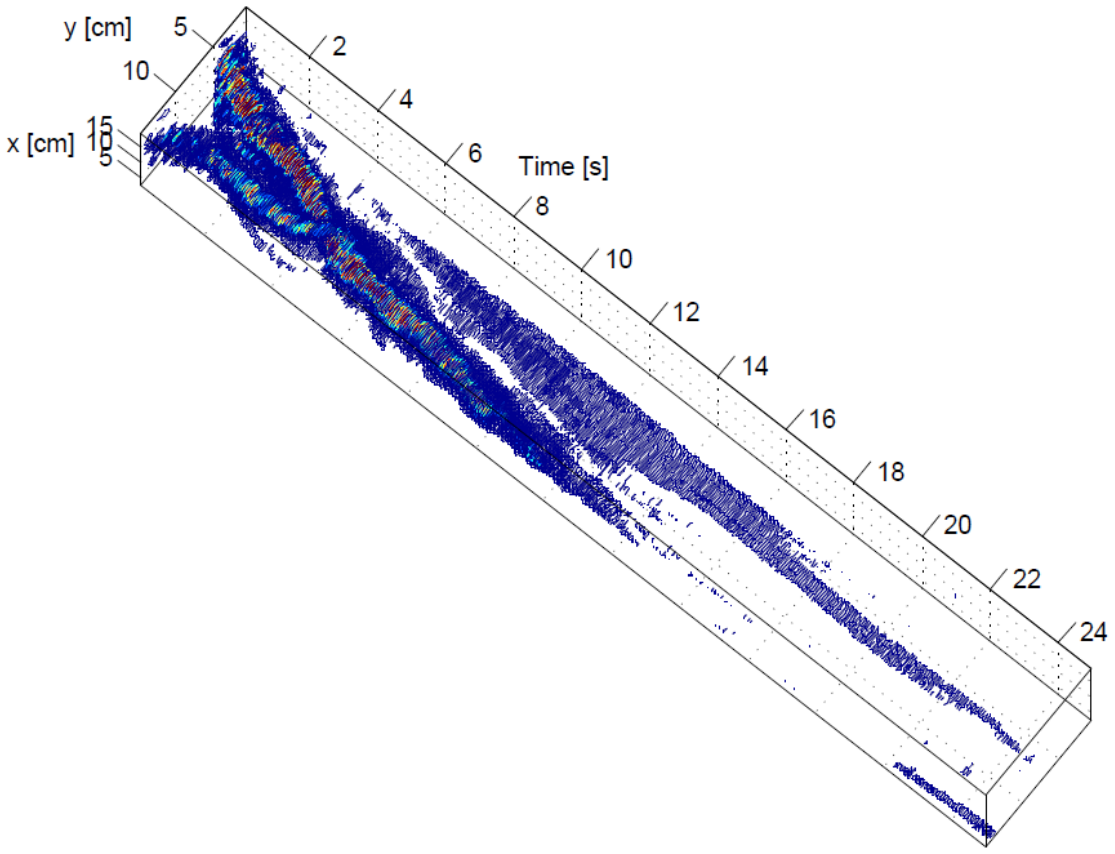

Figure 62 3D contour vorticity plot vs time for 0.75" separation at centerline asymmetric merger

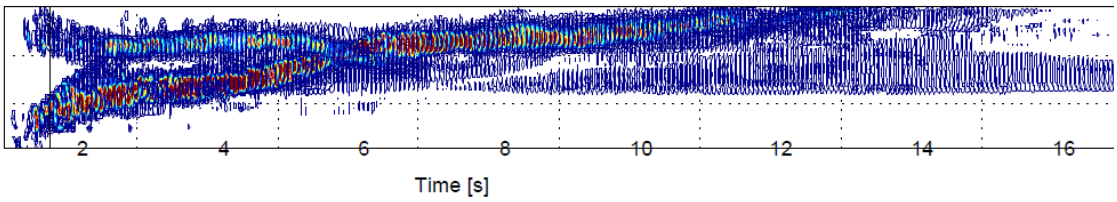

Figure 63 3D contour vorticity plot vs time for 0.75" separation at centerline side view symmetric merger

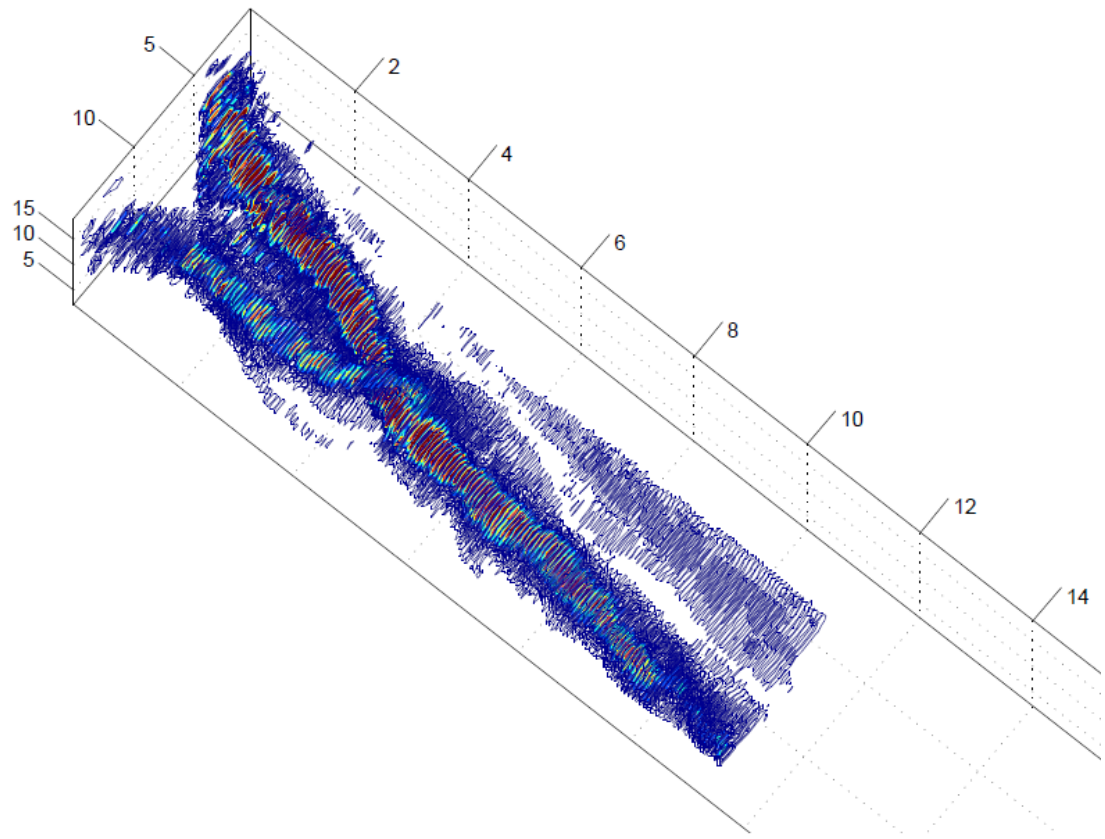

Figure 64 3D contour vorticity plot zoom in for 0.75" separation at centerline symmetric merger

As observed, the co-rotating vortex pair rotates around an axis perpendicular to the plane of the vortex pair and does a spiral turn and merges after one orbit period. The symmetric vortex pair merges nearly at half distance between the centers of the vortices whereas in asymmetric vortex pair, the stronger vortex influences the merger process. The stronger vortex is seen to follow its path and carries the weaker vortex along with itself and during this process the merger occurs. Figures 59, 60, 61 and Figures 62, 63, 64 show the symmetric and asymmetric mergers respectively.

4.5 Wall Effects on Vortex Merger

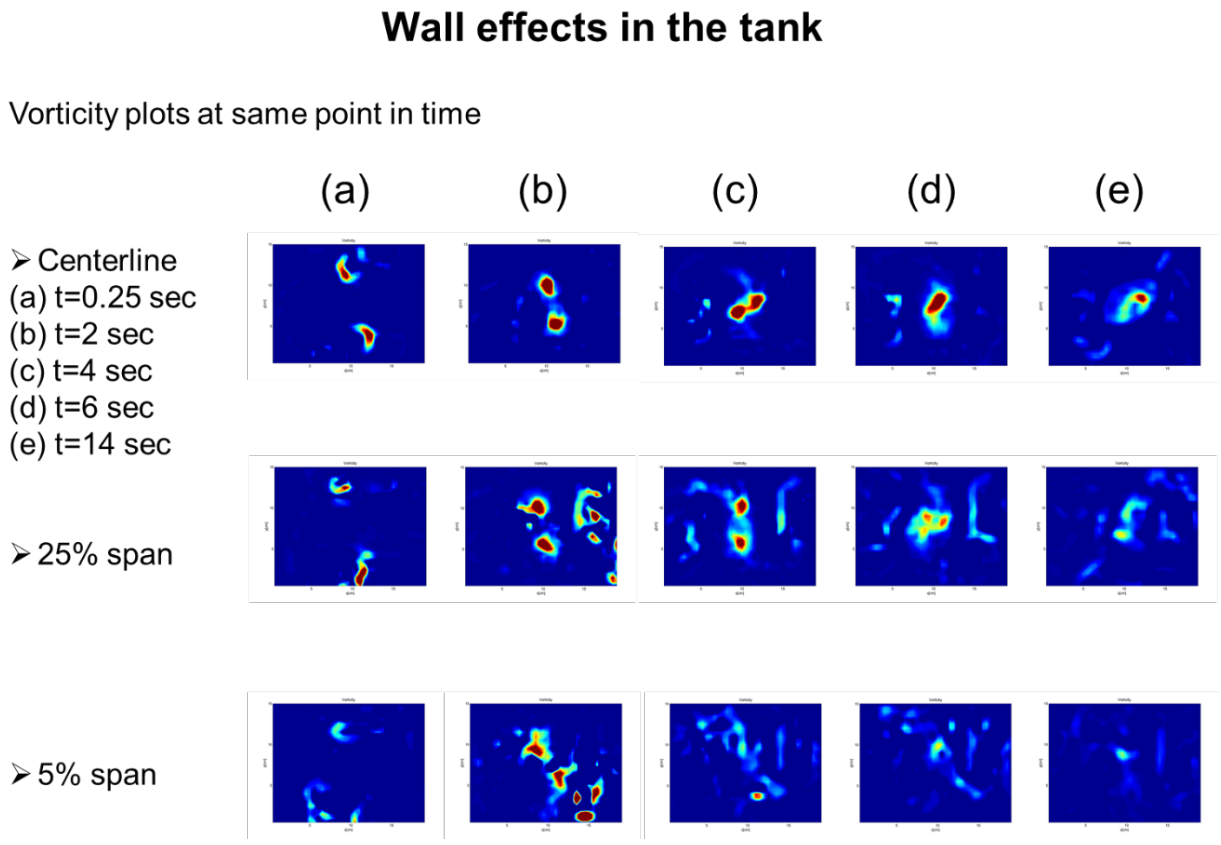

Figure 65 Wall effects on vortex merger at 0.75" separation

4.6 Vortex Center Position and Non Dimensional Analysis

In the Figures below, the red plot indicates the path of the center of Vortex 1 and blue plot indicates the path of center of Vortex 2. Figure 66, 67, 68 and 69 are vortex position and against non dimensionalized time with rotational speeds and with vortex properties.

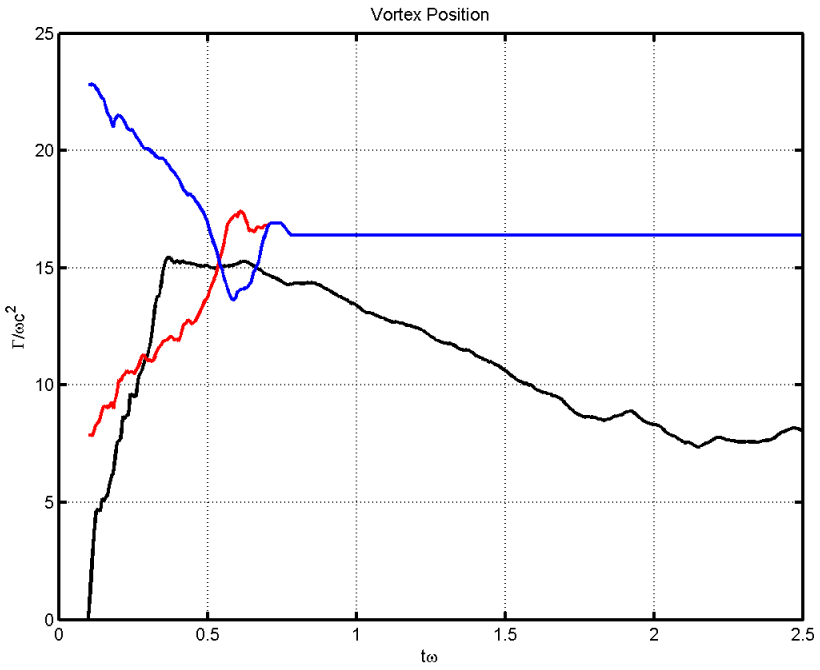

Figure 66 Vortex Position and Non Dimensional Analysis for 0.75" separation symmetric merger 6rpm, 6rpm

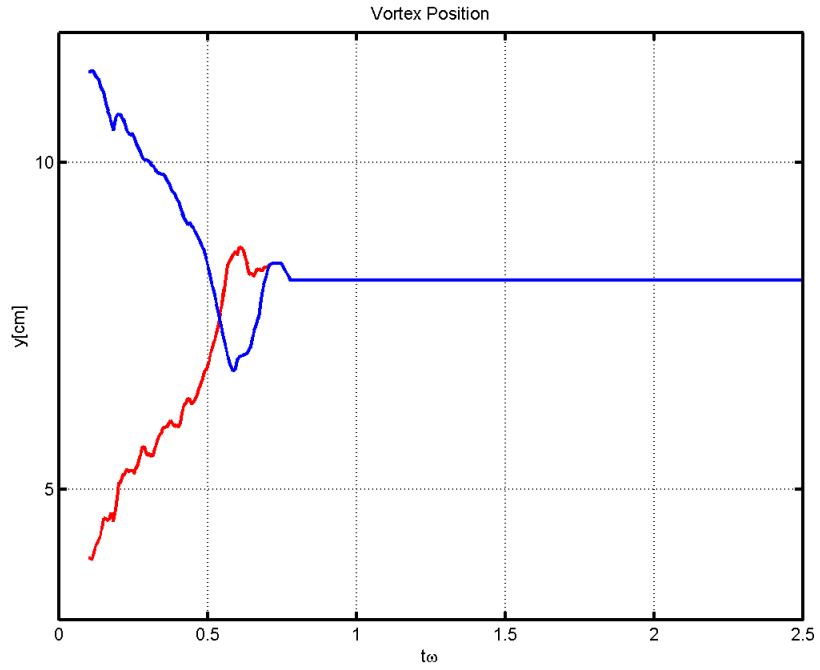

Figure 67 Vortex Positions vs time for 0.75" separation symmetric merger 6rpm, 6rpm

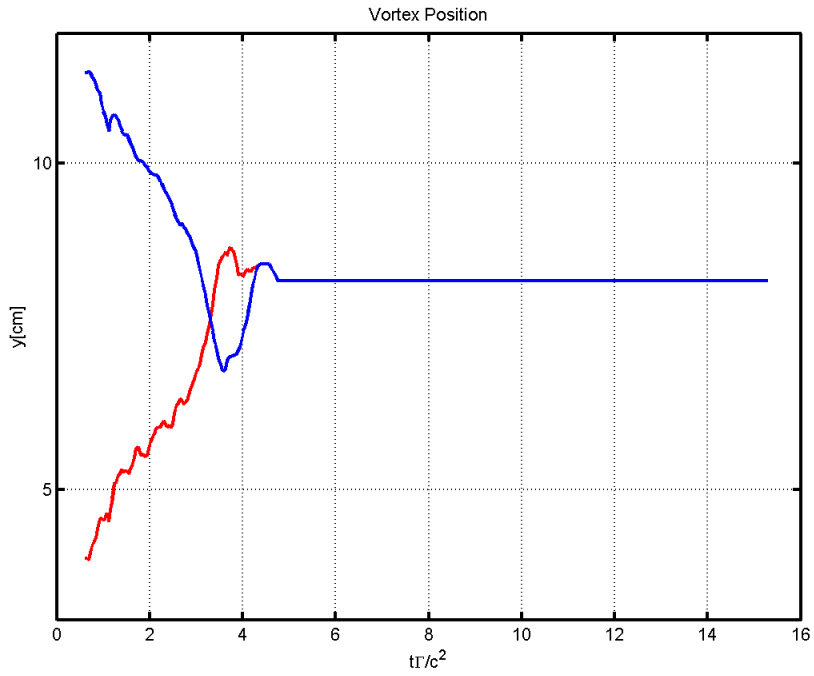

Figure 68 Vortex Position vs Non dimensional time for 0.75" separation symmetric vortex merger 6rpm, 6rpm

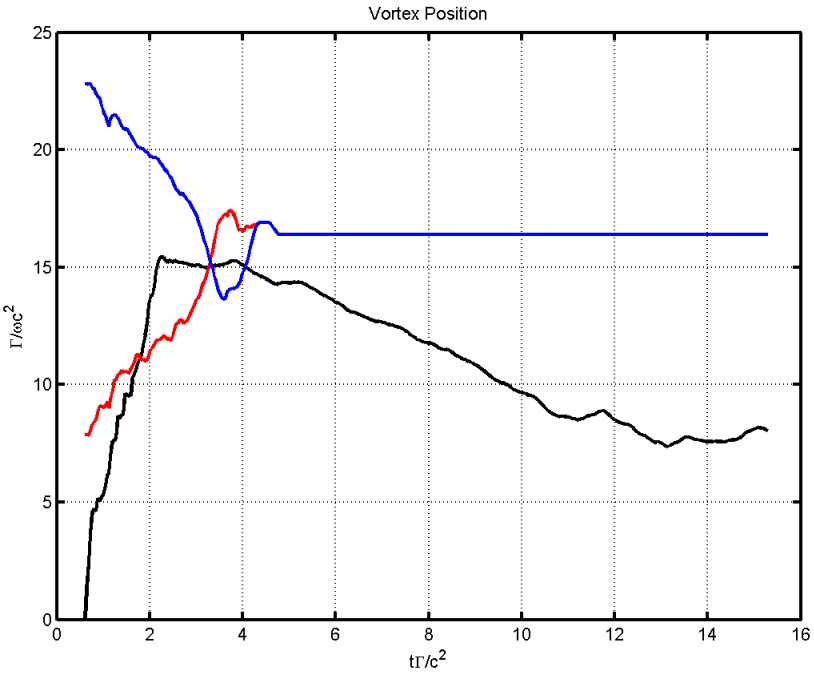

Figure 69 Vortex Position and Non Dimensional Analysis for 0.75" separation symmetric merger 6rpm, 6rpm

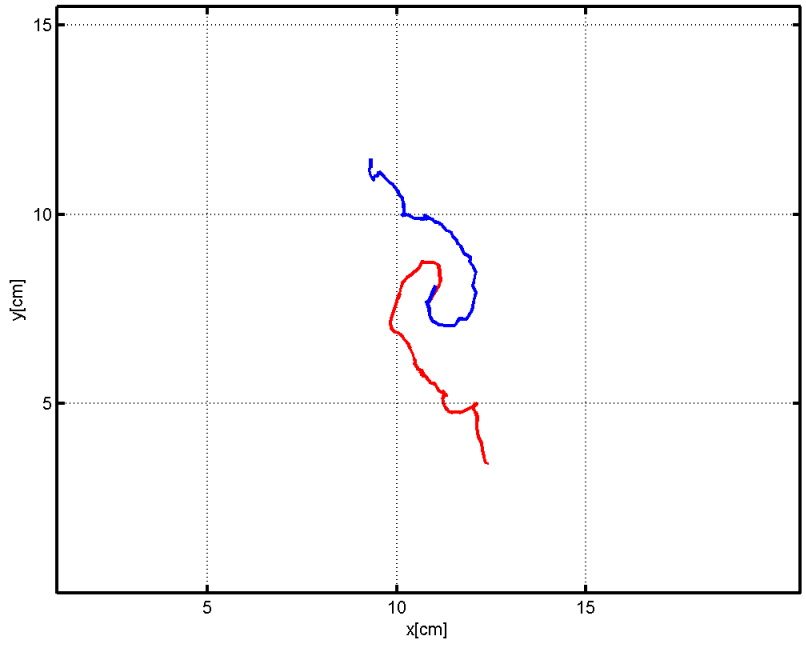

Figure 70 Hodograph for 0.75" separation symmetric merger 6rpm, 6rpm

Figure 66 and 67 show the vortex merger and is plotted with non-dimensional time $t\omega$ whereas Figure 68 and 69 show merger plotted against non-dimensional time$\frac{t\Gamma}{c^2}$. The difference between the two is a scaling factor. While the former compresses the scaling the later shows a much detailed characteristic of the merger.

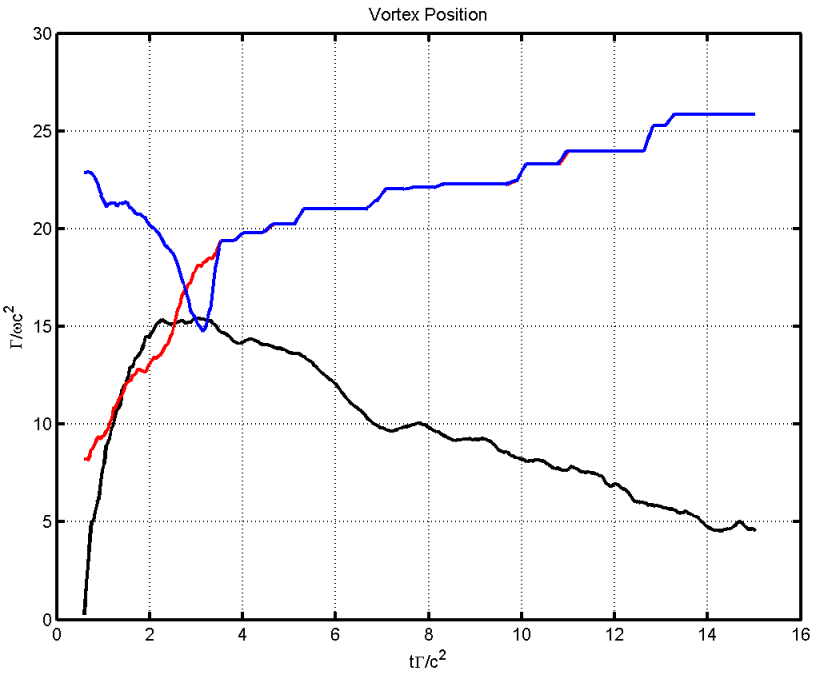

Figure 71 Vortex position and non-dimensional analysis for 0.75" separation asymmetric merger 6rpm, 9rpm

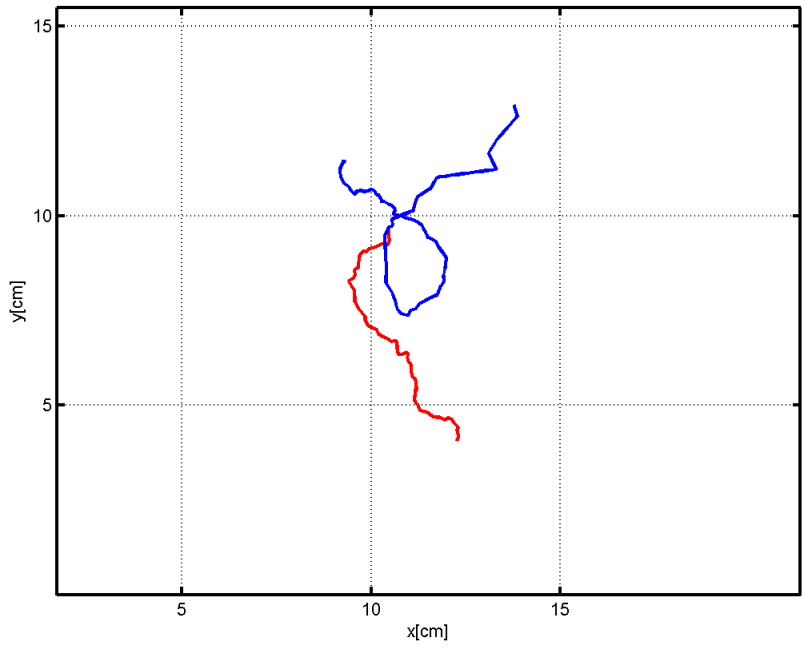

Figure 72 Hodograph for 0.75" separation asymmetric merger 6rpm, 9rpm

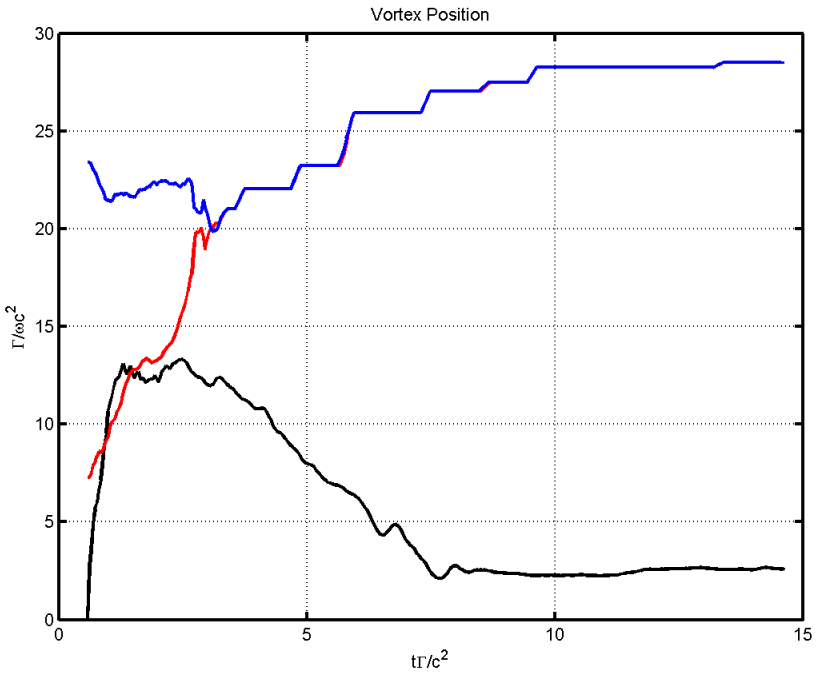

Figure 73 Vortex position and non-dimensional analysis for 0.75" separation asymmetric merger 6rpm, 12rpm

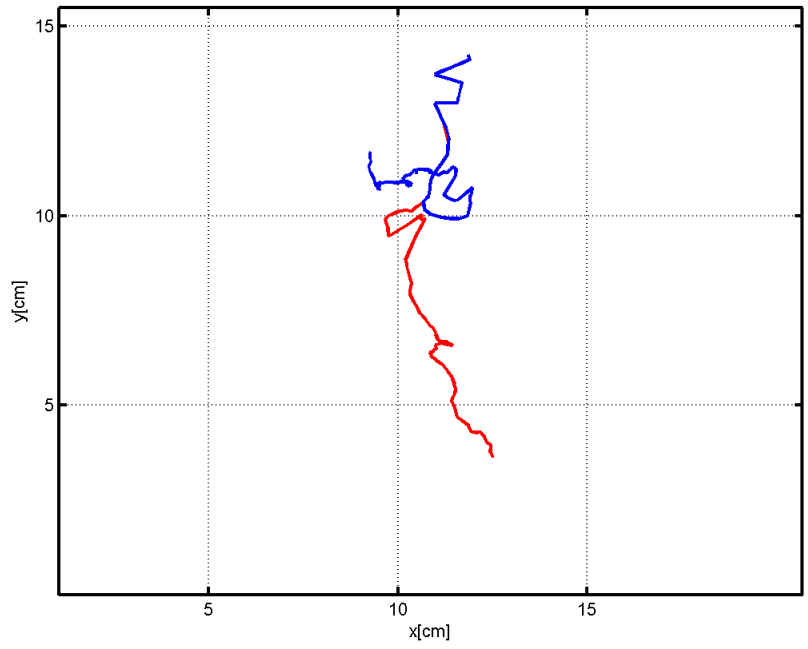

Figure 74 Hodograph for 0.75" separation asymmetric merger 6rpm, 12rpm

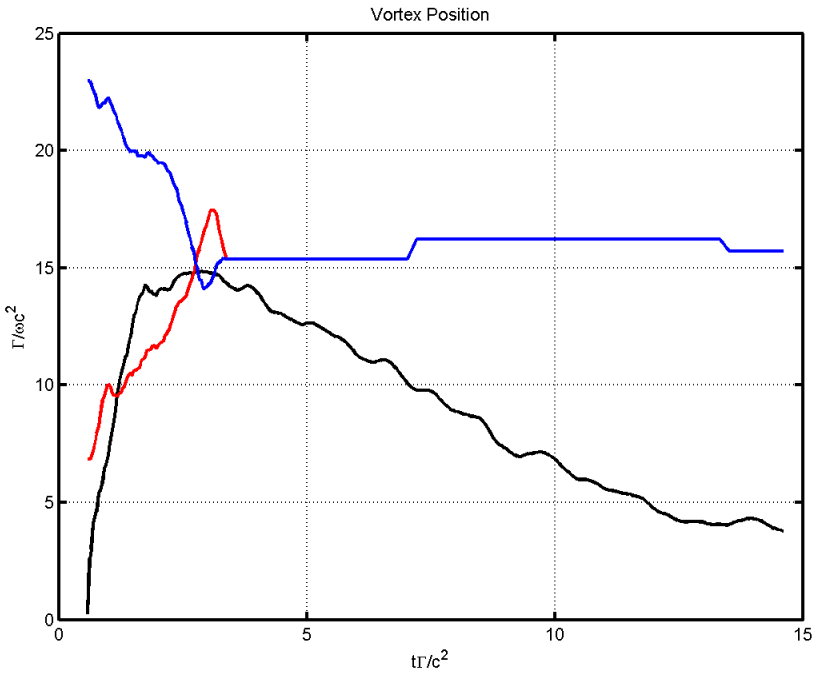

Figure 75Vortex position and non-dimensional analysis for 0.75" separation symmetric merger 9rpm, 9rpm

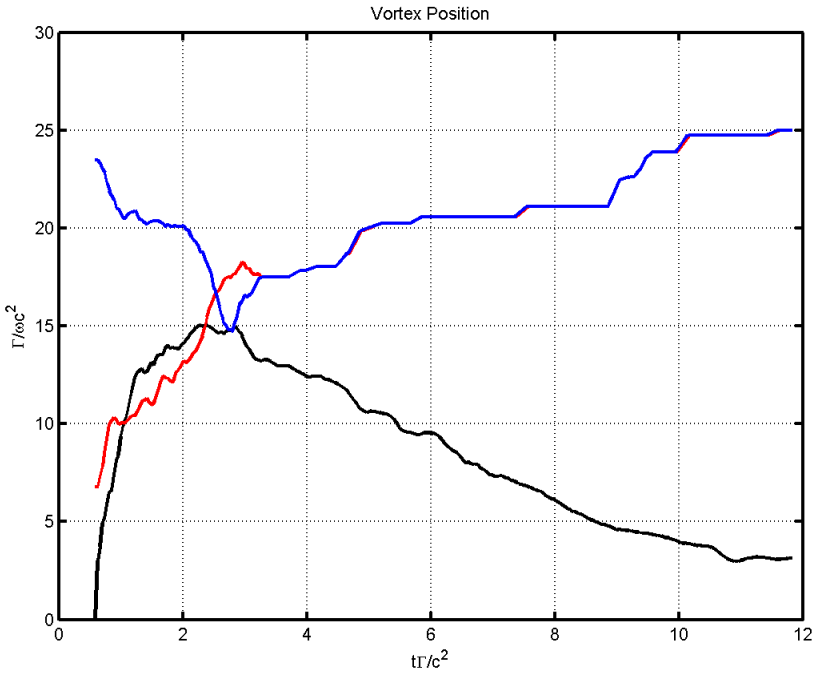

Figure 76 Vortex position and non-dimensional analysis for 0.75" separation asymmetric merger 9rpm, 12rpm

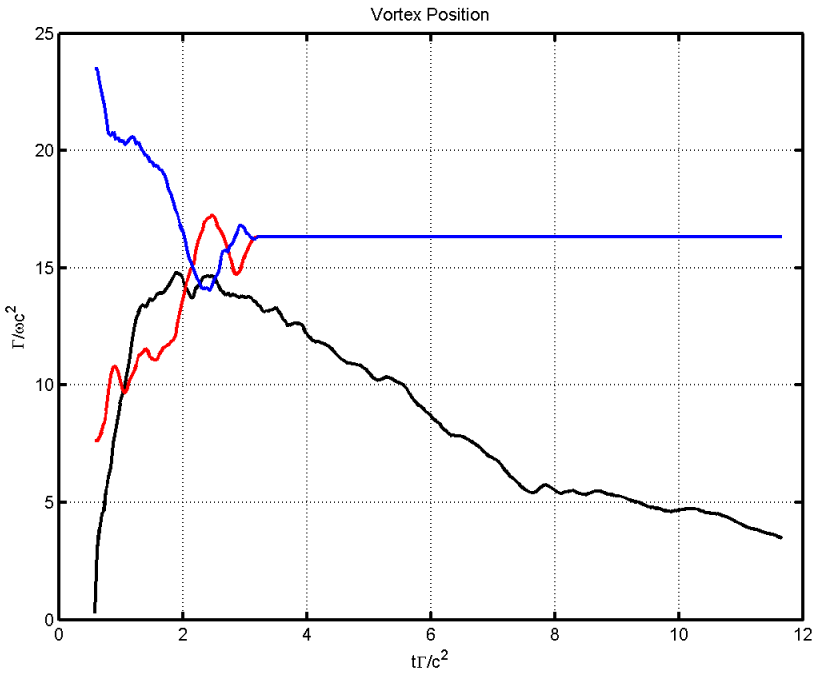

Figure 77 Vortex position and non-dimensional analysis for 0.75" separation symmetric merger 12rpm, 12rpm

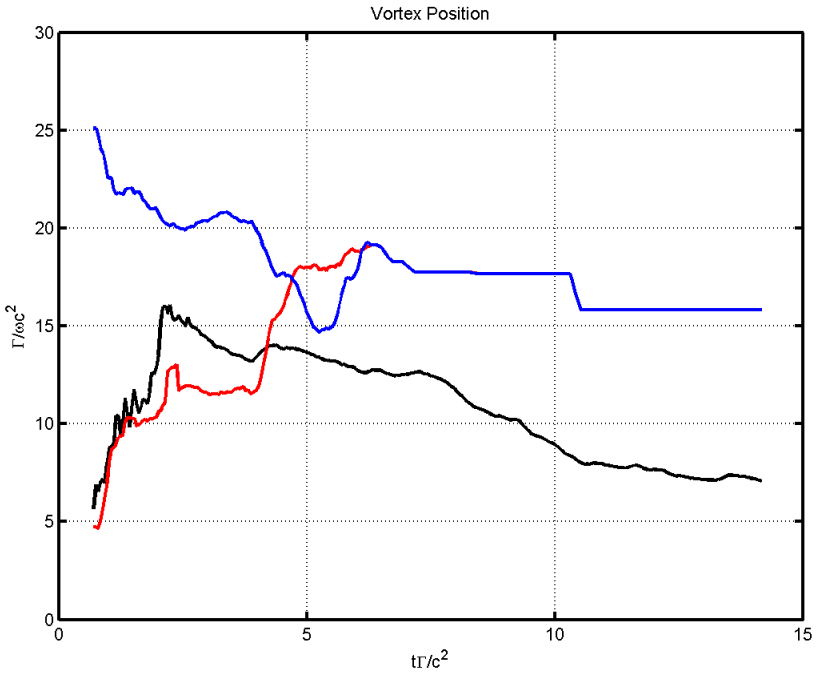

Figure 78 Vortex position and non-dimensional analysis for 0.75" separation at 25% span, symmetric merger 6rpm, 6rpm

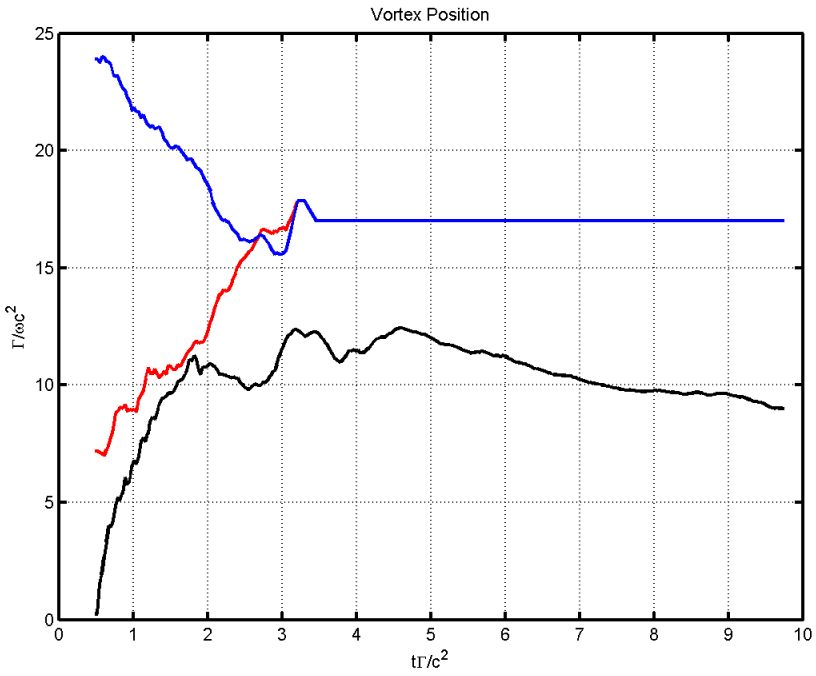

Figure 79 Vortex position and non-dimensional analysis for 1" separation symmetric merger 6rpm, 6rpm

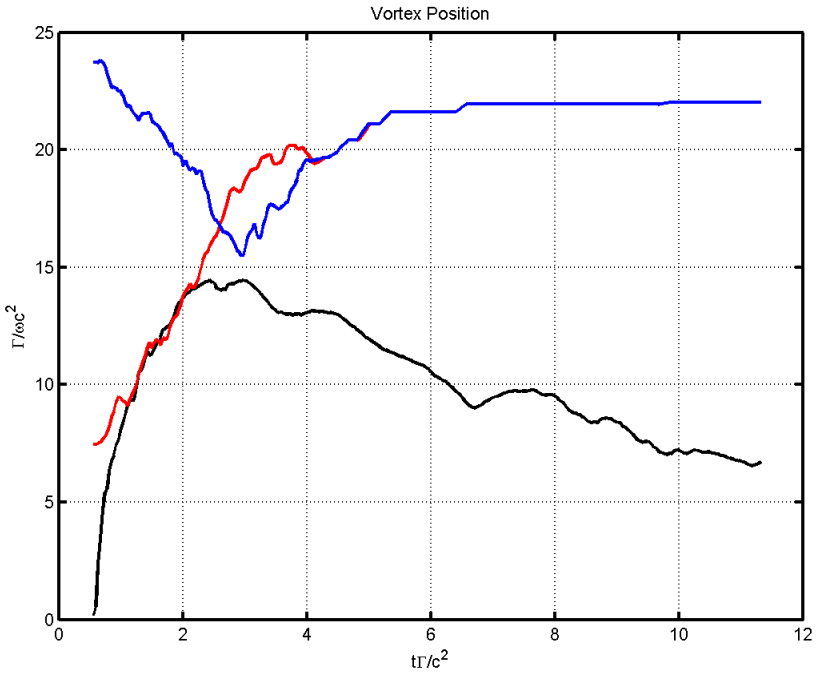

Figure 80 Vortex position and non-dimensional analysis for 1" separation asymmetric merger 6rpm, 9rpm

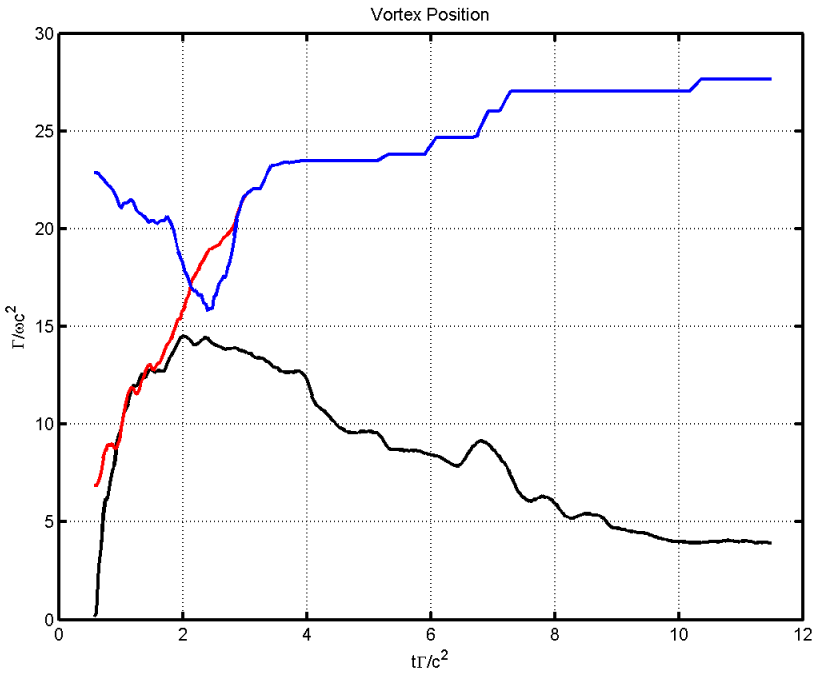

Figure 81 Vortex position and non-dimensional analysis for 1" separation asymmetric merger 6rpm, 12rpm

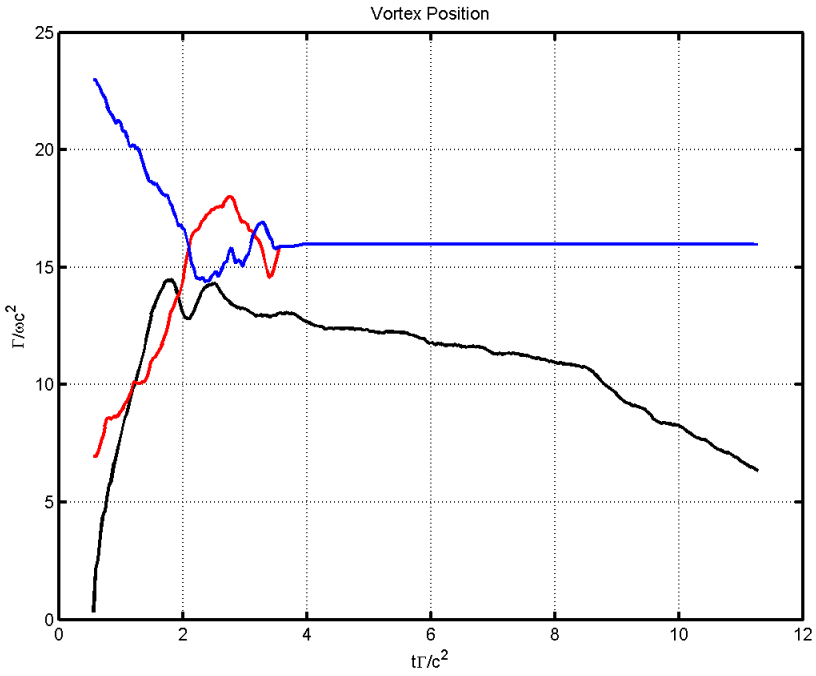

Figure 82 Vortex position and non-dimensional analysis for 1" separation symmetric merger 9rpm, 9rpm

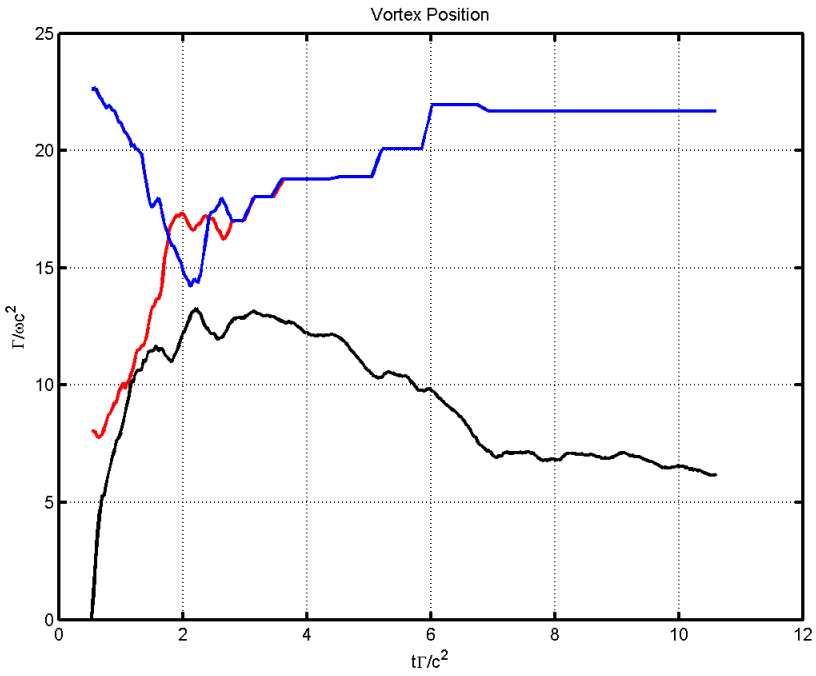

Figure 83 Vortex position and non-dimensional analysis for 1" separation asymmetric merger 9rpm, 12rpm

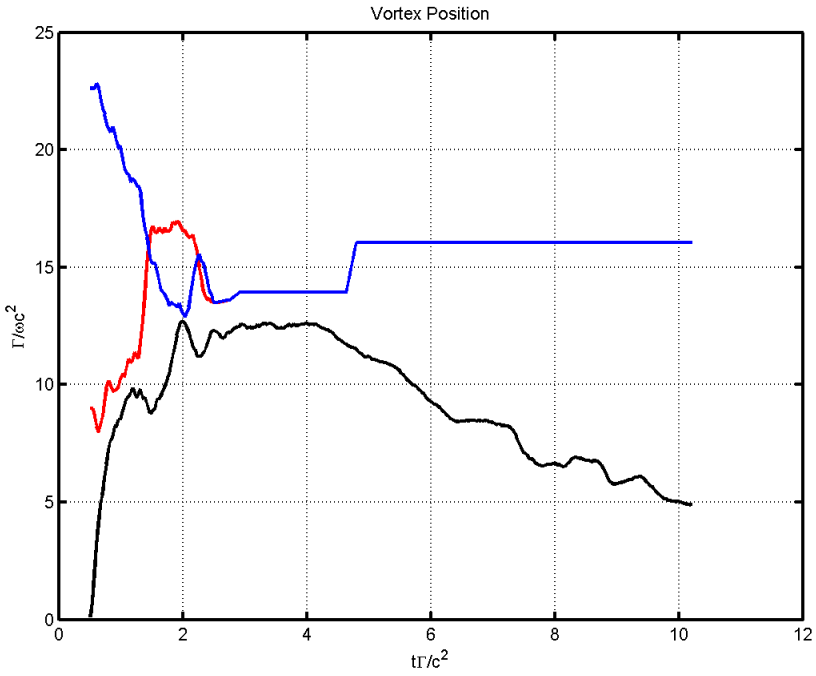

Figure 84 Vortex position and non-dimensional analysis for 1" separation symmetric merger 12rpm, 12rpm

CHAPTER V

CONCLUSION & FUTURE WORK

Conclusion:

In this thesis, effects of initial spacing and circulation strength, both symmetric and asymmetric, of a co-rotating vortex pair are studied. We observe that the co-rotating vortices always merge under present conditions. Symmetric vortex pair are observed to merge along the line perpendicular to the plane of the vortex pair while asymmetric vortex pair are seen to behave differently. The stronger vortex is seen to have a greater impact on the weaker vortex. It tends to break the weaker vortex into filaments and absorbs it as it continues to follow its path, though the asymmetric vortex pair is seen to rotate around each other as well.

The total strength of the vortex pair is seen to be conserved after the merger. Γ_1 and Γ_2 are individual strengths of the vortex pair. It is seen that the merged vortex appears to have strength almost equal to the addition of the two individual vortices. Having said some of

the energy is being lost in dissipation before the merger happens. But the experiments agree to $\Gamma_{total} = \Gamma_1 + \Gamma_2$. In symmetric vortex merger, pair of higher strengths merge at a faster rate and dissipate faster compared to those of lower strength pair. Figure 77, 82, 83 and 84 show that he higher strength vortex pair complete two orbital rotations around each other before merger while lower strength symmetric vortices complete one orbital rotation around each other. Initial separation distance between the centers of two co-rotating vortices also affects the number of rotations the pair finishes before merging.

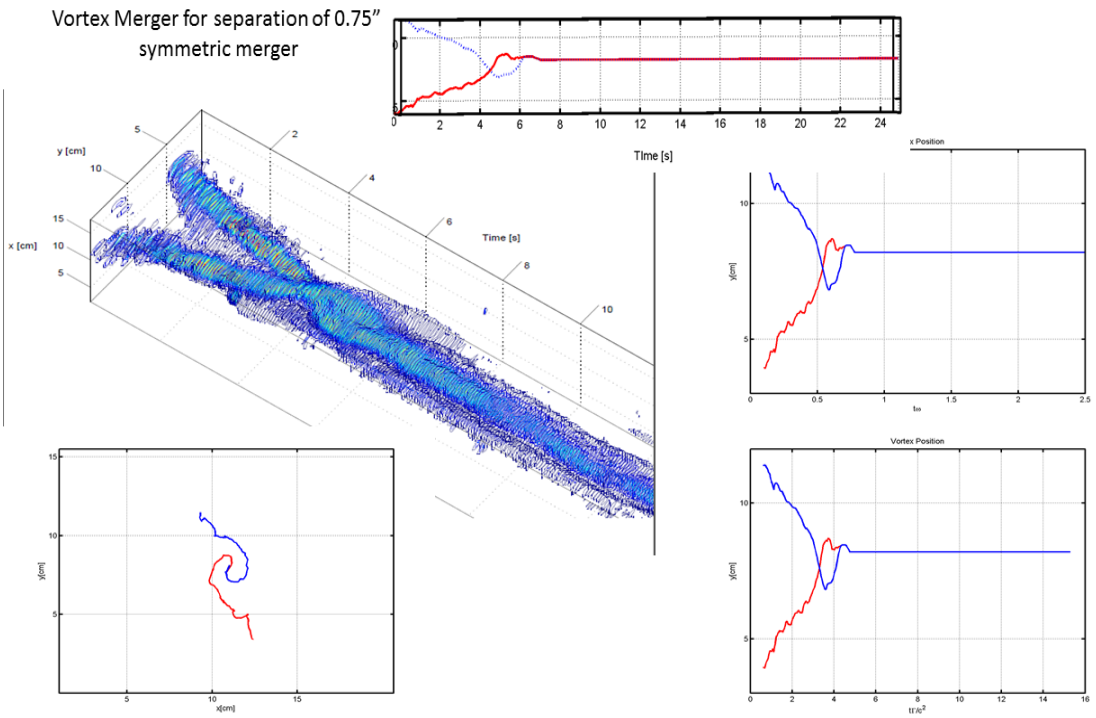

Figure 85 Symmetric Vortex Merger for 0.75" separation at 6rpm, 6rpm

Distance from the wall has been observed to have an effect on the merger time. Vorticity contour plots in Figure 65 compares vortex merger at specific time intervals to understand the position of individual vortex and wall effects on the merger. As strength of circulation increases merger time decreases and dissipation increases. Circulation is

conserved during the merger process for symmetric and asymmetric mergers. As we move from the center of the tank to the wall, the time for merger increases. Closer to the wall the dissipation rate decreases because of the wall effects. The vortex pair rotates faster around each other at the centerline while the rotational rate is slower near the wall. Comparing Figures 69 and 78 at centerline and 25% span respectively we see that orbital time of $\frac{t\Gamma}{c^2}$ is higher for 25% span than that for centerline. But from vorticity plots, we see a faster dissipation of the merger vortex. Thus the principles of braiding and stretching of vortex filaments are observed because of the shear closer to the wall.

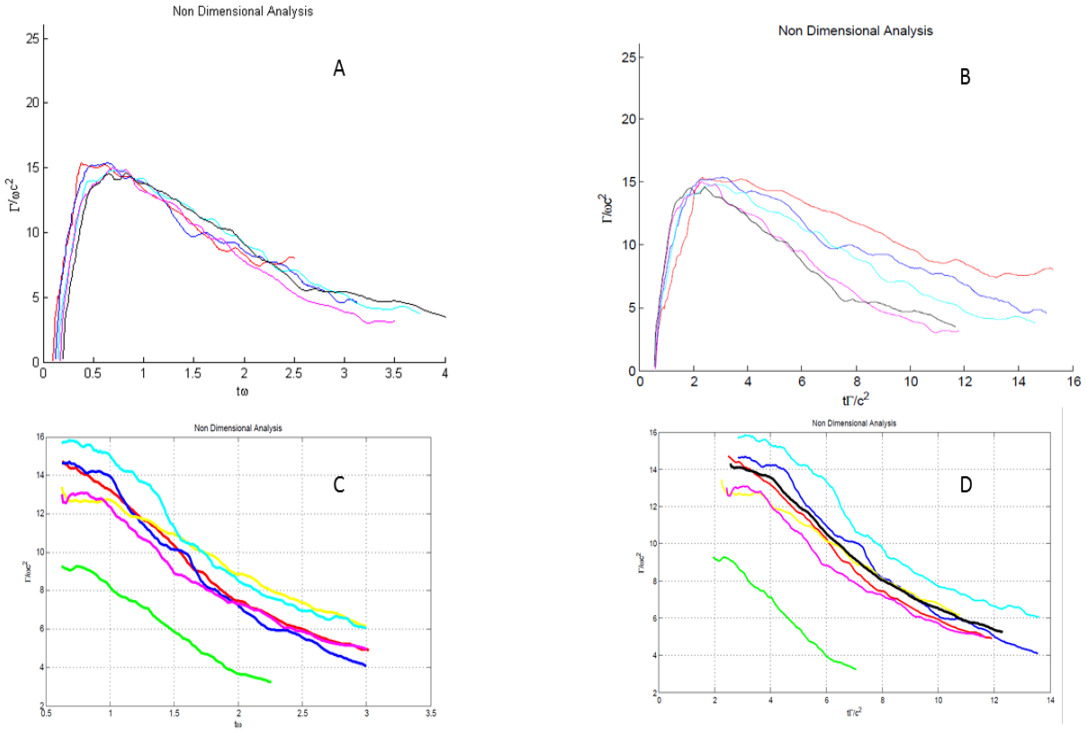

Figure 86 Non Dimensional Circulation vs Non Dimensional Time

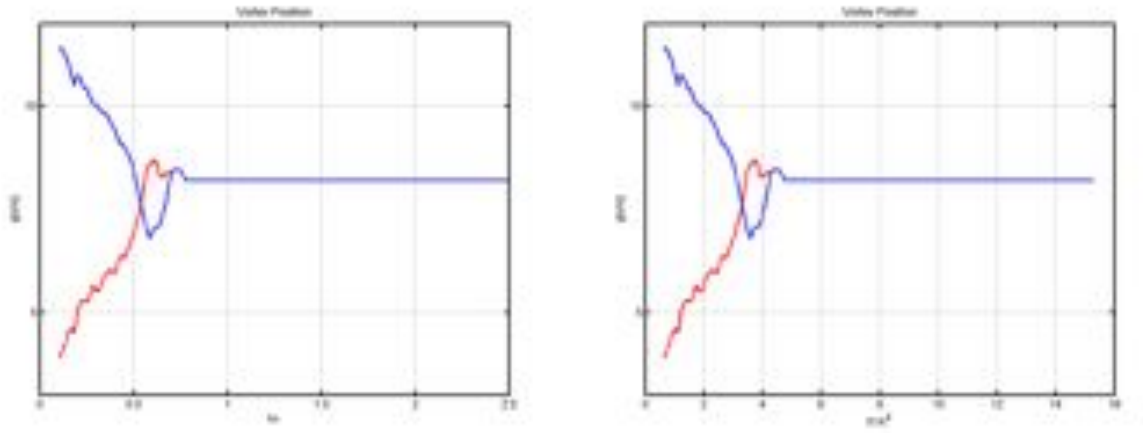

Figure 87 Non Dimensional Time comparison

Figure 86 and 87 shows a comparison of non-dimensional circulation vs non-dimensional time. For Plot (A) non-dimensional time is calculated using ω which is revolution of the pedal while for plot (B) time is non-dimensionalized using Γ and c^2. We see that it is just a scaling difference, and hence the merger time for $t\omega$ is around 0.5 whereas for time $\frac{t\Gamma}{c^2}$ is 4. In each case merger time is higher in the latter case, is because of the way time is non-dimensionalized. But when non-dimensionalized circulation is plotted against the two times, it's observed that $t\omega$ seems to follow a much composed trend than compared to $\frac{t\Gamma}{c^2}$. The same is observed for all the other cases. Vortex positions however seem to be more clearly observed in the $\frac{t\Gamma}{c^2}$ non dimensionalized plots than the $t\omega$ plots, and can be observed in Figure 87 and 137 respectively.

Future Work:

Comparisons with 3D vortex merger should be made. The setup for the 3D wind tunnel experiments is ready and set to be tested. The wing panels for the NACA 0015 wings are fabricated. The Labview codes for running the traverse by selecting the number of points to collect data and selecting the cross sectional area has been developed. The pressure scanner DSA 3217 is controlled by Labview to collect data using the 7-hole probe. The data collected can be processed using MatLab to get velocity plots. This analysis can then be compared with the 2D data from the vortex merger tank and non-dimensional circulation vs time.

REFERENCES

Ch Josserand, M. Rossi, "*The merging of two co-rotating vortices: a numerical study*", European Journam of Mechanics B/Fluids, 23 February 2006.

Fangxu Jing, Eva Kanso and Paul K Newton, *"Insights into symmetric and asymmetric vortex mergers using the core growth model*", American Institute of Physics, 5 July 2012.

Gregory G. Zilliac, "*Calibration of Seven-Hole Pressure Probes for Use in Fluid Flows with Large Angularity*", Ames Research Center California, December 1989.

Maziar Hemati, "*Vortex Merger: A Numerical Investigation*", University of California-Los Angeles Final Project, June 2009.

Xinyu Li and J.D.Jacob, "*Effect of Initial Spacing of Co-Rotating Vortex Formation and Merger*", University of Kentucky, October 2001.

Xinyu Li and J.D.Jacob, "*Effect of Initial Spacing of Co-Rotating Vortex Formation and Merger*", AIAA-2000-2219 Paper Published

Claude G> Matalanis and John K Eaton, "*Wake Vortex alleviation using rapidly actuated segmented gurney flaps*", The Stanford Thermal and Fluid Sciences Affiliates and Office of Naval Research, January 2007.

Xin Huang, Hirofumi Igashi, Paul Durbin and Hui Hu, "*Wind tunnel effects on wingtip vortices*", 48th AIAA Aerospace Sciences Meeting, January 2010.

S.L. Wakelin and N. Piley, "*Vortex ring interractions II. Inviscid models*", University of East Anglia, Norwich, December 1994.

A. L. Chen, J. D. Jacob and O. Savas, "*Dynamics of corotating vortex pairs in the wakes of flapped airfoils*", J. Fluid Mech. (1999), vol 382, pp. 155-193, August 1998.

O. U. Velasco Fuentes, "*Vortex filamentation: its onset and its role on axisymmetrization and merger*", Dynamics of Atmospheres and Oceans 40(2005) 23-42, December 2004.

C. Cerretelli and C. H. K. Williamson, "*The physical mechanism for margining of trailing vortices*", 41st Aerospace Sciences Meeting and Exhibit, January 2003

C. Cerretelli and C. H. K. Williamson, "*The physical mechanism for margining of trailing vortices*", J. Fluid Mech (2003), vol 475, pp 41-77, 2003.

P. Meunier and E. Villermaux, "*How vortices mix*", J. Fluid Mech. (2003), vol 476, pp 213-222, 2003.

APPENDICES

APPENDIX A

MATLAB Code for processing data from PIV for Circulation calculation.

```
function test
    % MATLAB Script to read ISSI-DPIV2 data and image files in tecplot format
    % Akshay Khandekar & Dr. Jamey Jacob, Nov. 9 2013
    clear all; close all;

    fprintf('Reading data and image files.\n')
    run='Camera 1';

   nx=39; ny=31; %Constant for DPIV program output for 2 iterations
%    nx=79; ny=63;
   nxc=1280; nyc=1024;   %camera size pixels

    %%%%%%%%SCALING TO CM/S %%%%%%%%%%%
    scale=550/(3*2.54);   %pixels/cm
    pulse=1/30;           %constant to remove the velocity/frame

    %%%%%%%%CONVERSION FACTORS TO CM/S%%%%%%%%%%
    convel=(scale*pulse);
    convor=(pulse);

   %change the path of where the data is located%
```

```
basepath=strcat('C:\Users\Akshay Khandekar\Desktop\Akshay Vortex Tank Data 0.75\Test_001');
titleinfo='';

%total number of data files
none=421;
nlas=421;
ntot=ceil((nlas/4)-(none/4))+1;

%%%%%%creating empty arrays%%%%%%
vorn=zeros(nx-1,ny-1);
vor=zeros(nx,ny);

m=1;
% read data file into header and tensor arrays
for i = none:4:nlas
   un=zeros(nx,ny);
   vn=zeros(nx,ny);
   [x,y,u,v,vel,vorticity,bat]=dpiv(run,i,basepath,scale,convel,convor,pulse);

   xllim=0; xulim=25; yllim=0; yulim=25;
   axis([xllim xulim yllim yulim])

   figure(1)
   h=quiver(x,y,u,v,3),axis equal,title(strcat(titleinfo,'Velocity Field'));


 %%%%%%% ACTIVATE CODE TO SAVE IMAGES OF VECTOR PLOTS %%%%%%%%%%
   filename = strcat(run,bat,'velocity plot');
   fileout=strcat(filename,'.png');
```

```
saveas(gcf,fileout,'png')

dx=(nxc/(scale*nx));

uu=reshape(u,nx,ny);
u=reshape(u,nx,ny);
v=reshape(v,nx,ny);
vv=reshape(v,nx,ny);
vorticity=reshape(vorticity,nx,ny);

for i=2:nx-1
   for j=2:ny-1
      vor1 = uu(i-1,j-1)+uu(i,j-1)+uu(i,j-1)+uu(i+1,j-1);
      vor2 = uu(i+1,j+1)+uu(i,j+1)+uu(i,j+1)+uu(i-1,j+1);
      vor3 = vv(i+1,j-1)+vv(i+1,j)+vv(i+1,j)+vv(i+1,j+1);
      vor4 = vv(i-1,j+1)+vv(i-1,j)+vv(i-1,j)+vv(i-1,j-1);
      vort(i,j) = (vor1 - vor2 + vor3 - vor4)/(8.*dx);
   end
end

vortex=rot90(rot90(rot90(vort)));

figure(3)
contourf(vortex,100);
axis equal, title(strcat(titleinfo,'Vorticity')),axis([1 nx-1 1 ny-1]),shading flat,caxis([0
2]),
set(gca,'xtick',[10 20 30]);
set(gca,'xticklabel',[5 10 15]);
set(gca,'ytick',[10 20 30]);
set(gca,'yticklabel',[5 10 15]);
xlabel('x[cm]');
```

```
ylabel('y[cm]');

un=u+un;
vn=v+vn;
vorn=vort+vorn;
vor=vorticity+vor;
gamma_vor=0;
gamma_vel=0;

%%%%%%%%%%%%find center of vortex%%%%%%%%%%%%
figure(3)
%    [xcen,ycen]=ginput(1);  %%manual selection of points
%    xcen=round(xcen);
%    ycen=round(ycen);

%    xcen=28;  %%manual point entry
%    ycen=11;
b=1;
%% auto scan for max circulation selection %%
for ycen=11:20
   a=1;
   for xcen=11:28

  boxwidth=10;

for iter=1:boxwidth

    cbox=iter;

    hold on;
    plot([xcen-cbox,xcen-cbox],[ycen-cbox,ycen+cbox],'y-')
```

```
plot([xcen+cbox,xcen+cbox],[ycen-cbox,ycen+cbox],'y-')
plot([xcen-cbox,xcen+cbox],[ycen-cbox,ycen-cbox],'y-')
plot([xcen-cbox,xcen+cbox],[ycen+cbox,ycen+cbox],'y-')
plot([xcen],[ycen],'c.','markersize',20)
hold off;

%%%%%%%%circulation via vorticity%%%%%%%%%%%%%
fprintf('\nCirculation via vorticity');
vor_gamma=0;
for p=xcen-cbox:xcen+cbox
   for q=ycen-cbox:ycen+cbox
      vor_gamma = vor_gamma + vortex(q,p);
   end
end
vor_gamma;

gamma_vor=(sum(sum(vortex(ycen-cbox:ycen+cbox, xcen-
cbox:xcen+cbox))))*dx^2;

un=reshape(un,nx,ny);
vn=reshape(vn,nx,ny);

%%%%%%%%%circulation via velocity%%%%%%%%

%       fprintf('Circulation via velocity \n');
for e=xcen-cbox:xcen+cbox
   gamma_vel=un(e,ycen+cbox)+gamma_vel;
   gamma_vel=-un(e,ycen-cbox)+gamma_vel;
end
for j=ycen-cbox:ycen+cbox
   gamma_vel=vn(xcen-cbox,j)+gamma_vel;
```

```
            gamma_vel=-vn(xcen+cbox,j)+gamma_vel;
        end
        gamma_vel=gamma_vel*dx;

        gamma_itervor(iter)=gamma_vor;
        gamma_itervel(iter)=-gamma_vel;
        gamma_voriter(iter)=vor_gamma;
 end

        individual_vorticity(a,b)=max(gamma_itervor);
        individual_velocity(a,b)=max(gamma_itervel);

    a=a+1;
       end
    b=b+1;
   end

      timebased_vorticity(m)=max(individual_vorticity(:));
%       timebased_velocity(m)=max(individual_velocity(:));

      [num, idx] = max(individual_vorticity(:));
      [x y] = ind2sub(size(individual_vorticity),idx);

      timebased_velocity(m)=individual_velocity(x,y);

      m=m+1;
    end

    disp(timebased_vorticity);
    disp(timebased_velocity);
```

```
figure(21)
hold on;
plot(timebased_vorticity,'b-');
plot(timebased_velocity,'r-');
title('Circulation via Velocity (red) & Vorticity (blue)');
set(gca,'xtick',[0 30 60 90 120 150 180 210 240 270 300 330 360]);
set(gca,'xticklabel',[0 2 4 6 8 10 12 14 16 18 20 22 24]);
xlabel('Time [sec]');
ylabel('\Gamma [cm^2/s]');
hold off

save('timebased_values','timebased*');
save('abc','individual*');
save('aaa','timebased*');

save('pqr','individual*');
save('ppp','timebased*');

return

function [x,y,u,v,vel,vorticity,bat]=dpiv(run,batch,basepath,scale,convel,convor,pulse)
%%%%%%%%%%%% MATLAB Function for DPIV output data files%%%%%%%%%

%read in the batch number for image number
bat=int2str(batch);

% file and path names

if batch < 10
   bat=strcat('_00000',bat);
```

```
    else
       if batch < 100
          bat=strcat('_0000',bat);
       else
          if batch < 1000
             bat=strcat('_000',bat);
          else
             bat=strcat('_00',bat);
          end
       end
    end

    lptfile=strcat(run,bat,'.dat');

    % read data file into header and tensor arrays

[x,y,u,v,vel,dum1,dum2,dum3,vorticity,dum5]=textread(lptfile,'%n%n%n%n%n%n%n%n%n%n','delimiter',',','headerlines',3);

    fprintf(' Reading single tensor file %s\n',lptfile)

    u=u/convel;
    v=v/convel;
    x=x/scale;
    y=y/scale;
    vorticity=vorticity/pulse;

    return
```

MatLab code for 3D contour volume visualization

```
load('xxx.mat')
ntot=375;        %Enter ntot value from the dimension of p matrix
[X,Y,Z]=meshgrid(1:38,1:30,1:ntot);
contourslice(X,Y,Z,p,[],[],[1:ntot],linspace(1,ntot,ntot));
grid on;
axis equal;
set(gca,'xtick',[10 20 30]);
set(gca,'xticklabel',[5 10 15]);
xlabel('x[cm]');
set(gca,'ytick',[10 20 30]);
set(gca,'yticklabel',[5 10 15]);
ylabel('y[cm]');
set(gca,'ztick',[0 30 60 90 120 150 180 210 240 270 300 330 360]);
set(gca,'zticklabel',[0 2 4 6 8 10 12 14 16 18 20 22 24]);
zlabel('Time [sec]');
camup([0 1 0]);
box on;
set(gca,'Color',[0.3 0.3 0.3]);
caxis([0 15]);
```

```
view([135 45 45]);
axis tight;
%%change perspective to X axis up
%#### for side view#######
%view([90 0 0]);
```

MatLab code for creating Non-Dimensional Analysis and plotting

```
a=(6/60)*(2*2.54)^2
b=(7.5/60)*(2*2.54)^2;
c=(9/60)*(2*2.54)^2;
d=(9/60)*(2*2.54)^2;
e=(10.5/60)*(2*2.54)^2;
f=(12/60)*(2*2.54)^2;
A=timebased_vorticity_075_001/a;
B=timebased_vorticity_075_002/b;
C=timebased_vorticity_075_003/c;
D=timebased_vorticity_075_004/d;
E=timebased_vorticity_075_005/e;
F=timebased_vorticity_075_006/f;
%%%%%%%%%%%%%%%%%%%%%%%%%%%%%%%%%%%%%%%%%
 p=max(A)/(2*2.54)^2;
q=max(B)/(2*2.54)^2;
r=max(C)/(2*2.54)^2;
s=max(D)/(2*2.54)^2;
t=max(E)/(2*2.54)^2;
u=max(F)/(2*2.54)^2;
```

```
time_a_new=time*p;
time_b_new=time*q;
time_c_new=time*r;
time_d_new=time*s;
time_e_new=time*t;
time_f_new=time*u;

hold on;
xlabel('t\Gamma/c^2');
ylabel('\Gamma/\omegac^2');
plot(time_a_new,smooth(A),'r-');
plot(time_b_new,smooth(B),'b-');
plot(time_c_new,smooth(C),'g-');
plot(time_d_new,smooth(D),'c-');
plot(time_e_new,smooth(E),'m-');
plot(time_f_new,smooth(F),'k-');
title('Non Dimensional Analysis');
hold off

hold on;
xlabel('t\Gamma/c^2');
ylabel('\Gamma/\omegac^2');
plot(time_a_new,(A),'r-');
plot(time_b_new,(B),'b-');
```

```
plot(time_c_new,(C),'g-');
plot(time_d_new,(D),'c-');
plot(time_e_new,(E),'m-');
plot(time_f_new,(F),'k-');
title('Non Dimensional Analysis');
hold off
%%%%%%%%%%%%%%%%%%%%%%%%%%%%%%%%%%%%%%%%%%%%%%
hold on;
set(gca,'xtick',[0 30 60 90 120 150 180 210 240 270 300 330 360]);
set(gca,'xticklabel',[0 2 4 6 8 10 12 14 16 18 20 22 24]);
xlabel('Time [sec]');
ylabel('\Gamma/\omega*c^2');
plot(A,'r-');
plot(B,'b-');
plot(C,'g-');
plot(D,'c-');
plot(E,'m-');
plot(F,'k-');
title('Non Dimensional Analysis');
hold off
#####NON DIMENSIONAL TIME DATA#####
hold on;
xlabel('t\omega');
ylabel('\Gamma/\omegac^2');
plot(time_a,A,'r-');
```

```
plot(time_b,B,'b-');

plot(time_c,C,'g-');

plot(time_d,D,'c-');

plot(time_e,E,'m-');

plot(time_f,F,'k-');

title('Non Dimensional Analysis');

hold off


omega_b=((6+9)/2)/60;

omega_a=((6+6)/2)/60;

omega_c=((6+12)/2)/60;

omega_d=((9+9)/2)/60;

omega_e=((9+12)/2)/60;

omega_f=((12+12)/2)/60;

time=linspace(1,total_time,ntot);

time_a=time*omega_a;

time_b=time*omega_b;

time_c=time*omega_c;

time_d=time*omega_d;

time_e=time*omega_e;

time_f=time*omega_f;

%COMPARISON FOR TEST 001-006 Non Analysis%%%%%%%%%

hold on;

scatter(time_a(51:300),A(51:300),'r'); scatter(time_b(51:300),B(51:300),'b') ;
scatter(time_c(51:300),C(51:300),'g');scatter(time_d(51:300),D(51:300),'c');scatter(time_
e(51:300),E(51:300),'m');scatter(time_f(51:300),F(51:300),'k');
```

```
Total=[A(1:300);B(1:300);C(1:300);D(1:300);E(1:300);F(1:300)];

Total_100C=mean(Total,1);

total_time=[time_a(1:300);time_b(1:300);time_c(1:300);time_d(1:300);time_e(1:300);ti
me_f(1:300)];

total_time_100C=mean(total_time,1);

scatter(total_time_100C(51:300),Total_100C(51:300),'y');

xlabel('t\omega');

ylabel('\Gamma/\omegac^2');

title('Non Dimensional Analysis');

hold off

hold on;

plot(total_time_075(51:300),smooth(Total_075(51:300)),'r-');

plot(total_time_075B(51:300),smooth(Total_075B(51:300)),'b-');

plot(total_time_075C(51:225),smooth(Total_075C(51:225)),'g-');

plot(total_time_100(51:300),smooth(Total_100(51:300)),'y-');

plot(total_time_100B(51:300),smooth(Total_100B(51:300)),'c-');

plot(total_time_100C(51:300),smooth(Total_100C(51:300)),'m-');

xlabel('t\omega');

ylabel('\Gamma/\omegac^2');

title('Non Dimensional Analysis');

box on;

grid on;

hold off
```

MatLab code for Vortex Position and plotting of non dimensional analysis

```
load('positions.mat')

load('PARAMATARS_075.mat')


%%Create x, y vortex position matrix

xc_a_075B_001=[xc_a(1),xc_a(1),xc_a(1),xc_a];

yc_a_075B_001=[yc_a(1),yc_a(1),yc_a(1),yc_a];

xc_b_075B_001=[xc_b(1),xc_b(1),xc_b(1),xc_b];

yc_b_075B_001=[yc_b(1),yc_b(1),yc_b(1),yc_b];


%%%%plot vortex position with time%%%%

figure(1)

hold on;

xlabel('t\omega');

ylabel('\Gamma/\omegac^2');

box on; grid on;

title('Vortex Position');

h1=plot(time_a,smooth(A),'k-');

h2=plot(time_a,smooth(yc_a_075B_001),'r');
h3=plot(time_a,smooth(yc_b_075B_001),'b');
```

```
set(h1,'Linewidth',2);
set(h2,'Linewidth',2);
set(h3,'Linewidth',2);
set(gca,'Linewidth',2);
hold off
saveas(gcf,'VortexPosition_075B_001-1','png')

figure(2)
hold on;
title('Vortex Position');
xlabel('t\omega');
set(gca,'ytick',[10 20 30]);
set(gca,'yticklabel',[5 10 15]);
ylabel('y[cm]');
box on; grid on;
h=plot(time_a,smooth(yc_a_075B_001),'r'); j=plot(time_a,smooth(yc_b_075B_001),'b');
set(h,'Linewidth',2);
set(j,'Linewidth',2);
set(gca,'Linewidth',2);
saveas(gcf,'VortexPosition_075B_001-2','png')
hold off

figure(3)
hold on;
title('Vortex Position');
```

```
xlabel('t\Gamma/c^2');

set(gca,'ytick',[10 20 30]);

set(gca,'yticklabel',[5 10 15]);

ylabel('y[cm]');

box on; grid on;

h=plot(time_a_new,smooth(yc_a_075B_001),'r');
j=plot(time_a_new,smooth(yc_b_075B_001),'b');

set(h,'Linewidth',2);

set(j,'Linewidth',2);

set(gca,'Linewidth',2);

saveas(gcf,'VortexPosition_075B_001-3','png')

hold off


figure(4)

hold on;

xlabel('t\Gamma/c^2');

ylabel('\Gamma/\omegac^2');

box on; grid on;

title('Vortex Position');

h1=plot(time_a_new,smooth(A),'k-');

h2=plot(time_a_new,smooth(yc_a_075B_001),'r');
h3=plot(time_a_new,smooth(yc_b_075B_001),'b');

set(h1,'Linewidth',2);

set(h2,'Linewidth',2);

set(h3,'Linewidth',2);

set(gca,'Linewidth',2);
```

```
saveas(gcf,'VortexPosition_075B_001-4','png')
hold off
```

APPENDIX B

ADDITIONAL PLOTS:

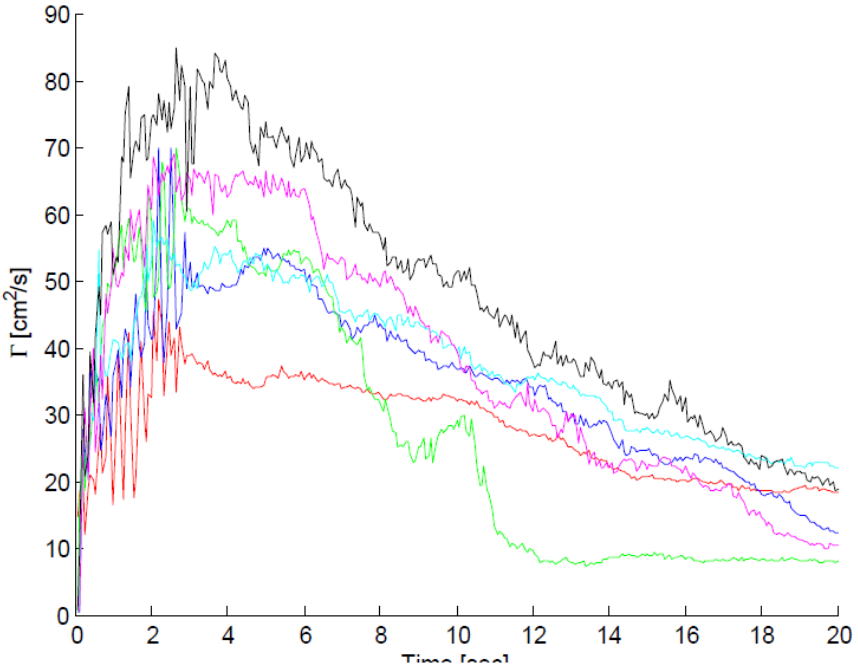

Figure 88 Circulation vs time for 0.75" separation at 25% span

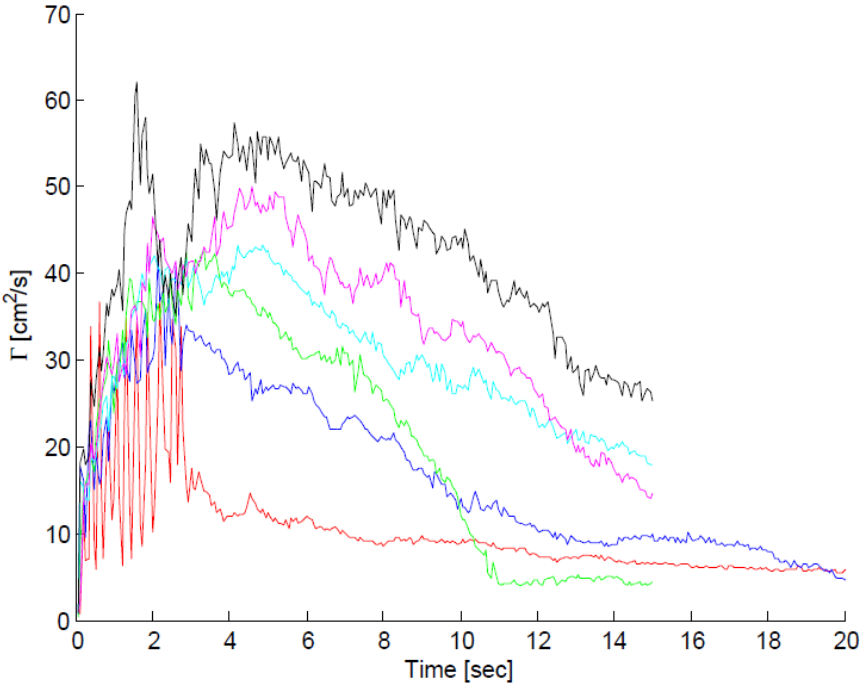

Figure 89 Circulation vs time for 0.75" separation at 5% span

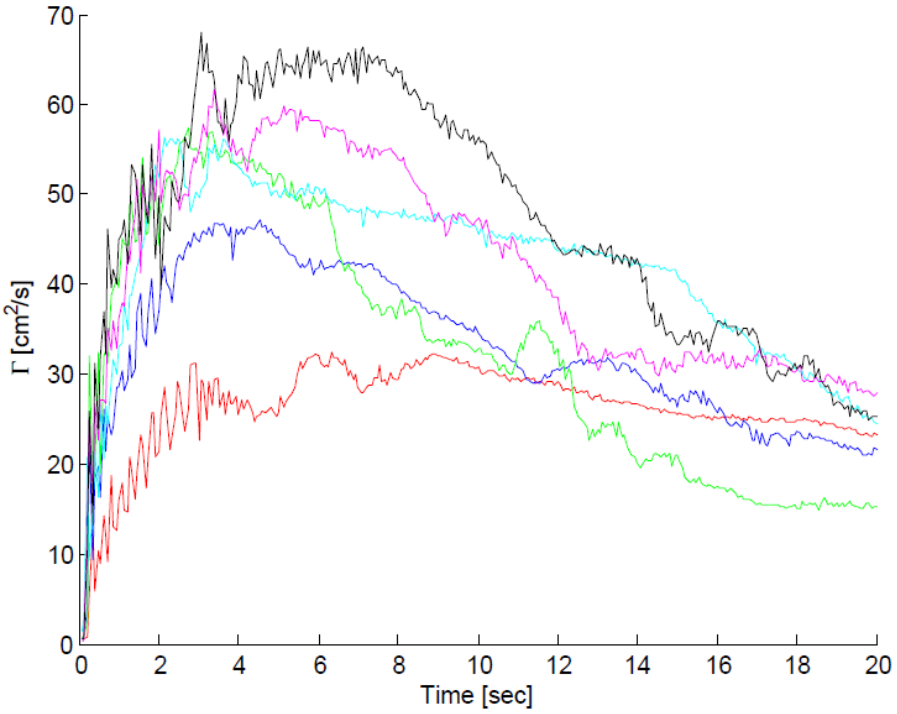

Figure 90 Circulation vs time for 1" separation at centerline

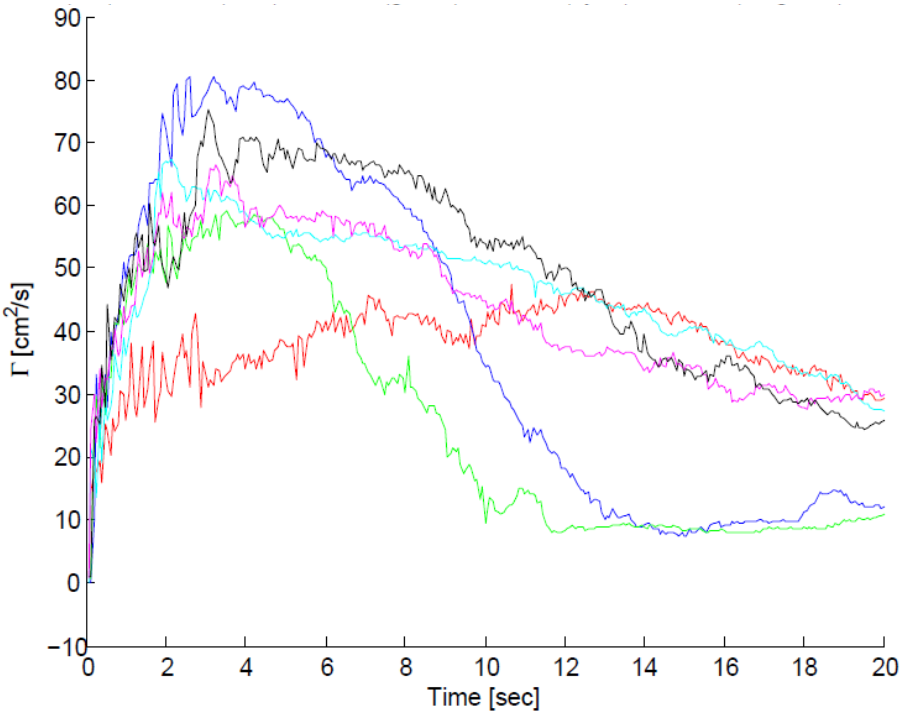

Figure 91 Circulation vs time for 1" separation at 25% span

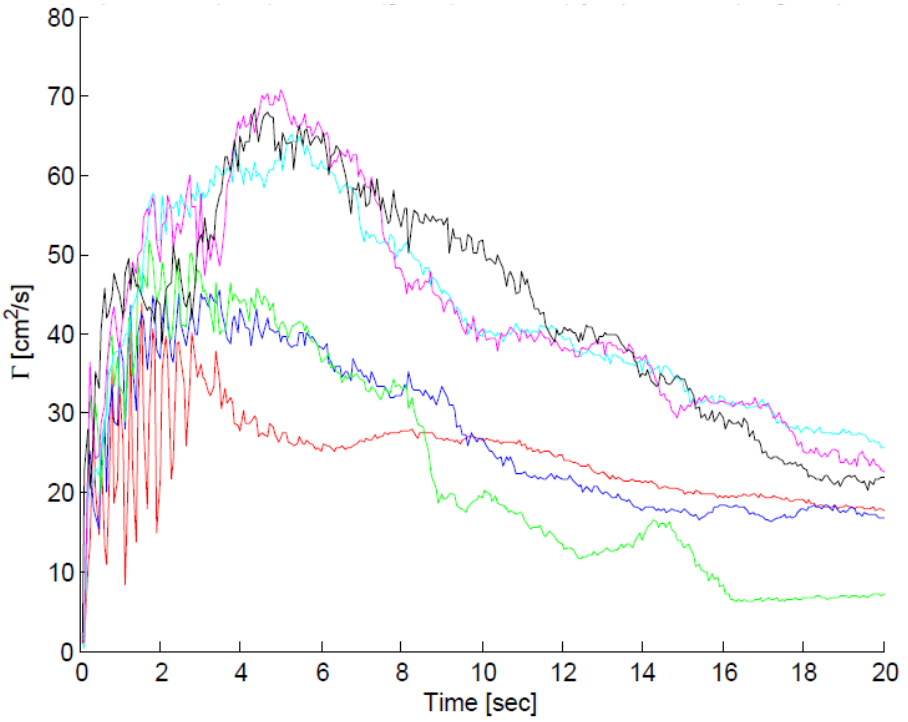

Figure 92 Circulation vs time for 1" separation at 5% span

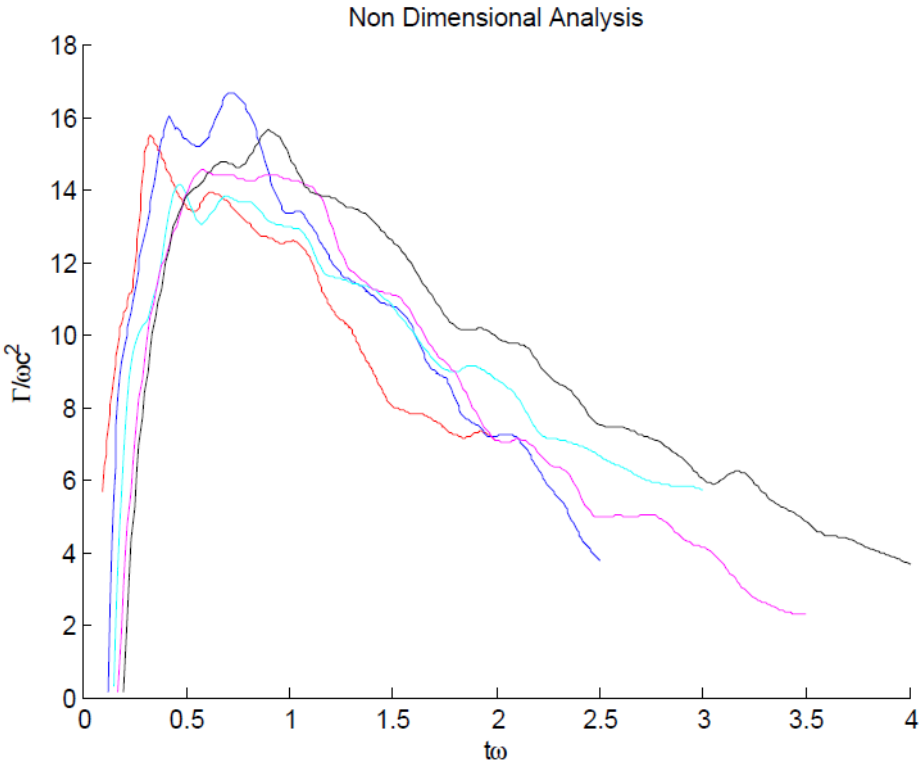

Figure 93 Non Dimensional Analysis for 0.75" separation at 25% span

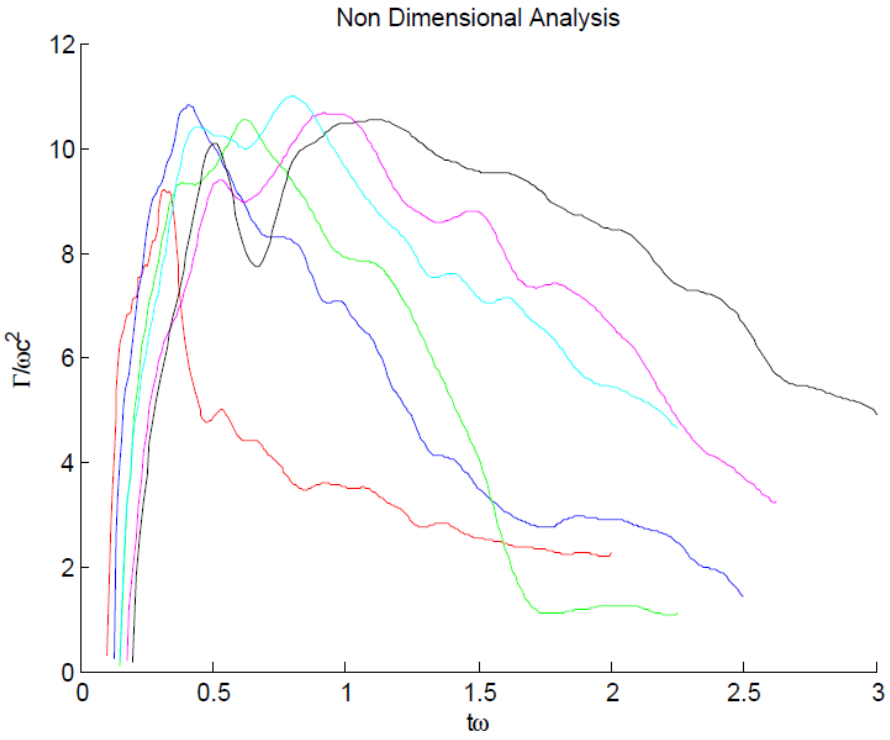

Figure 94 Non Dimensional Analysis for 0.75" separation at 5% span

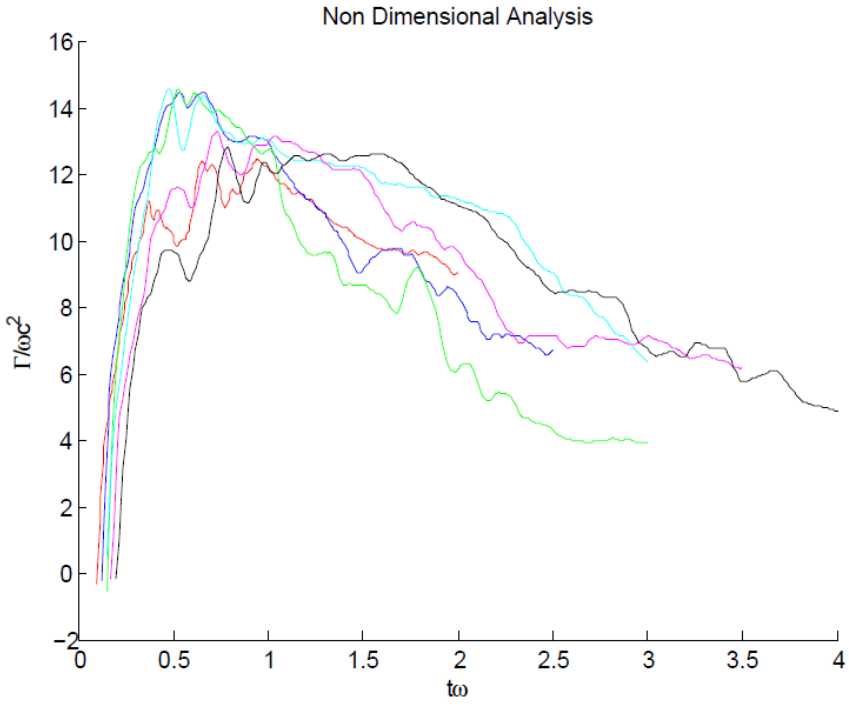

Figure 95 Non Dimensional Analysis for 1" separation at centerline

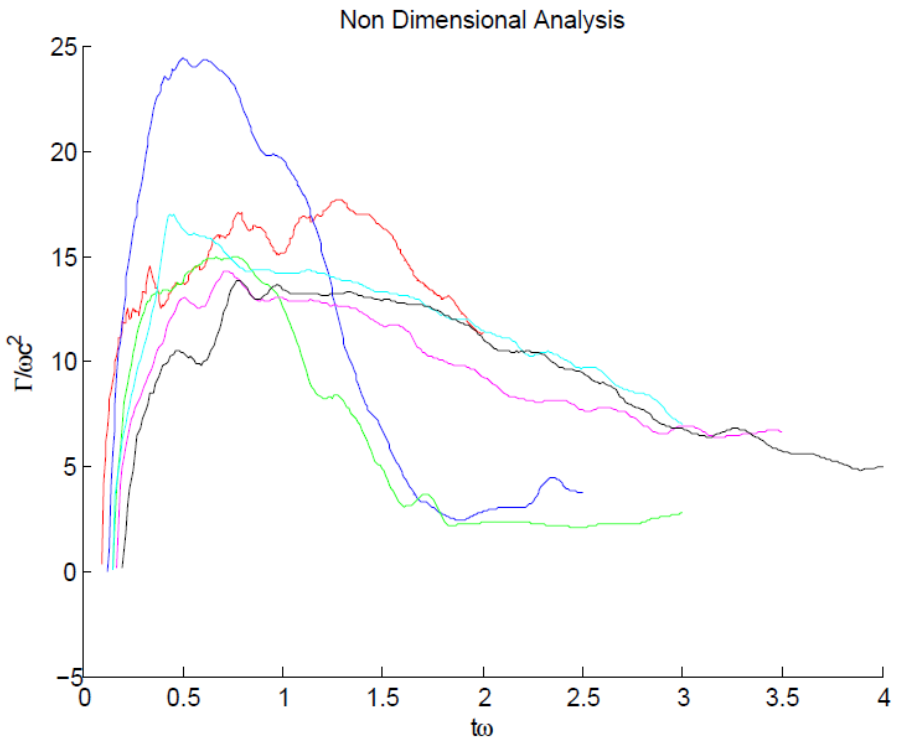

Figure 96 Non Dimensional Analysis for 0.75" separation at 25% span

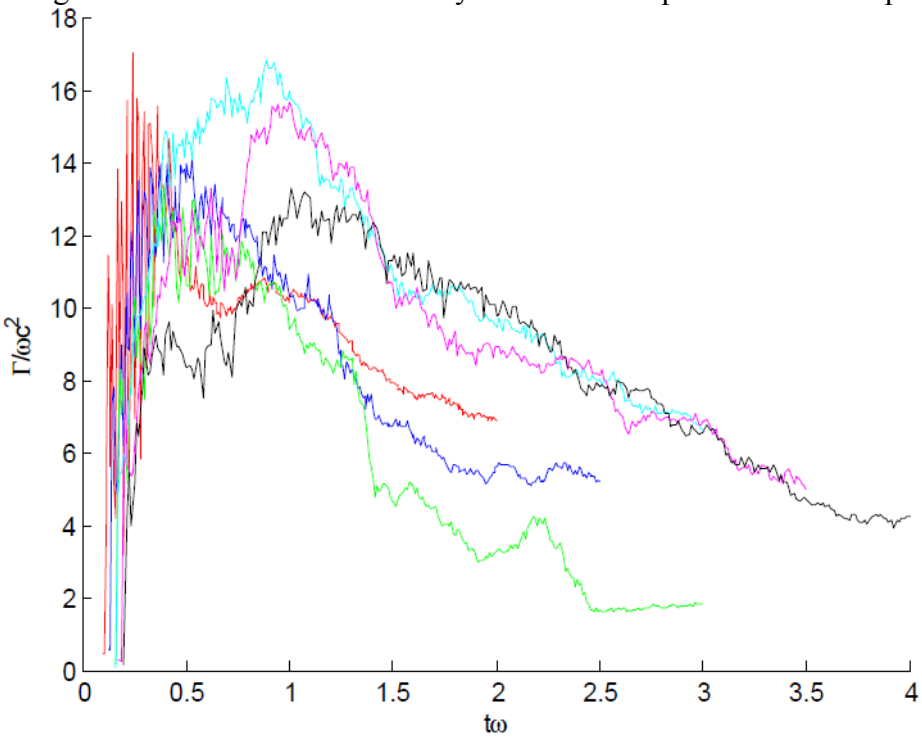

Figure 97 Non Dimensional Analysis for 0.75" separation at 5% span

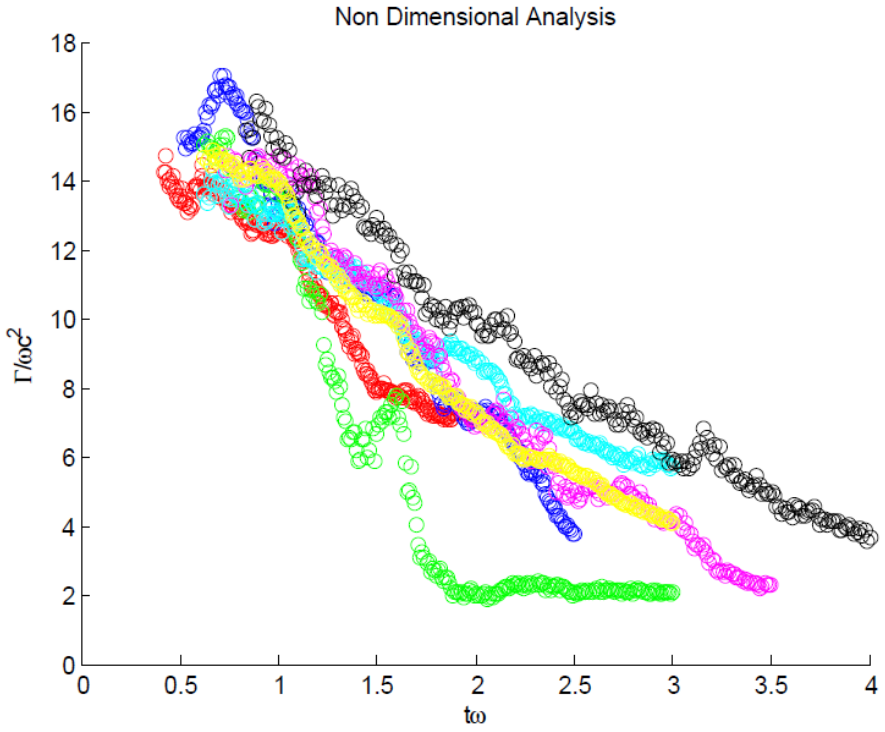

Figure 98 Non Dimensional Analysis for 0.75" separation at 25% span scatter plo

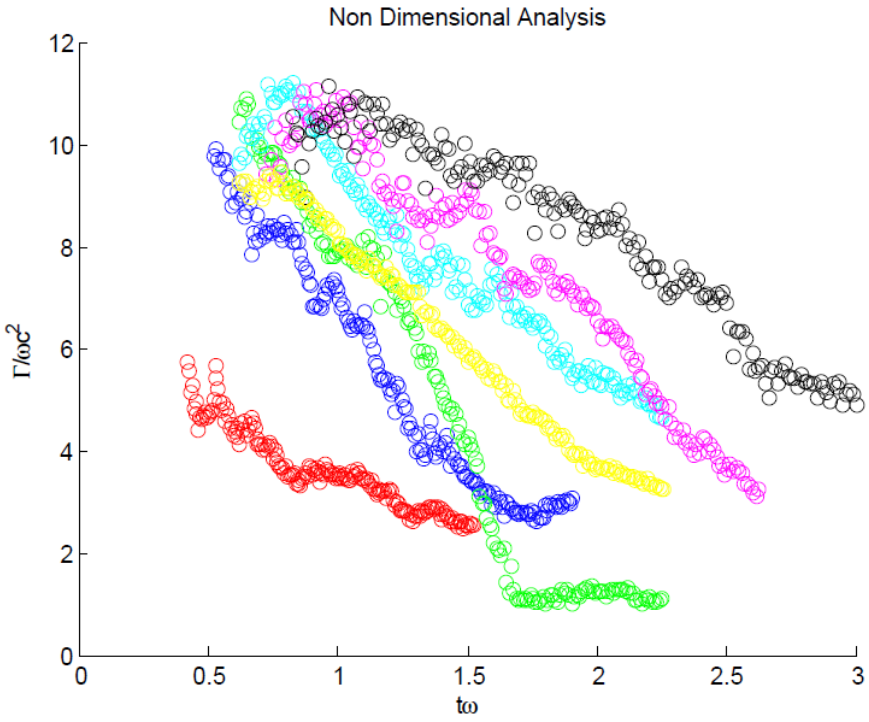

Figure 99 Non Dimensional Analysis for 0.75" separation at 5% span scatter plot

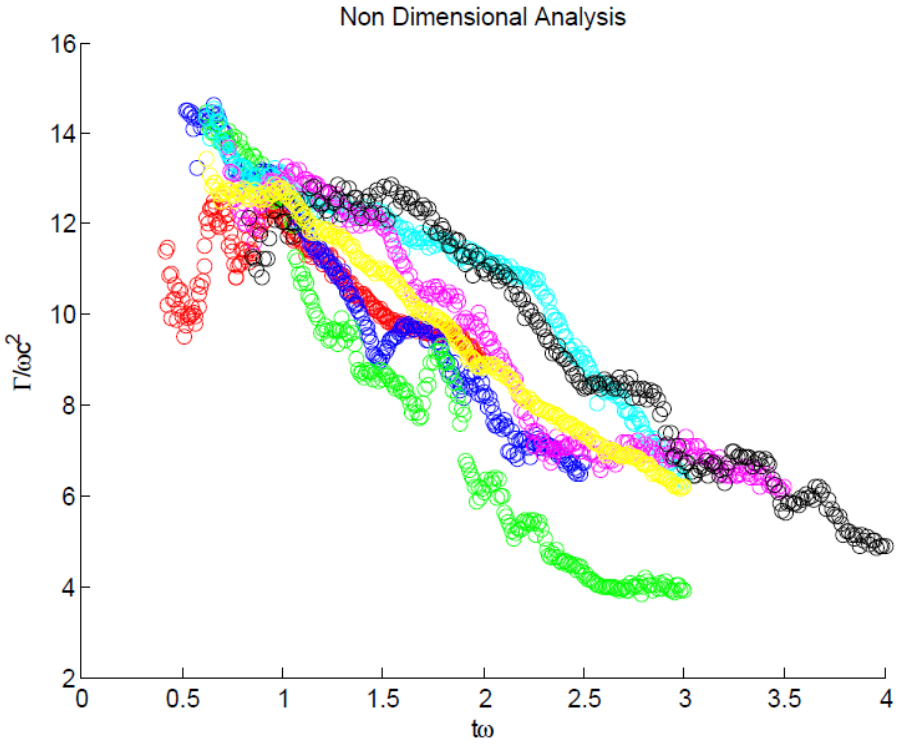

Figure 100 Non Dimensional Analysis for 1" separation at centerline scatter plot

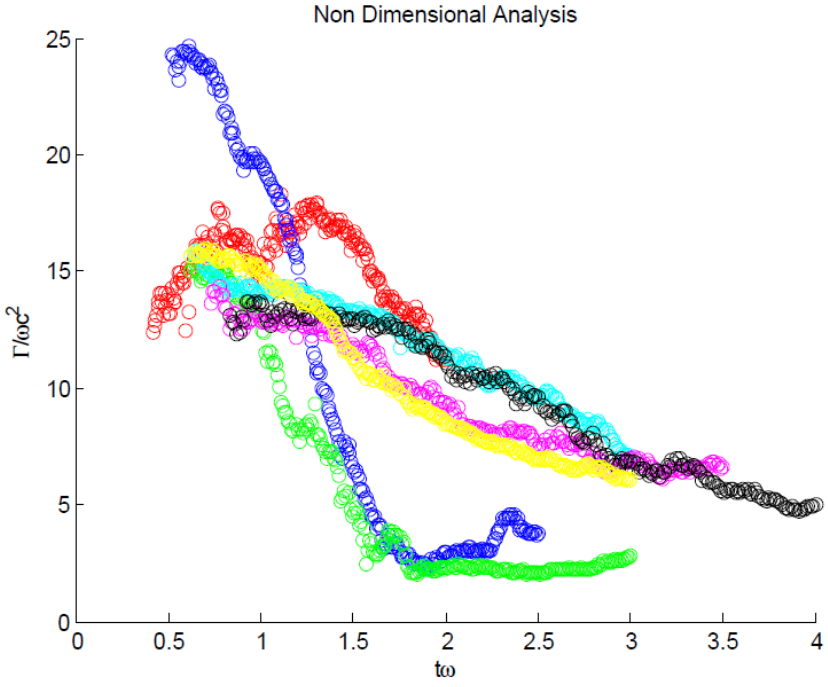

Figure 101 Non Dimensional Analysis for 1" separation at 25% span scatter plot

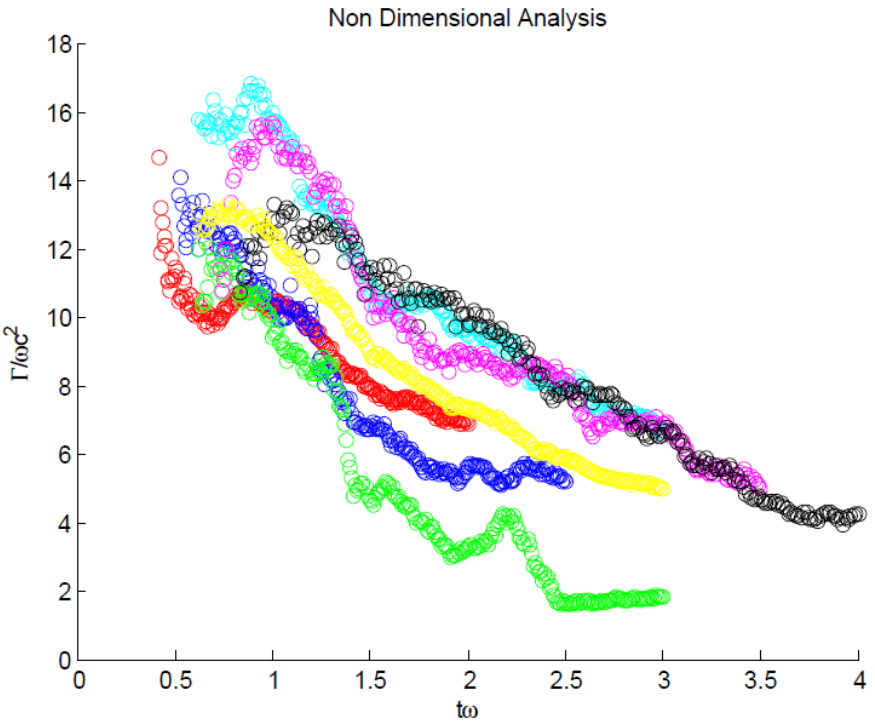

Figure 102 Non Dimensional Analysis for 1" separation at 5% span scatter plot

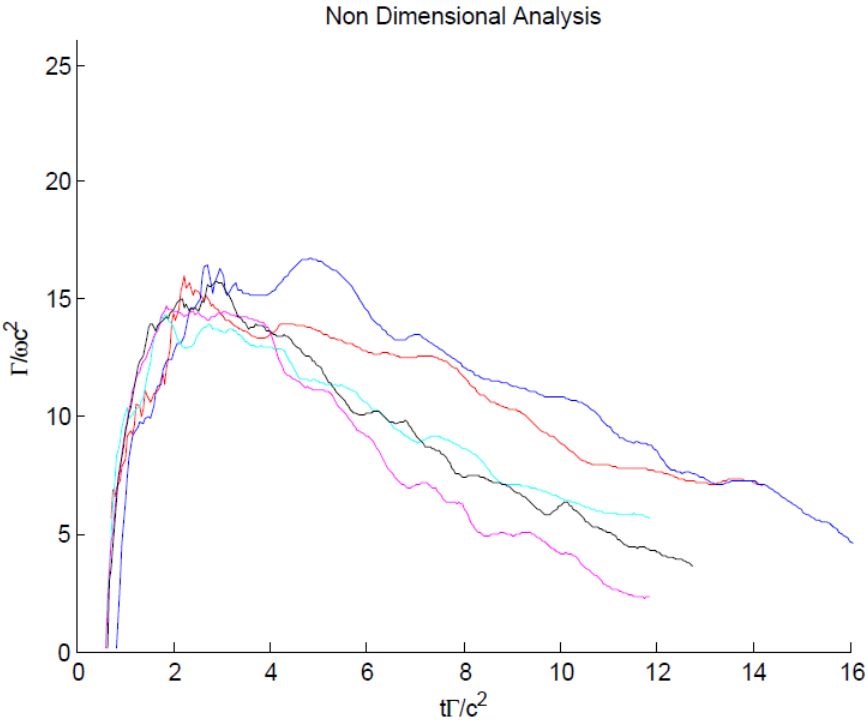

Figure 103 Non Dimensional Analysis for 0.75" separation at 25% span

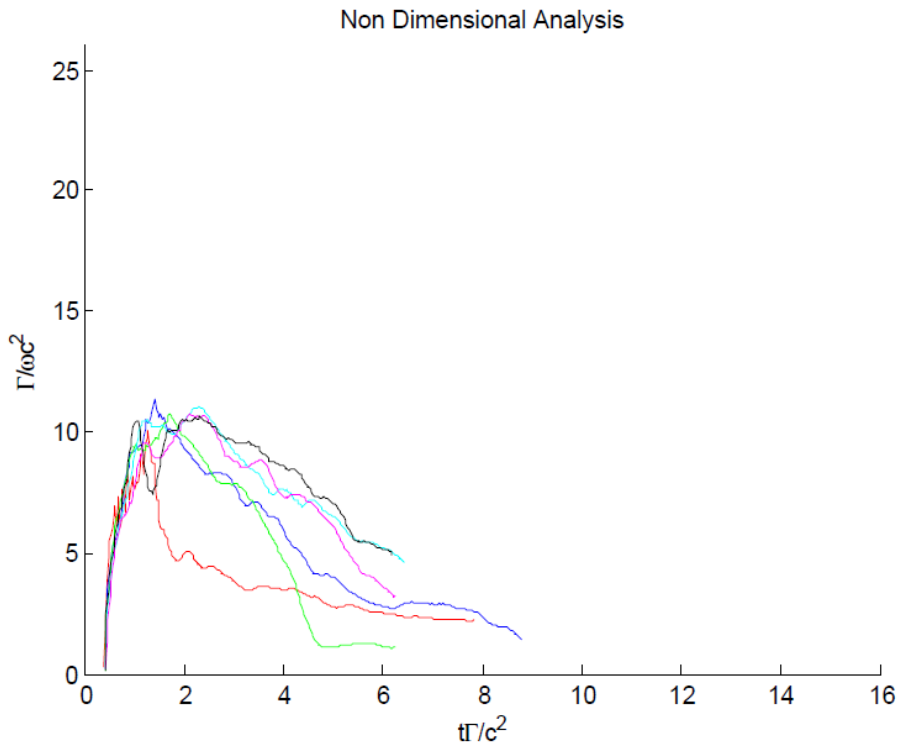

Figure 104 Non Dimensional Analysis for 0.75" separation at 5% span

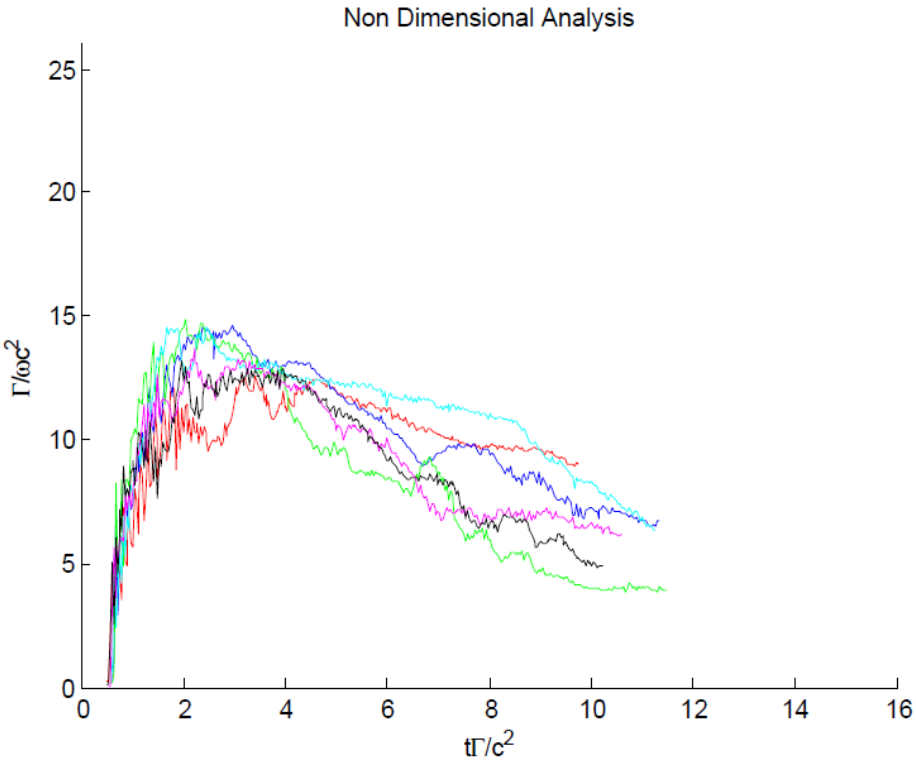

Figure 105 Non Dimensional Analysis for 1" separation at centerline

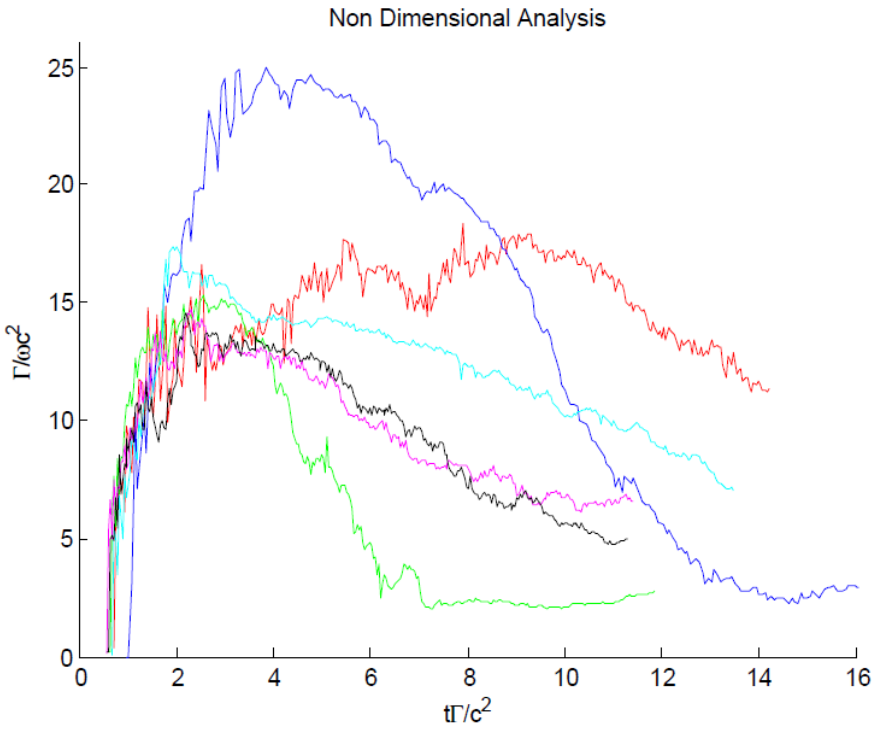

Figure 106 Non Dimensional Analysis for 1" separation at 25% span

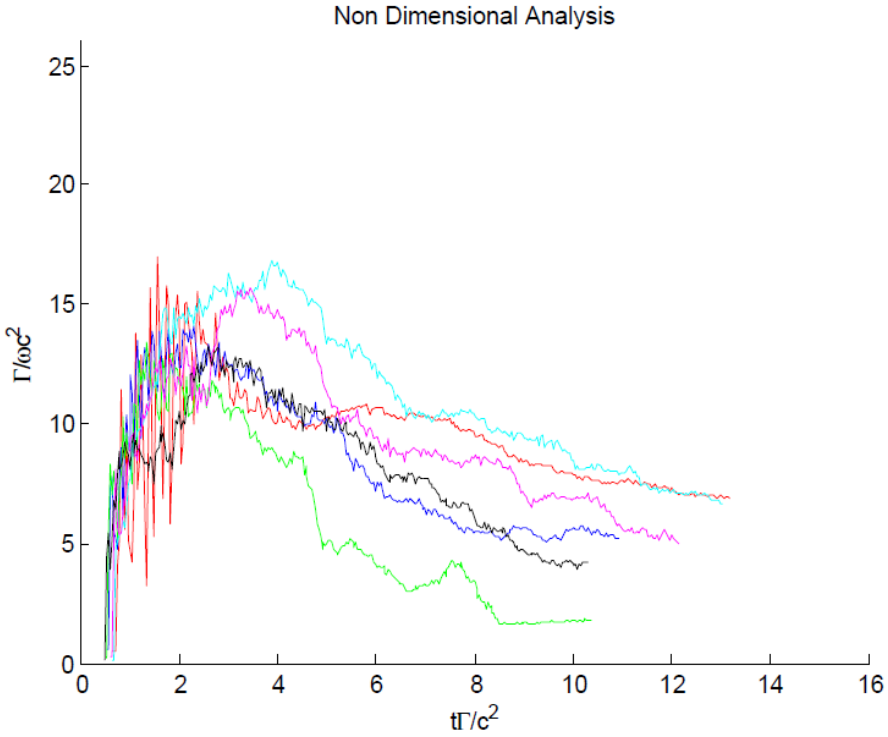

Figure 107 Non Dimensional Analysis for 1" separation at 5% span

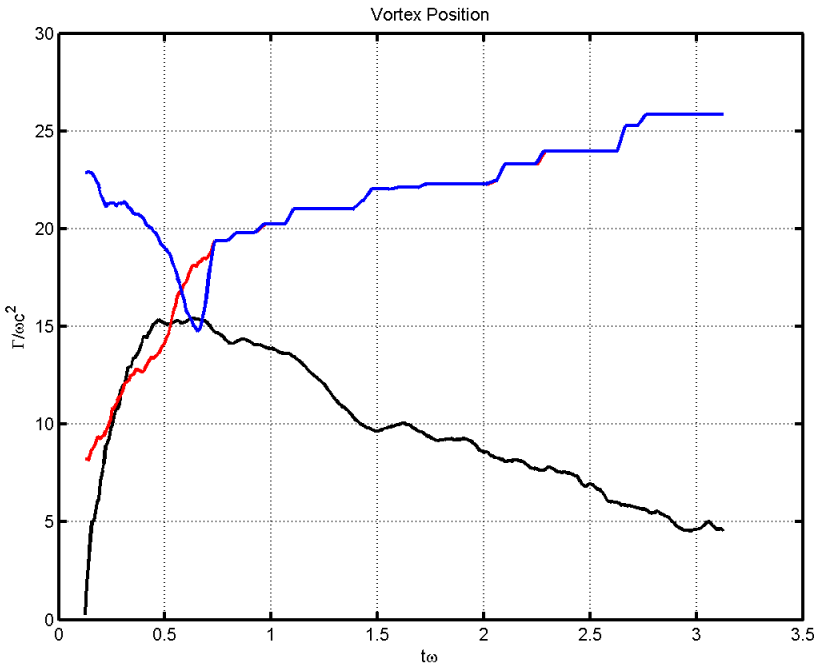

Figure 108 Vortex Position and Non Dimensional Analysis for 0.75" separation asymmetric merger 6rpm, 9rpm

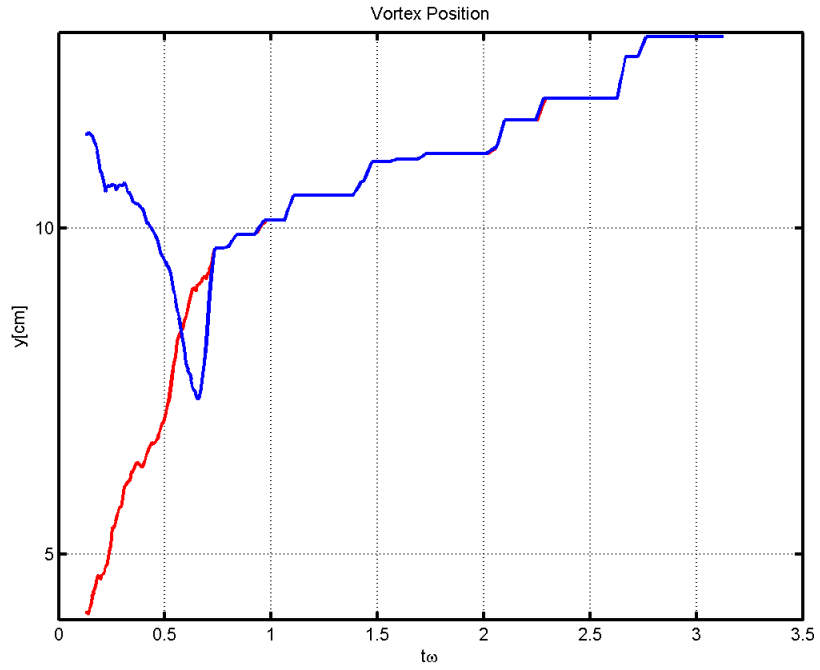

Figure 109 Vortex Positions vs time for 0.75" separation symmetric merger 6rpm, 9rpm

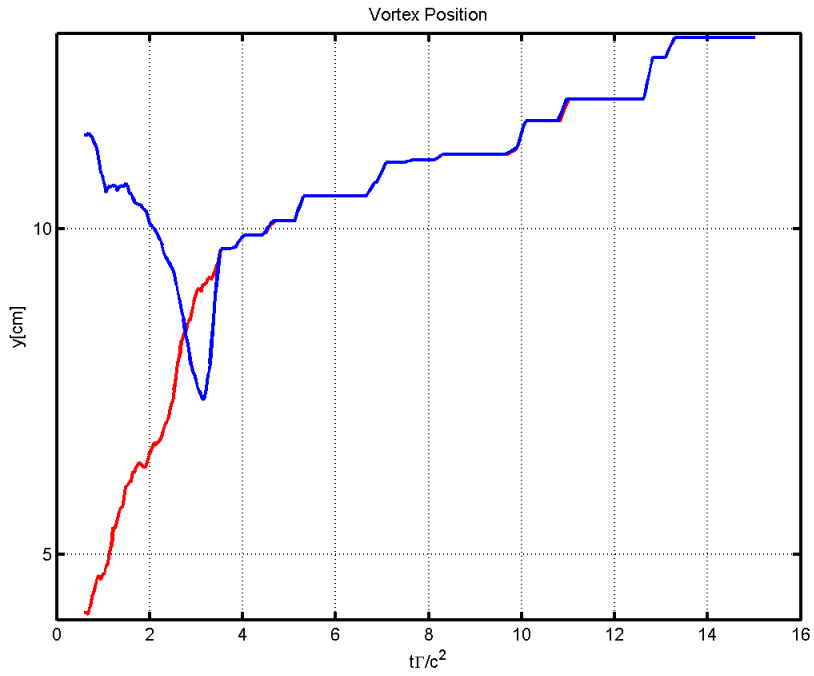

Figure 110 Vortex Position vs Non dimensional time for 0.75" separation asymmetric vortex merger 6rpm, 9rpm

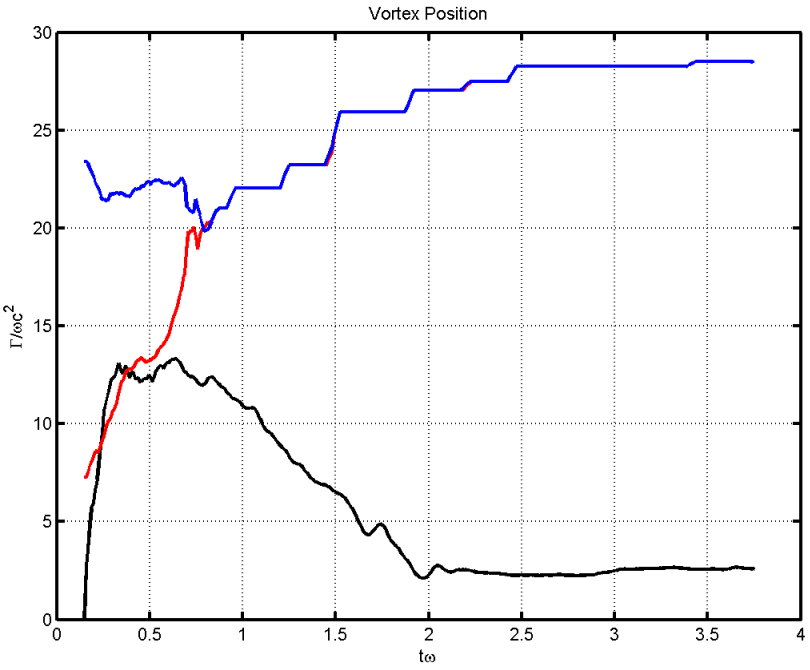

Figure 111 Vortex Position and Non Dimensional Analysis for 0.75" separation asymmetric merger 6rpm, 12rpm

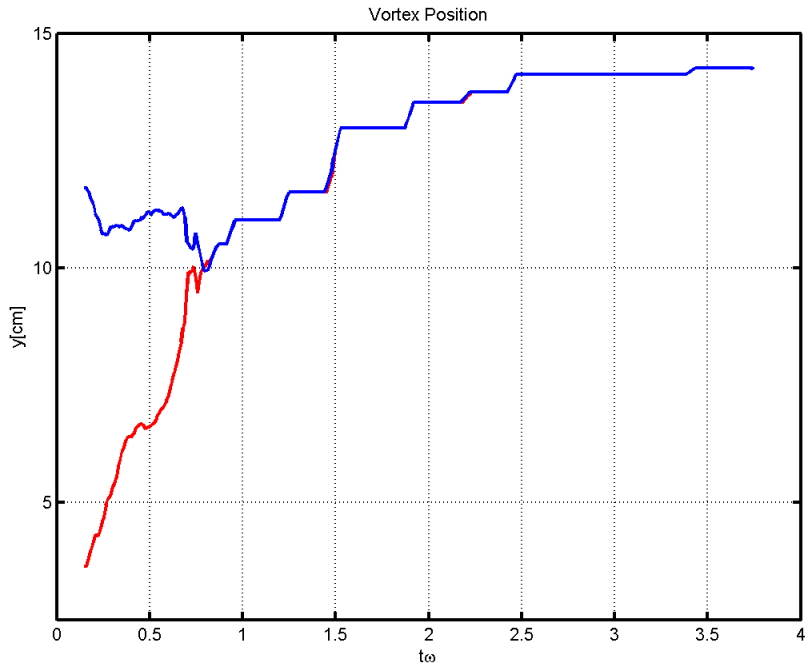

Figure 112 Vortex Positions vs time for 0.75" separation asymmetric merger 6rpm, 12rpm

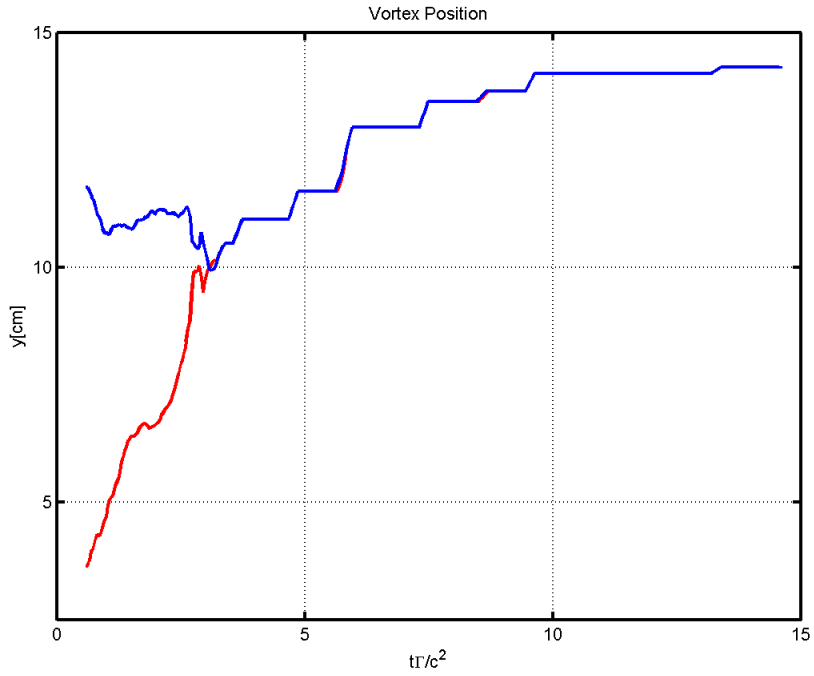

Figure 113 Vortex Position vs Non dimensional time for 0.75" separation asymmetric vortex merger 6rpm, 12rpm

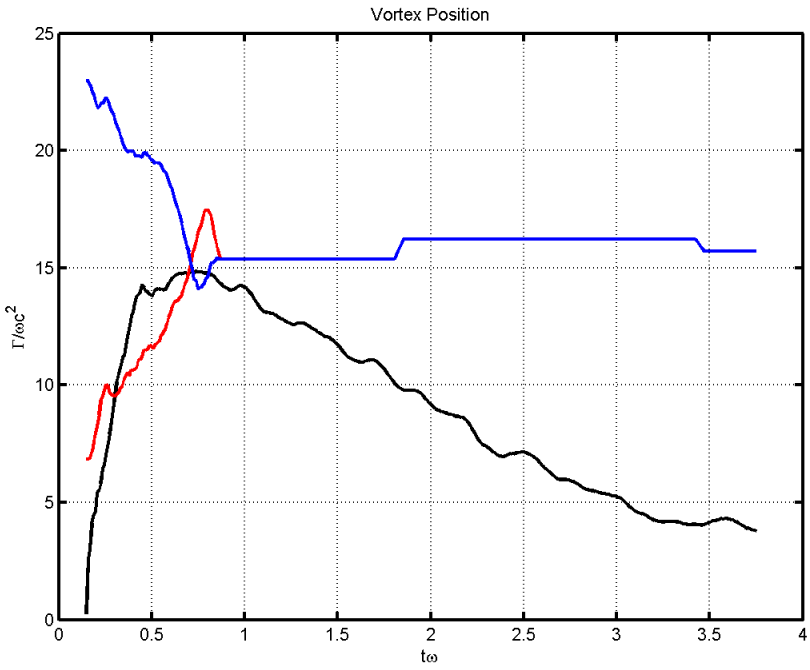

Figure 114 Vortex Position and Non Dimensional Analysis for 0.75" separation symmetric merger 9rpm, 9rpm

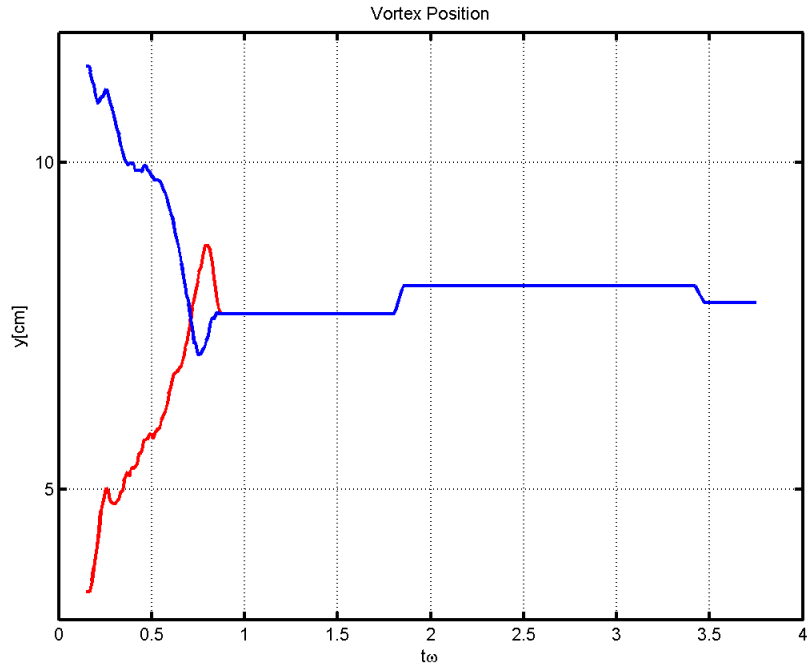

Figure 115 Vortex Positions vs time for 0.75" separation symmetric merger 6rpm, 9rpm

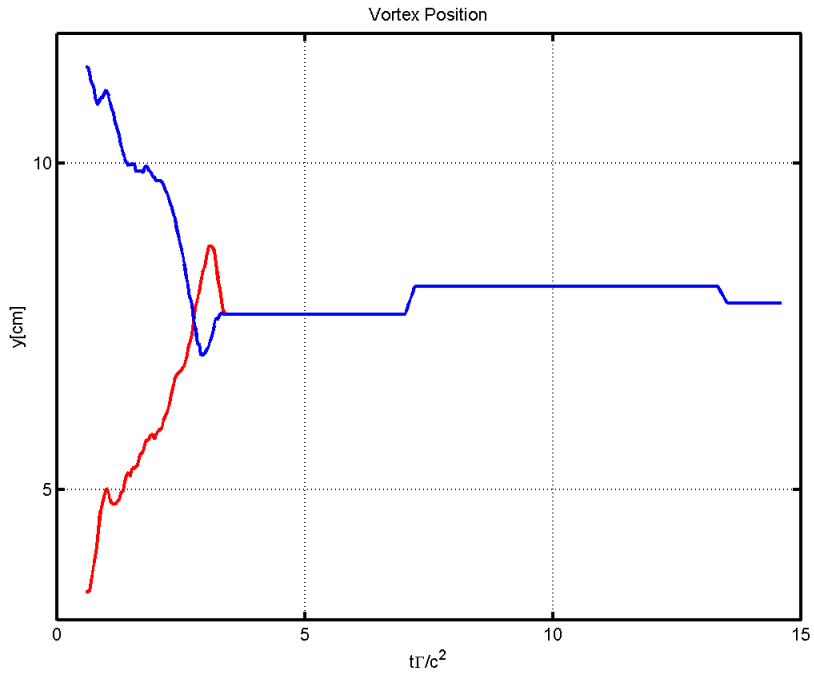

Figure 116 Vortex Position vs Non dimensional time for 0.75" separation symmetric vortex merger 9rpm, 9rpm

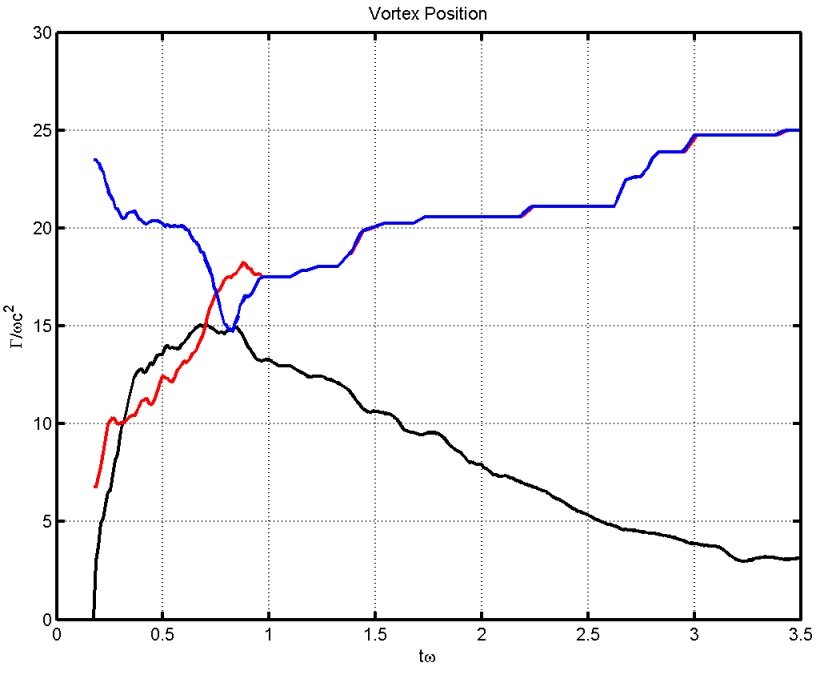

Figure 117 Vortex Position and Non Dimensional Analysis for 0.75" separation symmetric merger 9rpm, 12rpm

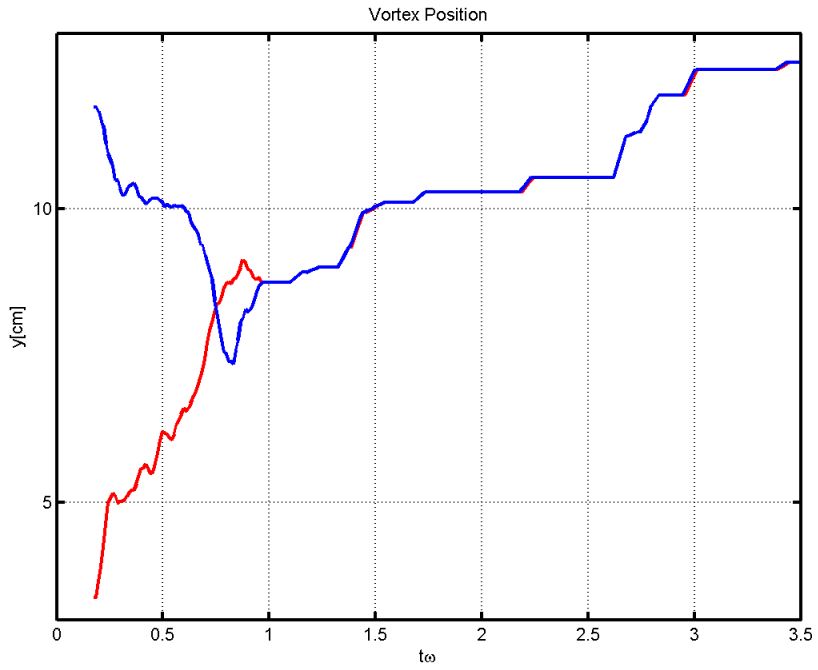

Figure 118 Vortex Positions vs time for 0.75" separation asymmetric merger 9rpm, 12rpm

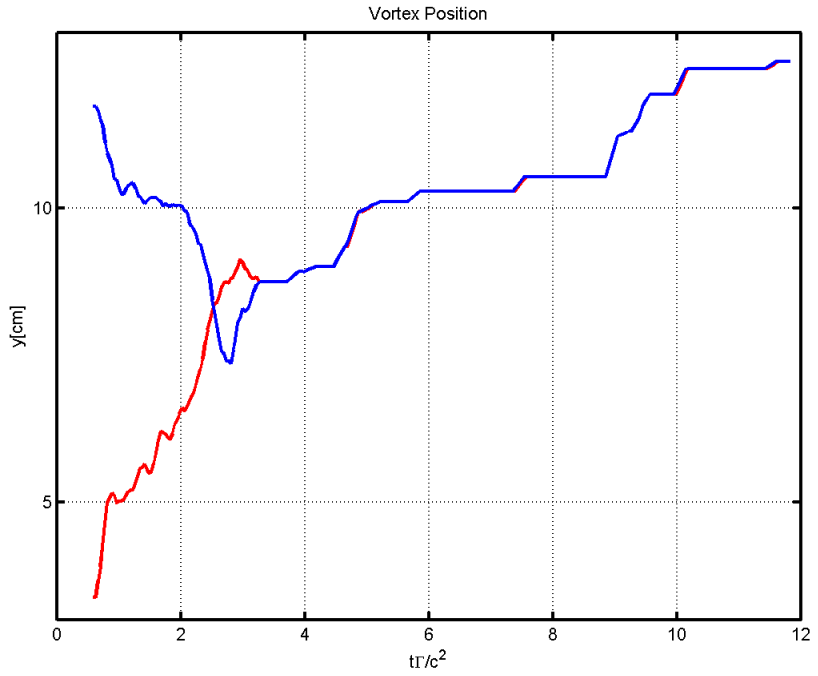

Figure 119 Vortex Position vs Non dimensional time for 0.75" separation asymmetric vortex merger 9rpm, 12rpm

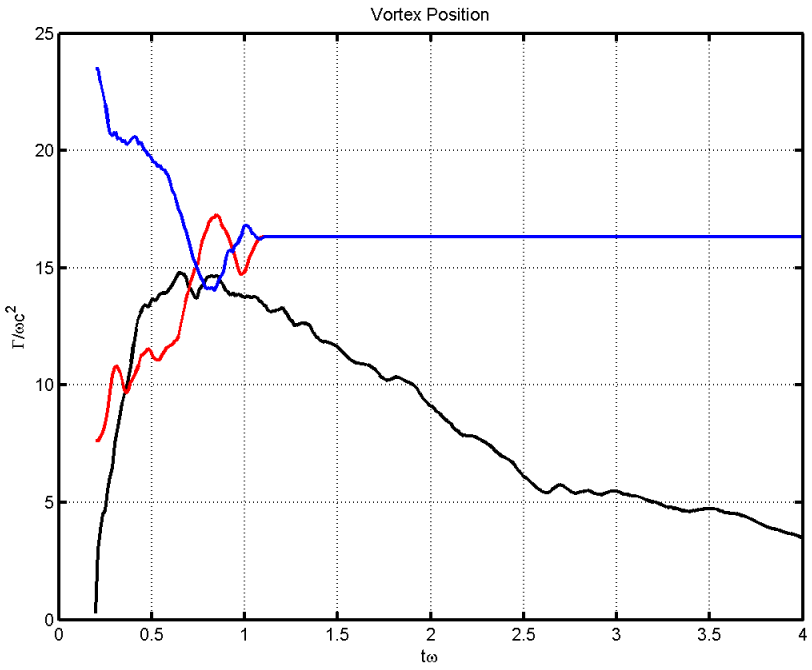

Figure 120 Vortex Position and Non Dimensional Analysis for 0.75" separation symmetric merger 12rpm, 12rpm

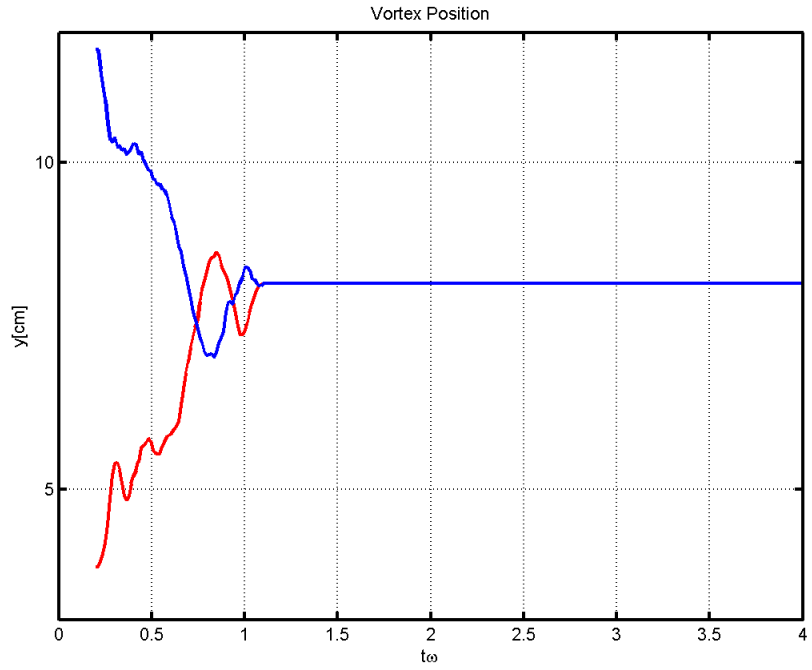

Figure 121 Vortex Positions vs time for 0.75" separation symmetric merger 12rpm, 12rpm

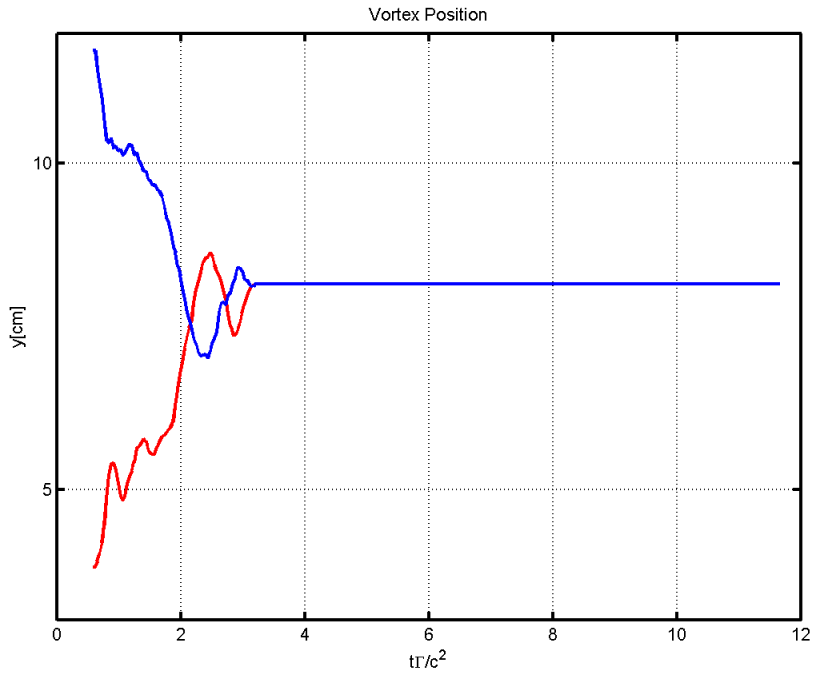

Figure 122 Vortex Position vs Non dimensional time for 0.75" separation symmetric vortex merger 12rpm, 12rpm

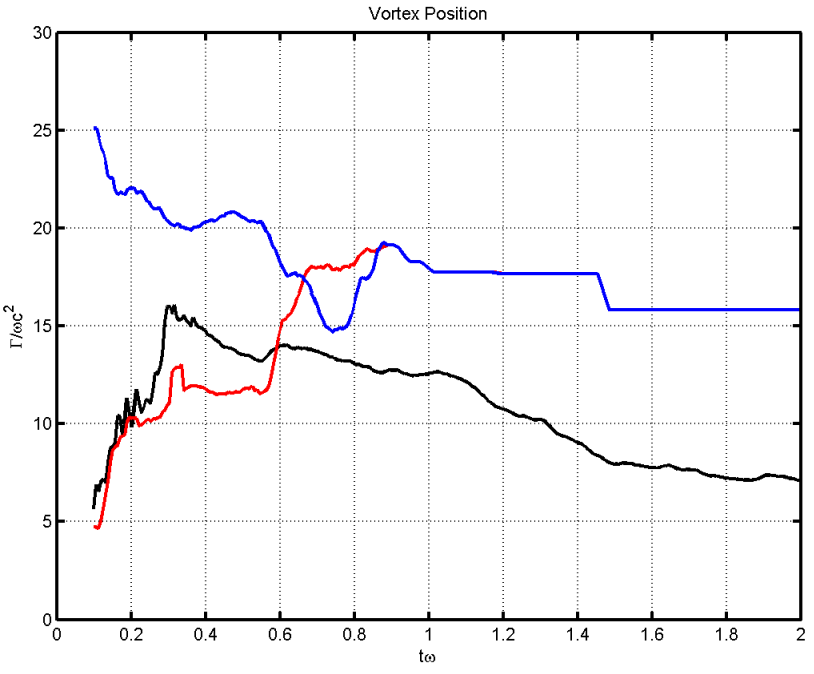

Figure 123 Vortex Position and Non Dimensional Analysis for 0.75" separation symmetric merger 6rpm, 6rpm at 25% span

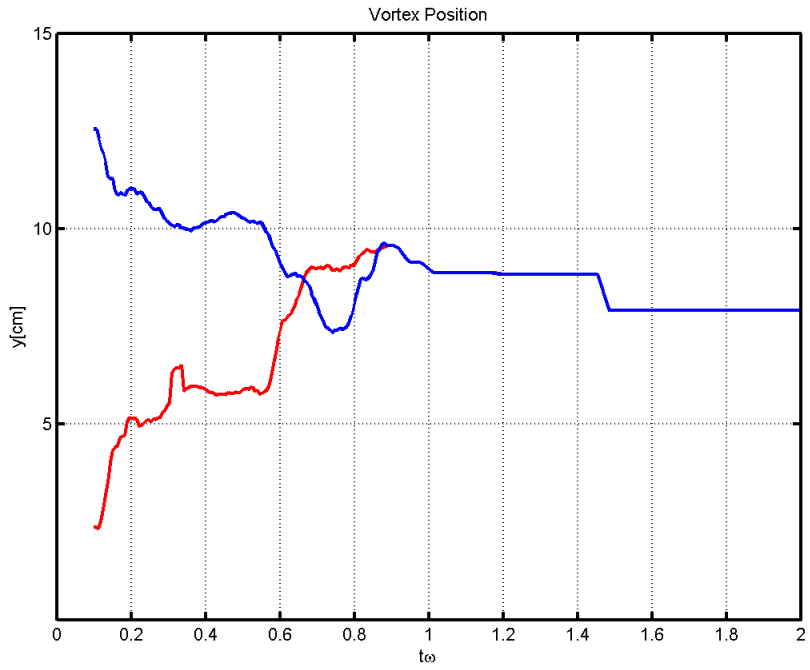

Figure 124 Vortex Positions vs time for 0.75" separation symmetric merger 6rpm, 6rpm at 25% span

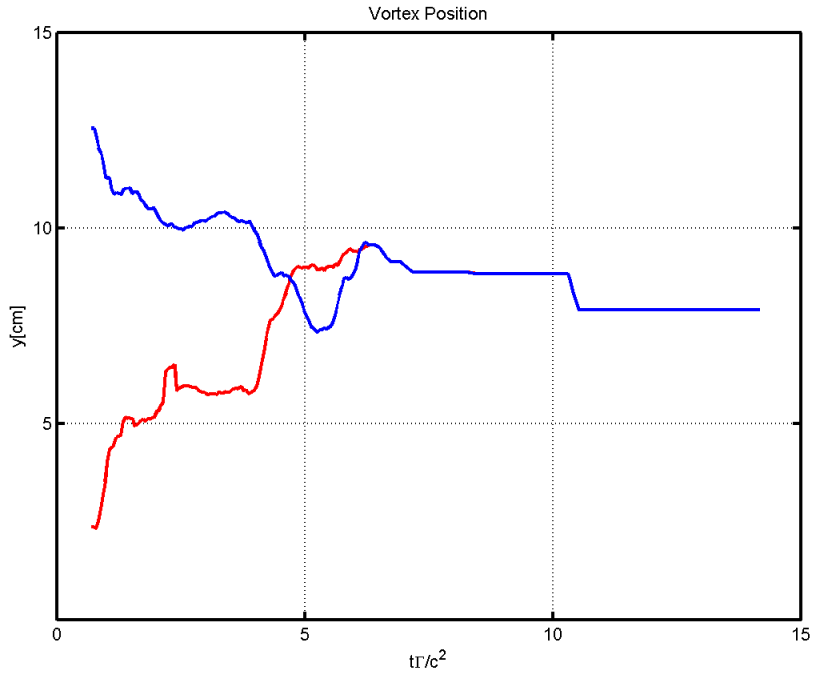

Figure 125 Vortex Position vs Non dimensional time for 0.75" separation symmetric vortex merger 6rpm, 6rpm at 25% span

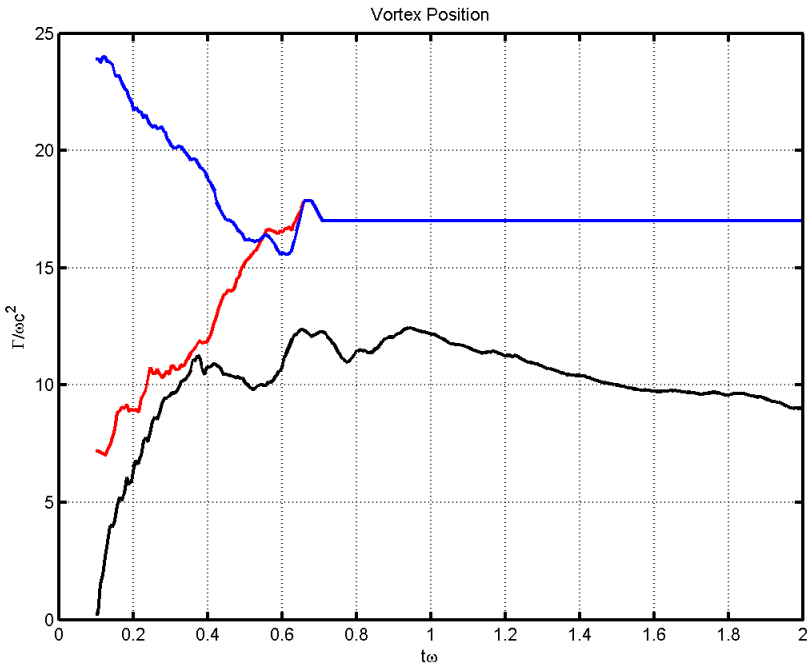

Figure 126 Vortex Position and Non Dimensional Analysis for 1" separation symmetric merger 6rpm, 6rpm

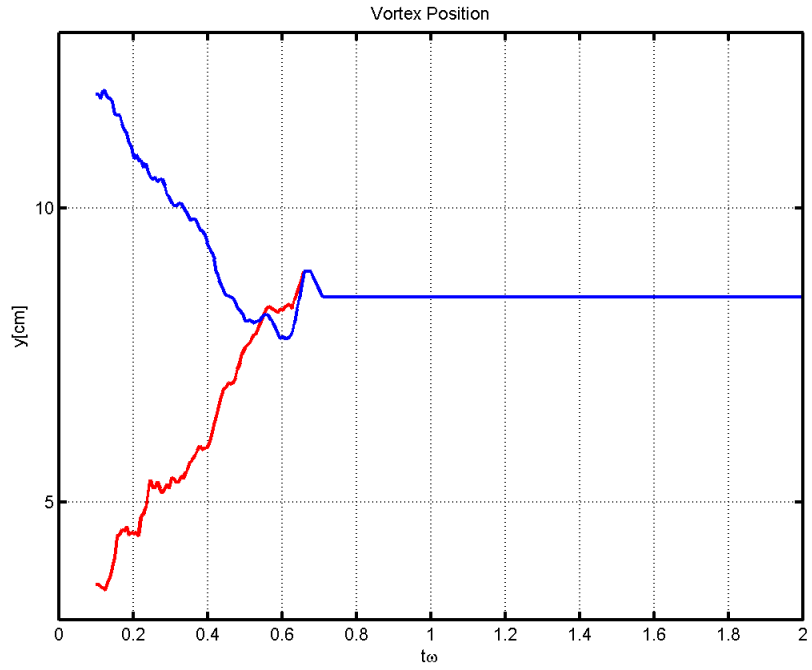

Figure 127 Vortex Positions vs time for 1" separation symmetric merger 6rpm, 6rpm

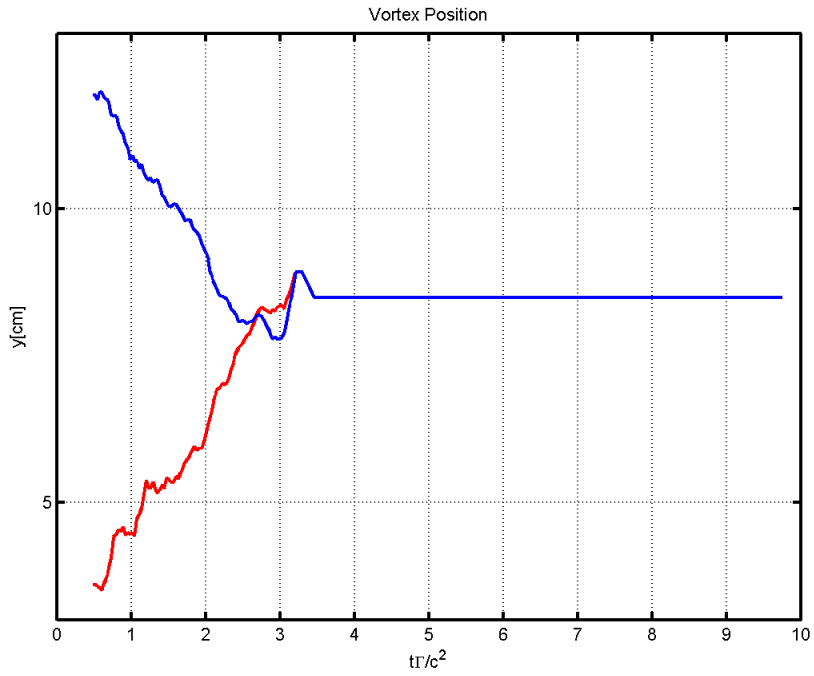

Figure 128 Vortex Position vs Non dimensional time for 1" separation asymmetric vortex merger 6rpm, 9rpm

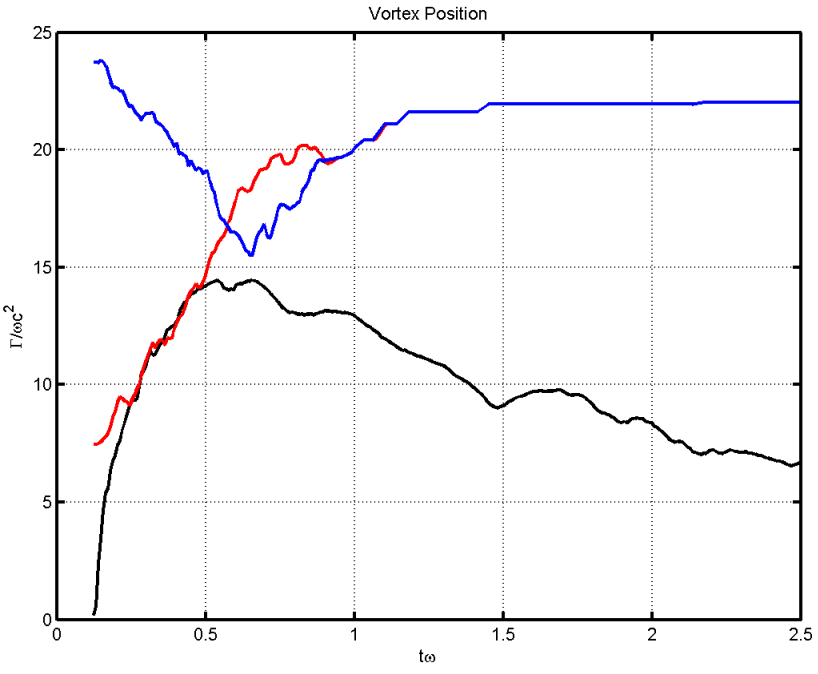

Figure 129 Vortex Position and Non Dimensional Analysis for 1" separation symmetric merger 6rpm, 9rpm

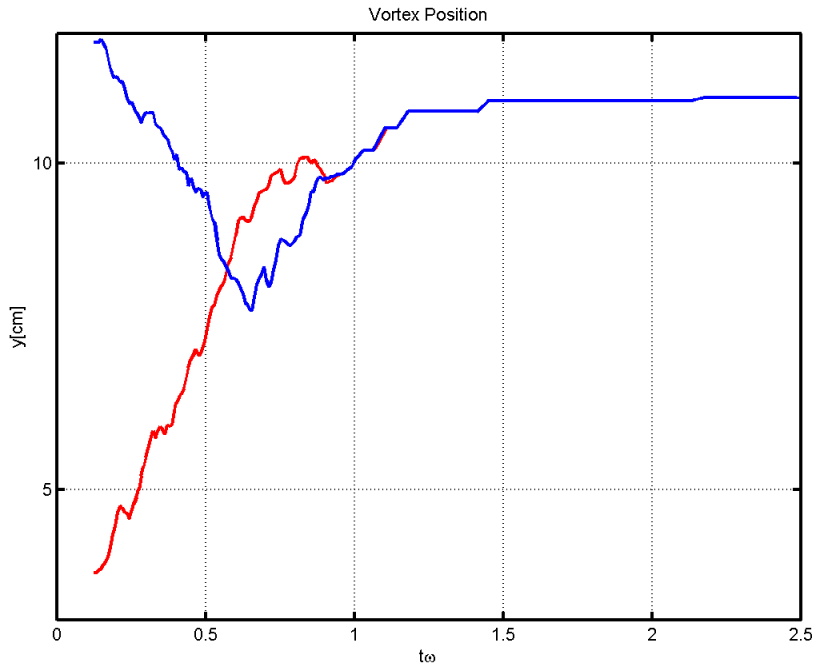

Figure 130 Vortex Positions vs time for 1" separation asymmetric merger 6rpm, 9rpm

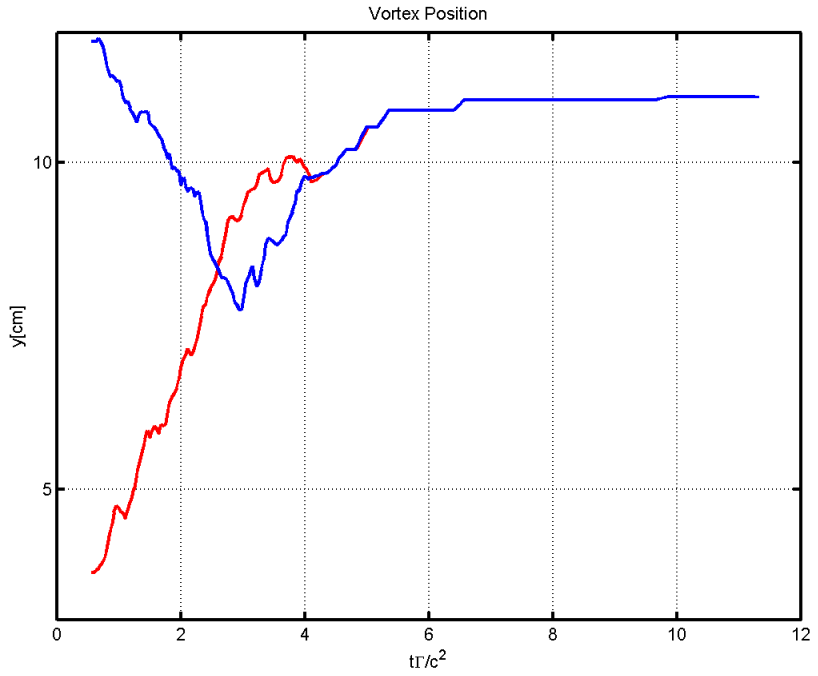

Figure 131 Vortex Position vs Non dimensional time for 1" separation asymmetric vortex merger 6rpm, 9rpm

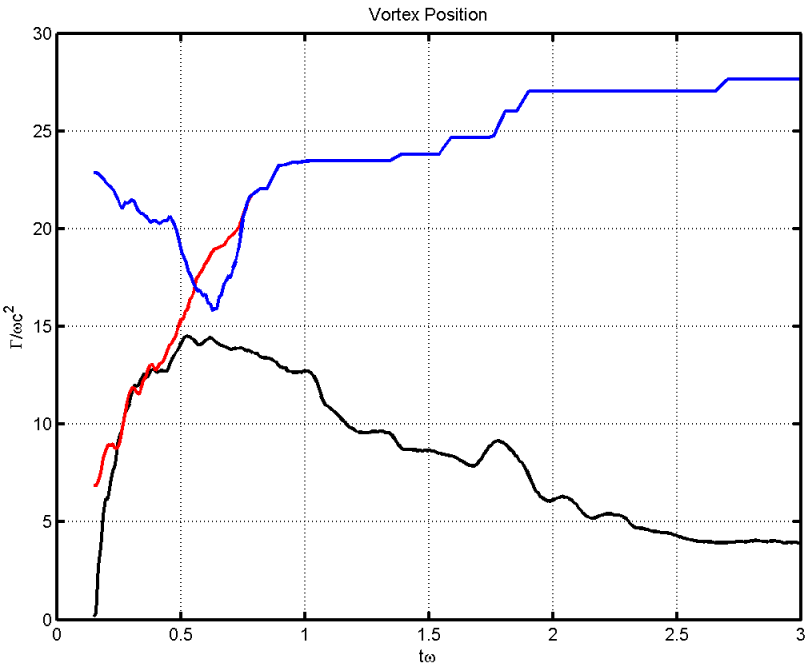

Figure 132 Vortex Position and Non Dimensional Analysis for 1" separation asymmetric merger 6rpm, 12rpm

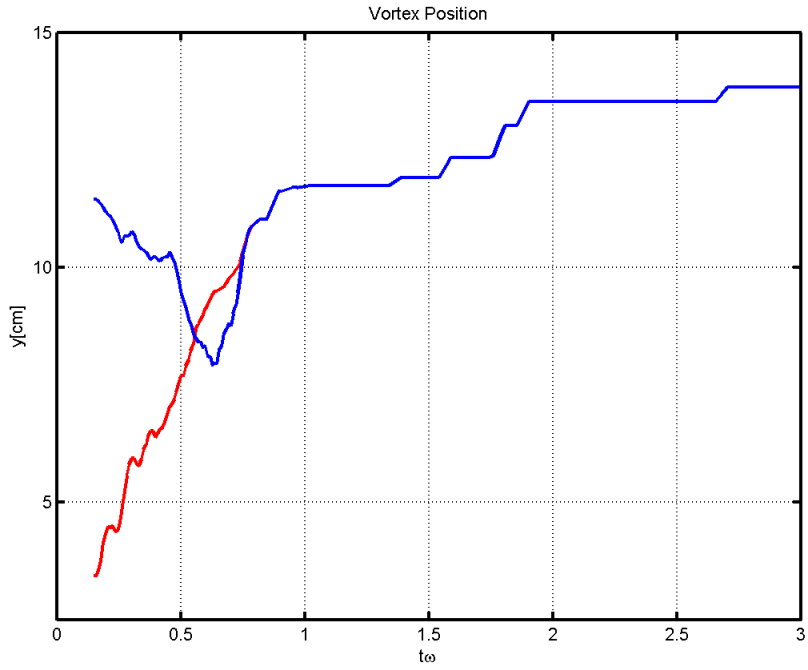

Figure 133 Vortex Positions vs time for 1" separation asymmetric merger 6rpm, 12rpm

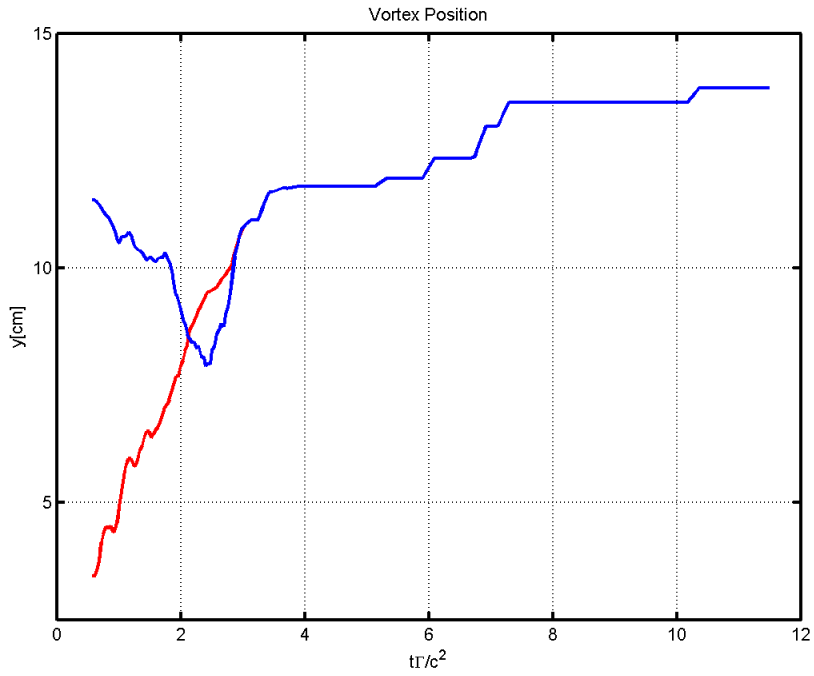

Figure 134 Vortex Position vs Non dimensional time for 1" separation asymmetric vortex merger 6rpm, 12rpm

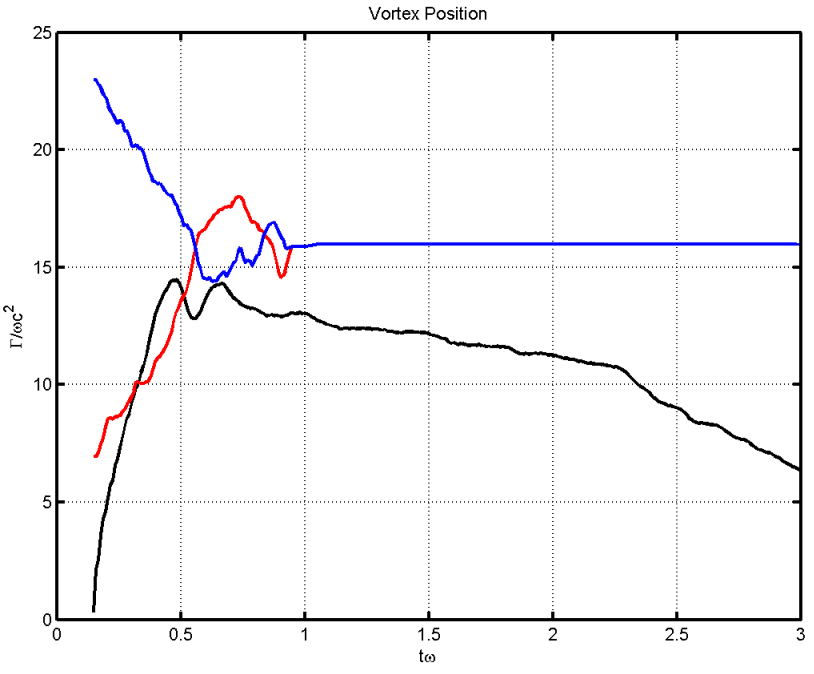

Figure 135 Vortex Position and Non Dimensional Analysis for 1" separation symmetric merger 9rpm, 9rpm

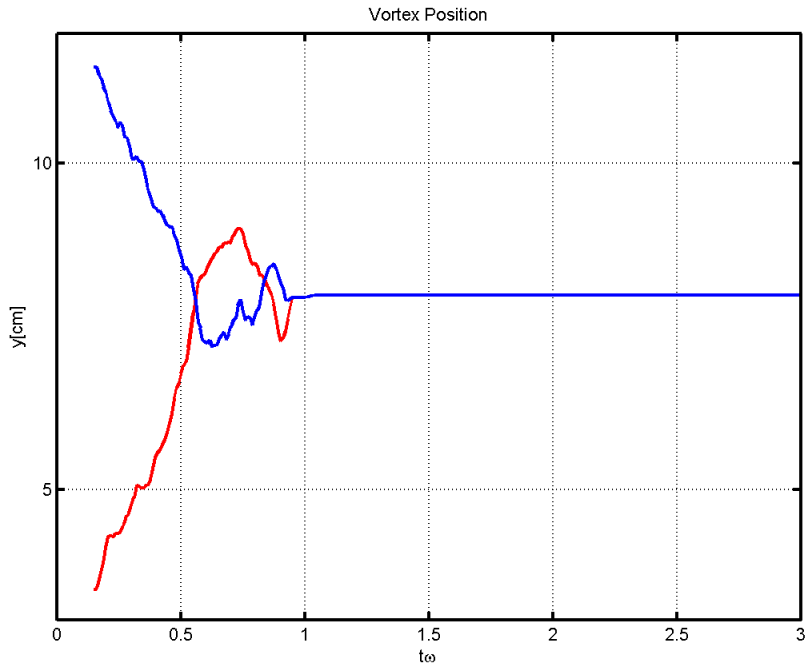

Figure 136 Vortex Positions vs time for 1" separation symmetric merger 9rpm, 9rpm

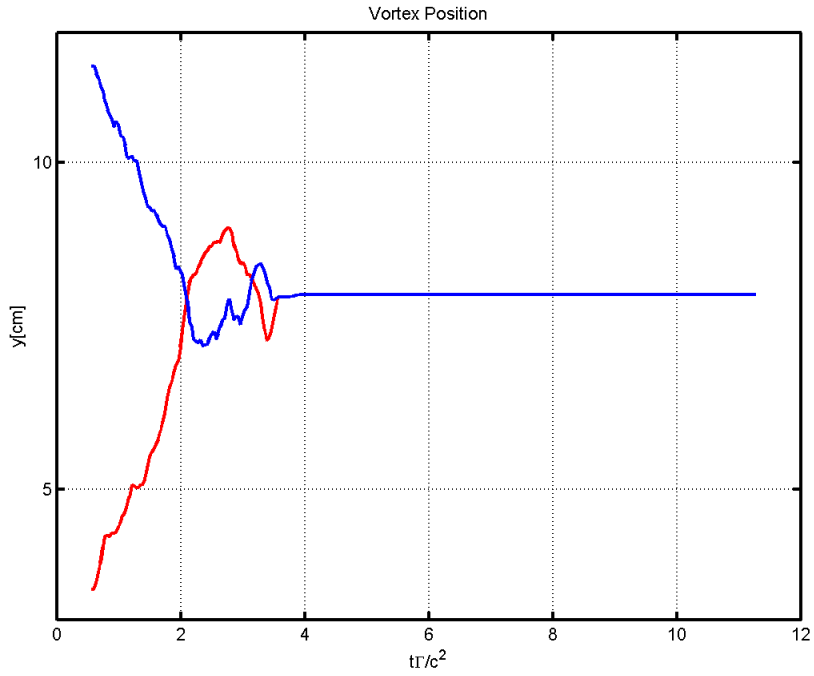

Figure 137 Vortex Position vs Non dimensional time for 1" separation symmetric vortex merger 9rpm, 9rpm

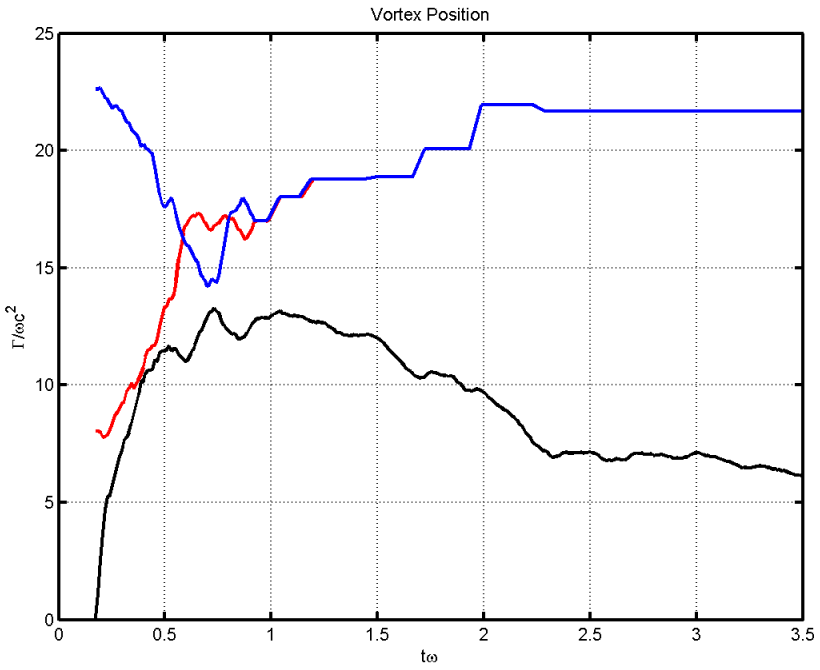

Figure 138 Vortex Position and Non Dimensional Analysis for 1" separation asymmetric merger 9rpm, 12rpm

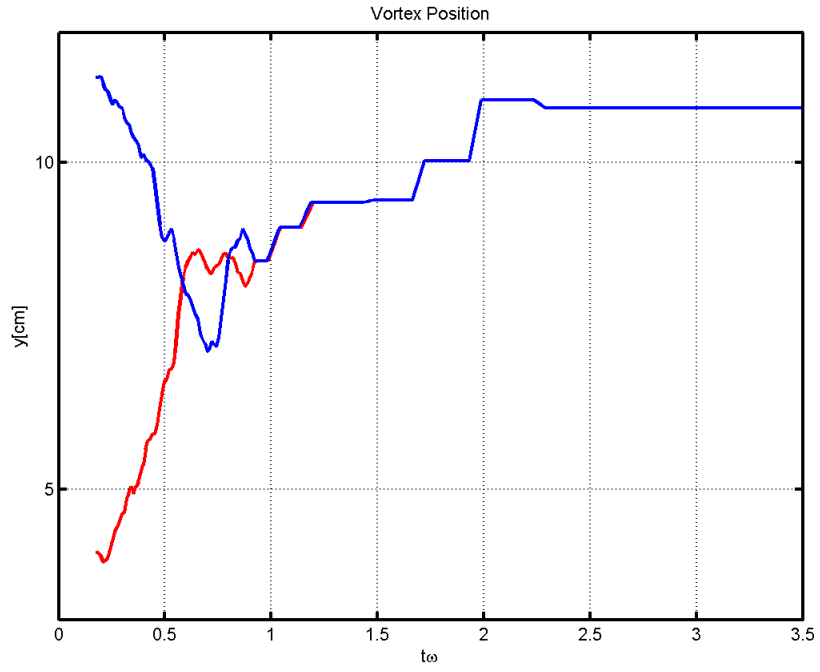

Figure 139 Vortex Positions vs time for 1" separation asymmetric merger 9rpm, 12rpm

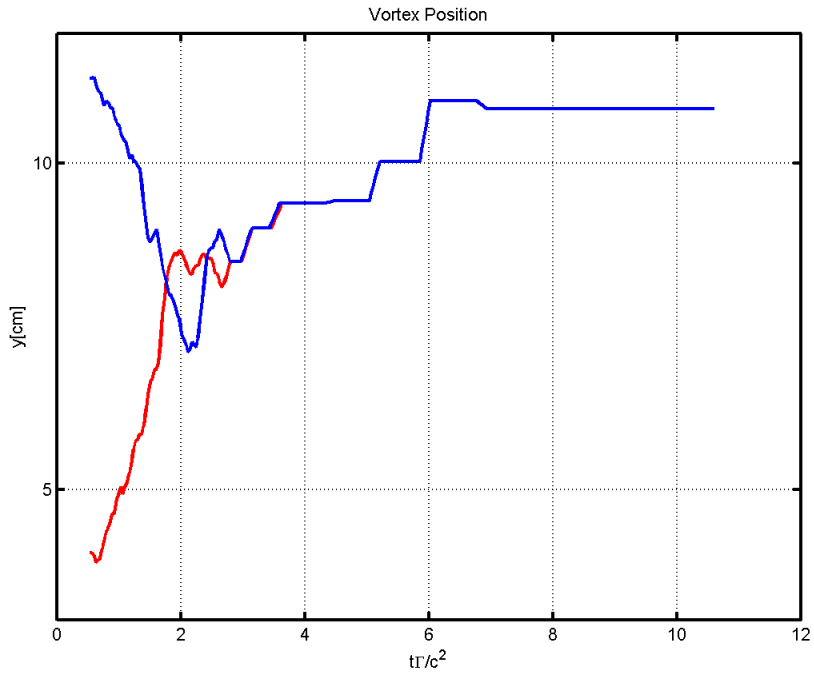

Figure 140 Vortex Position vs Non dimensional time for 1" separation asymmetric vortex merger 9rpm, 12rpm

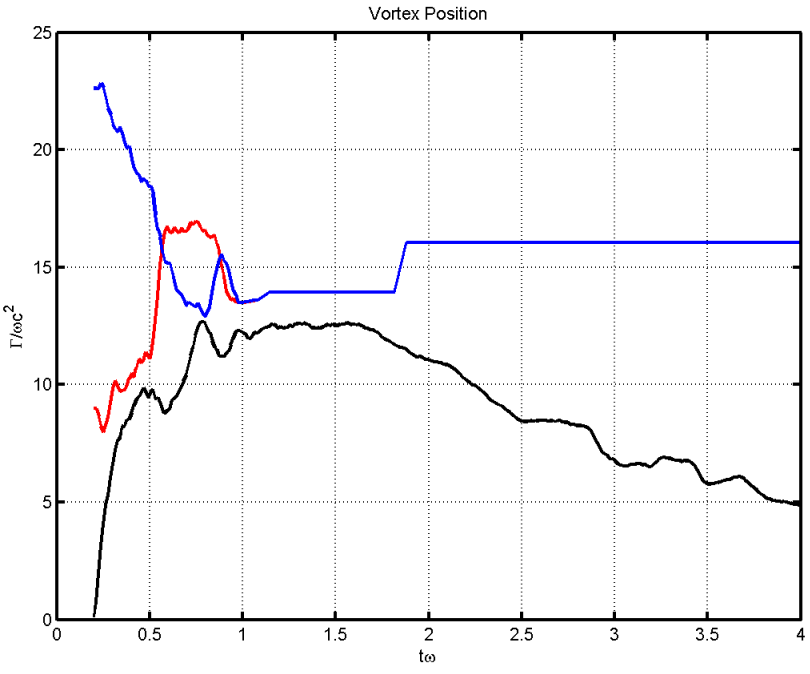

Figure 141 Vortex Position and Non Dimensional Analysis for 1" separation symmetric merger 12rpm, 12rpm

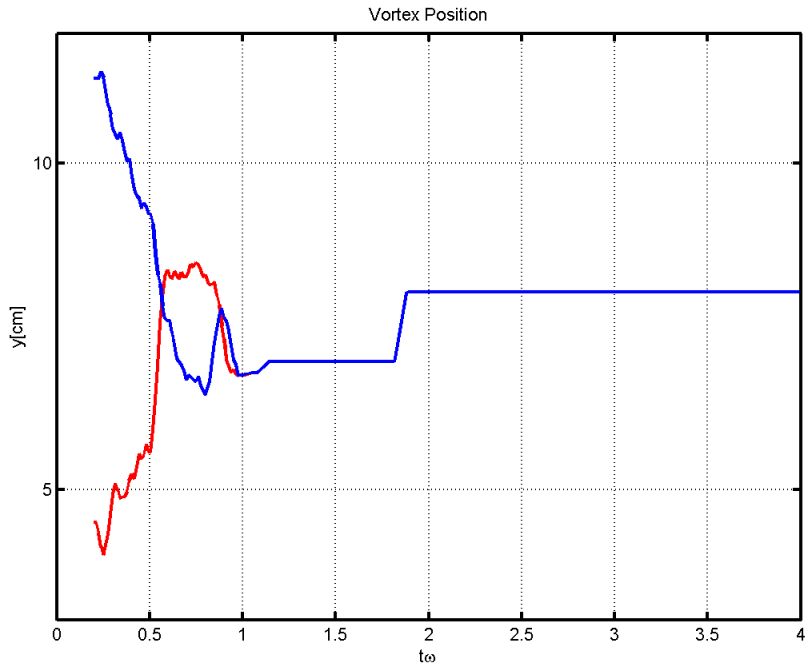

Figure 142 Vortex Positions vs time for 1" separation symmetric merger 12rpm, 12rpm

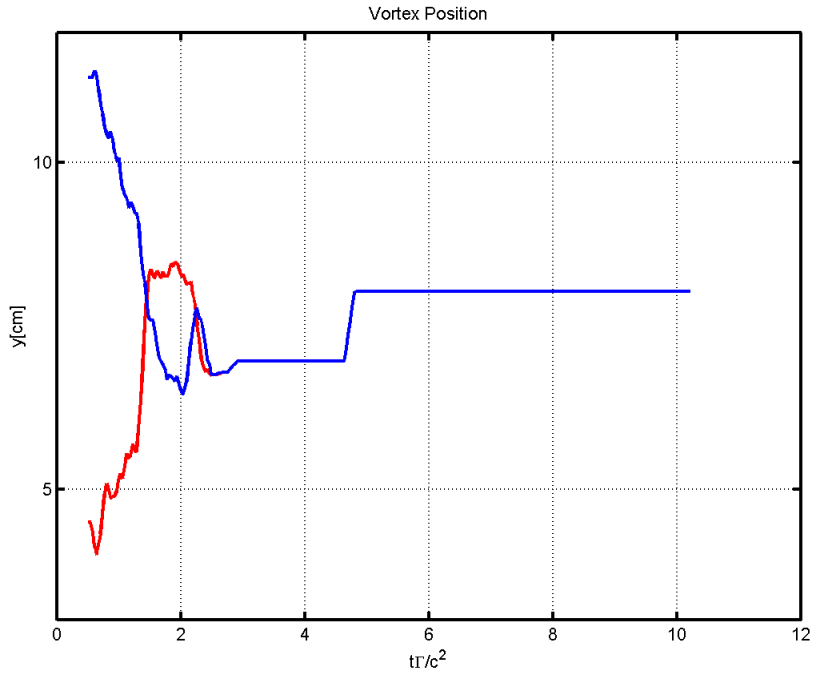

Figure 143 Vortex Position vs Non dimensional time for 1" separation symmetric vortex merger 12rpm, 12rpm

VITA

Akshay Girish Khandekar

Candidate for the Degree of

Master of Science

Thesis: DYNAMICS OF QUASI 2D and 3D CO-ROTATING VORTEX MERGER

Major Field: Mechanical & Aerospace Engineering

Biographical:

Education:

Completed the requirements for the Bachelor of Science/Arts in Mechanical Engineering at Oklahoma State University, Stillwater, Oklahoma in May, 2011.

Experience:

Graduate Teaching Assistant, Mechanical & Aerospace Engineering at Oklahoma State University, Stillwater, Oklahoma in January 2012 to May 2014.

Graduate Research Assistant, Mechanical & Aerospace Engineering at Oklahoma State University, Stillwater, Oklahoma in January 2012 to May 2014.

Professional Memberships: AIAA, APS, AUVSI, ASME, Pi Tau Sigma, GoldenKey